1521-009X/49/10/947–960$35.00
DRUG METABOLISM AND DISPOSITION

https://doi.org/10.1124/dmd.121.000497
Drug Metab Dispos 49:947–960, October 2021

Static and Dynamic Projections of Drug-Drug Interactions Caused by Cytochrome P450 3A Time-Dependent Inhibitors Measured in Human Liver Microsomes and Hepatocytes[S]

Elaine Tseng, Heather Eng, Jian Lin, Matthew A. Cerny, David A. Tess, Theunis C. Goosen, and R. Scott Obach

Medicine Design, Worldwide Research and Development, Pfizer Inc., Groton, Connecticut

Received April 8, 2021; accepted July 1, 2021

ABSTRACT

Cytochrome P450 3A (CYP3A) is a frequent target for time-dependent inhibition (TDI) that can give rise to drug-drug interactions (DDI). Yet many drugs that exhibit in vitro TDI for CYP3A do not result in DDI. There were 23 drugs with published clinical DDI evaluated for CYP3A TDI in human liver microsomes (HLM) and hepatocytes (HHEP), and these data were used in static and dynamic models for projecting DDI caused by inactivation of CYP3A in both liver and intestine. TDI parameters measured in HHEP, particularly the maximal rate of enzyme inactivation, were generally lower than those measured in HLM. In static models, the use of estimated average unbound organ exit concentrations offered the most accurate projections of DDI with geometric mean fold errors of 2.0 and 1.7 for HLM and HHEP, respectively. Use of maximum organ entry concentrations yielded marked overestimates of DDI. When evaluated in a binary fashion (i.e., projection of DDI of 1.25-fold or greater), data from HLM offered the greatest sensitivity (100%) and specificity (67%) and yielded no missed DDI when average unbound organ exit concentrations were used. In dynamic physiologically based pharmacokinetic modeling, accurate projections of DDI were obtained with geometric mean fold errors of 1.7 and 1.6 for HLM and HHEP, respectively. Sensitivity and specificity were 100% and 67% when using TDI data generated in HLM and Simcyp modeling. Overall, DDI caused by CYP3A-mediated TDI can be reliably projected using dynamic or static models. For static models, average organ unbound exit concentrations should be used as input values otherwise DDI will be markedly overestimated.

SIGNIFICANCE STATEMENT

CYP3A time-dependent inhibitors (TDI) are important in the design and development of new drugs. The prevalence of CYP3A TDI is high among newly synthesized drug candidates, and understanding the potential need for running clinical drug-drug interaction (DDI) studies is essential during drug development. Ability to reliably predict DDI caused by CYP3A TDI has been difficult to achieve. We report a thorough evaluation of CYP3A TDI and demonstrate that DDI can be predicted when using appropriate models and input parameters generated in human liver microsomes or hepatocytes.

Introduction

Alterations in the catalytic activities of cytochrome P450 enzymes represent a common mechanism of drug-drug interactions (DDI). Administration of one drug (the precipitant or perpetrator) which inhibits, inactivates, or induces the expression of a P450 enzyme will lead to changes in exposure to a second drug (the object or victim) that is cleared by that enzyme. The scientific and medical literature describe myriad examples of DDI that arise via this mechanism, and a large public database that summarizes the knowledge of DDI has been assembled (https://didb.druginteractionsolutions.org/).

Our understanding of the human P450 enzymes and their substrate and inhibitor specificities, along with the development of methods and algorithms to translate in vitro drug metabolism data to in vivo

This work received no external funding.

The authors are employees of Pfizer and report no conflicts of interest. The authors alone are responsible for the content and writing of the paper.

http://dx.doi.org/10.1124/dmd.121.000497.

[S] This article has supplemental material available at dmd.aspetjournals.org.

ABBREVIATIONS: AUC, area under the concentration versus time curve; AUCR, area under the plasma concentration-time curve ratio in the inhibited and control state; C_{avg}, average concentration values; $C_{avg,portal,u}$, unbound average portal vein concentration; $C_{avg,systemic,u}$, unbound average systemic concentration; $C_{avg,u}$, unbound average concentration values; $C_{max,portal,u}$, unbound steady state maximum portal vein concentration; CYP3A, cytochrome P450 3A; DDI, drug-drug interaction; F_a, fraction absorbed after oral dose; FN, false negative; FP, false positive; f_u, fraction unbound; $f_{u,mic}$, free fraction determined in microsomes; $f_{u,plasma}$, plasma free fraction; GMFE, geometric mean absolute fold error; HHEP, human hepatocyte; HLM, human liver microsome; [I], inhibitor concentration; $[I]_g$, intestinal inhibitor concentration; $[I]_h$, liver inhibitor concentration; iQC, inhibitor quality control; k_a, inhibitor absorption rate constant; k_{deg}, enzyme degradation rate constant; K_i, reversible inhibition constant; K_I, time-dependent inhibition constant; $K_{I,u}$, time-dependent inhibition constant, unbound; k_{inact}, maximal rate of enzyme inactivation; k_{obs}, rate constant for inhibition; $K_{p,uu}$, unbound partition coefficient in hepatocyte; LC-MS/MS, liquid chromatography-tandem mass spectrometry; MBI, mechanism-based inactivator; NPE, negative predictive error; NPV, negative predictive value; P450, cytochrome P450; PBPK, physiologically based pharmacokinetic modeling; PPE, positive predictive error; PPV, positive predictive value; RMSFE, root mean square fold error; TDI, time-dependent inhibition\inhibitor; TN, true negative; TP, true positive; V_{ss}, steady-state volume of distribution; WEM, Williams' E medium.

pharmacokinetics through the use of equations and physiologically based pharmacokinetic (PBPK) modeling platforms, has led to the routine collection of in vitro P450 inhibition data. DDI are an undesired phenomenon in new drugs, and in vitro P450 inhibition data are used in drug design and the selection of candidate compounds for further development as drugs. Such data are also used in developing strategies to evaluate DDI in the clinical phase of drug development, to decide what clinical pharmacokinetic studies need to be conducted in anticipation of observing a DDI (Grimm et al., 2009; Zhang et al., 2010; FDA, 2020).

Among the human P450 enzymes, CYP3A is the most important, since it is involved in the metabolic clearance of many drugs (Guengerich, 1995; Zhou, 2008). Thus, this enzyme is of focus for in vitro evaluation of the potential for DDI. Furthermore, this enzyme is prone to time-dependent inhibition (TDI), wherein the degree of inhibition observed increases with increasing incubation time. Some of the most notorious perpetrators of DDI are TDI of CYP3A, including clarithromycin, verapamil, diltiazem, and mibefradil, among others (Backman et al., 1994; Gorski et al., 1998; Mullins et al., 1998; Jones et al., 1999). In fact, mibefradil was withdrawn from clinical use due to CYP3A TDI (Prueksaritanont et al., 1999). Among CYP3A TDI, most are mechanism-based inactivators (MBI) in that the compound must be acted upon by the enzyme for the inhibition to occur. In P450 incubations, TDI and MBI can be distinguished in that the latter require the inclusion of NADPH, the cosubstrate required for P450 catalysis. MBI of P450 enzymes can occur via several biochemical mechanisms, and the most well known are 1) the formation of a complex between a metabolic intermediate of the inactivator and the heme iron (referred to as an M-I complex); 2) adduction of the inactivator to porphyrin, or 3) adduction of the inactivator to the protein backbone of the enzyme. Irrespective of the biochemical mechanism of MBI, all three will result in permanent cessation of the activity of enzyme molecules and DDI, with DDI abating only upon stopping treatment with the perpetrator drug and resynthesis of the enzyme in vivo (Zhou et al., 2004). Thus, during the drug research and development processes, considerable attention is focused on TDI of CYP3A to avoid this unwanted property.

Observations in our laboratories arising through the routine deployment of CYP3A TDI assays (unpublished observations) and those reported by others (Zimmerlin et al., 2011) have shown the preponderance of CYP3A TDI among test compounds to be high. Yet, for several compounds that have shown CYP3A TDI and which were predicted to demonstrate DDI, the result in clinical pharmacokinetic studies with sensitive CYP3A marker substrates, such as midazolam, showed no DDI (Ring et al., 2005; Wang et al., 2013). A reason for this mismatch is currently unknown. Others have attempted to engineer the conditions of in vitro incubations in an attempt to better represent the in vivo situation by the inclusion of plasma in the in vitro incubations (Mao et al., 2011, 2012). In a previous report, it was demonstrated that several drugs that showed measurable TDI of CYP3A in human liver microsomes (HLM) and hepatocytes (HHEP) do not cause DDI in vivo (Eng et al., 2021). In that work, the focus was on the use of CYP3A TDI data in an early drug research stage when drug design teams are seeking and selecting compounds lacking potential TDI. The conclusion from that study was that a cutoff for the observed inactivation rate constant, k_{obs} (run at a test concentration of 30 μM), is needed under which no compounds will cause in vivo DDI. Even with such a cutoff, several drugs with k_{obs} over that boundary were still not perpetrators of DDI. Such a boundary can be considered oversimplified, as it is known that other factors besides k_{obs} will influence whether a DDI will be observed (e.g., dose and exposure). Nevertheless, this was an important finding and defines a better understanding of how to use in vitro CYP3A TDI data in decision making.

In the present report, the objective was to build upon the observations from Eng et al., 2021 and query the fidelity of CYP3A TDI data in the projection of DDI using measurements of k_{inact} and K_I generated from both HLM and HHEP assays, along with several other necessary input values (e.g., various exposure parameters, plasma free fraction, estimated intestinal exposure, among others). Simple equations that relate in vitro TDI data to in vivo DDI (a.k.a. static methods) (Ernest et al., 2005; Obach et al., 2007; Grimm et al., 2009) as well as PBPK modeling (a.k.a. dynamic methods) (Rowland Yeo et al., 2011; Mao et al., 2013) were used, and various input parameters were evaluated. These methods were tested with 23 drugs that have reported clinical pharmacokinetic studies with sensitive CYP3A marker substrates (mostly midazolam). This represents the largest dataset for this purpose generated under the same experimental conditions. The results have shown that in vitro TDI data tend to over-project DDI, but that with application of established input parameters, success can be obtained using either HLM or HHEP.

Materials and Methods

Materials

Research was conducted on human tissue acquired from a vendor that was verified as compliant with internal policies, including institutional review board/independent ethics committee approval. Pooled HLM, consisting of 36 male and 14 female donors, were purchased from Sekisui XenoTech (Kansas City, KS). Cryopreserved pooled HHEP, consisting of 4 male and 6 female donors, pooled mixed-gender human plasma collected with K_3EDTA, and male human liver homogenate were purchased from BioIVT (Westbury, NY). Monobasic and dibasic potassium phosphate buffers, magnesium chloride, NADPH, HEPES, Dulbecco's PBS, and DMSO were purchased from Sigma (St. Louis, MO). M-PER™ buffer was purchased from Thermo Fisher Scientific (Waltham, MA). Midazolam was purchased from USP (Rockville, MD). 1'-Hydroxymidazolam and [$^2H_4$]1'-hydroxymidazolam were synthesized at Pfizer (Groton, CT). Williams' E medium was purchased from Gibco (Dublin, Ireland). Commercially obtained chemicals and solvents were of high-performance liquid chromatography or analytical grade. Tested drugs (typical purity >95%) were either synthesized internally at Pfizer (Groton, CT) or purchased from one of the following sources: Sigma-Aldrich (St. Louis, MO), Toronto Research Chemicals (North York, Ontario, Canada), MedChemExpress (Monmouth Junction, NJ), TCI (Portland, OR), or APExBio (Houston, TX).

Identification of Test Drugs

The University of Washington Drug Interaction Database (https://www.druginteractionsolutions.org) was used to compile a list of drugs for which clinical CYP3A interaction studies were conducted (Table 1). Studies in which midazolam was dosed via the oral route were preferred. In a couple of instances, studies containing midazolam dosed via the intravenous route or other CYP3A probe substrates were chosen. The magnitude of DDI (AUCR) was determined based on the ratio of the probe substrate AUC in the presence (area under the concentration versus time curve when coadministered with an inhibitor) and absence (AUC) of the test drug. For drugs where more than one interaction study was published at the same dose and route, the weighted average AUCR based on the number of subjects per study was calculated using eq. 1 below:

$$W = \frac{\sum_{i=1}^{n} w_i X_i}{\sum_{i=1}^{n} w_i} \quad (1)$$

where the weighted average AUCR (W) is the quotient between the summation of the product of each observed mean AUCR (X_i) and the number of subjects in that study (w_i) divided by the total number of subjects in all studies.

Binding to Plasma, Liver Microsomes, and Liver Homogenate

Binding of the test drugs to human plasma, liver microsomes, and liver homogenate were determined based on methods previously described by Di et al., 2017. Briefly, binding experiments were performed by equilibrium

TABLE 1

Summary of observed clinical drug-drug interactions for CYP3A cleared drugs

Drug Name	Inhibitor Dose	Substrate Dose[b]	Clinical Interaction (AUCR)	Clinical Interaction Reference
Azithromycin	500 mg once a day; 3 d	15 mg oral midazolam	1.23[a]	(Yeates et al., 1996; Zimmermann et al., 1996)
Boceprevir	800 mg three times a day; 6 d	4 mg oral midazolam	5.05	(FDA, 2011)
Carfilzomib	27 mg/m^2 i.v.; various	2 mg oral midazolam	1.10	(Wang et al., 2013)
Clarithromycin	500 mg twice a day; 7 d	4 mg oral midazolam	6.69[a]	(Gorski et al., 1998; Gurley et al., 2006; Gurley et al., 2008; Quinney et al., 2008; Prueksaritanont et al., 2017)
Conivaptan	40 mg twice a day; 5 d	2 mg oral midazolam[c]	5.76	(FDA, 2005)
Diltiazem	60 mg three times a day; 2 d	2 mg oral midazolam	3.93[a]	(Backman et al., 1994; Friedman et al., 2011)
Disulfiram	500 mg single dose	1 mg i.v. midazolam	1.05	(Kharasch et al., 1999)
Eplerenone	100 mg once a day; 6 d	10 mg oral midazolam	0.96	(Cook et al., 2004)
Erythromycin	500 mg three times a day; 7 d	4 mg oral midazolam	4.12[a]	(Olkkola et al., 1993; Zimmermann et al., 1996)
Imatinib	400 mg once a day; 7 d	40 mg oral simvastatin	2.92	(O'Brien et al., 2003)
Midostaurin	100 mg single dose	4 mg oral midazolam	1.00	(Dutreix et al., 2013)
Nelfinavir	1250 mg twice a day; 14 d	2 mg oral midazolam 1 mg i.v. midazolam	4.29[a] 1.83	(Kirby et al., 2011)
Nitrendipine	20 mg single dose	0.07 mg/kg i.v. plus infusion midazolam	0.93 change in CL	(Handel et al., 1988)
Panobinostat	20 mg every other day; 15 d	5 mg oral midazolam	1.04	(Einolf et al., 2017)
Paroxetine	20 mg once a day; 15 d	60 mg oral terfenadine[d]	0.97	(Martin et al., 1997)
Propiverine	15 mg twice a day; 7 d	2 mg oral midazolam	1.46	(Tomalik-Scharte et al., 2005)
Propranolol	40 mg four times a day; 2 d	0.5 mg oral triazolam	0.89	(Friedman et al., 1988)
Simvastatin	10 mg once a day; 14 d	15 ug/kg oral midazolam	1.24	(Kokudai et al., 2009)
Tabimorelin	3 mg/kg once a day; 7 d	7.5 mg oral midazolam	1.93	(Zdravkovic et al., 2003)
Tadalafil	10 mg once a day; 14 d	15 mg oral midazolam	0.90	(Ring et al., 2005)
Telaprevir	750 mg three times a day; 16 d	2 mg oral midazolam 0.5 mg i.v. midazolam	13.5 4.92	(Garg et al., 2012)
Terfenadine	120 mg once a day; 3 d	10 mg oral buspirone	1.19	(Lamberg et al., 1999)
Verapamil	80 mg three times a day; 2 d	15 mg oral midazolam	2.92	(Backman et al., 1994)

[a]AUCR was calculated as a weighted average AUCR based on number of subjects in each study at the same dose per route (eq. 1).
[b]Substate (single dose) was given at the final day of inhibitor dose.
[c]Substrate (once a day), 5 days.
[d]Substrate (twice a day), days 8 to 15, 8 days.

dialysis. The matrix was spiked with 1 μM of test drug (donor) and allowed to dialyze against Dulbecco's PBS (receiver) for a duration of 6 hours with a 12000–14000 molecular weight cutoff membrane in a humidified incubator supplemented with 5% CO_2 at 37°C. All incubations were performed in quadruplicate. At equilibrium, matrix and buffer samples were collected and matrix matched before addition of 4 volumes of acetonitrile containing a cocktail of internal standards (50 ng/ml tolbutamide and 5 ng/ml terfenadine). Samples were vortexed and centrifuged for 5 minutes at approximately 2300 x *g* at room temperature. The supernatant was collected and analyzed directly by LC-MS/MS (method details are in Supplemental Table 2). Determination of the fraction unbound (f_u) in human plasma, liver microsomes, and liver homogenate were determined by methods described in (Riccardi et al., 2017).

Human Hepatocyte Unbound Partition Coefficient

The unbound partition coefficient in HHEP for each of the test drugs was determined following the methods described by Riccardi et al., 2018. Briefly, HHEP (0.5 million hepatocytes/ml) suspended in WEM supplemented with L-glutamine and HEPES (50 mM) were incubated with 1 μM of test drug for 2 hours. At the end of the incubation, the HHEP were centrifuged at 40 x *g* for approximately 5 minutes to pellet the cells. The supernatant was reserved for analysis. The pellet was washed three times with ice-cold PBS, and the final pellet was lysed with M-PER™ buffer. The reserved supernatant and lysate were matrix matched before the addition of 4 volumes of acetonitrile containing a cocktail of internal standards (200 ng/ml diclofenac and 25 ng/ml indomethacin). Samples were vortexed and centrifuged for 5 minutes at approximately 2300 x *g* at room temperature. The supernatant was mixed with an equal volume of water containing 0.2% formic acid and analyzed directly by LC-MS/MS (Supplemental Table 2). In vitro $K_{p,uu}$ of the test drugs in HHEP were calculated by methods described by Riccardi et al., 2018. Partitioning into hepatocytes was demonstrated to be fairly rapid, and equilibrium was generally achieved by 10 minutes (Treyer et al., 2018, 2019).

IC_{50} Determination in Human Liver Microsomes and Human Hepatocytes

HLM and HHEP were used to determine the IC_{50} of CYP3A enzyme activity. HLM incubations (0.01 mg/ml) were supplemented with $MgCl_2$ (3.3 mM) and NADPH (1.3 mM) in potassium phosphate buffer (100 mM, pH 7.4). HHEP (0.2 million hepatocytes/ml) were suspended in WEM supplemented with L-glutamine and HEPES (50 mM). Drug stocks, at incrementing concentrations, were prepared at 100 times the final incubation concentration (up to 100 μM final) in a mixture of organic and aqueous solvents, typically acetonitrile and water (Supplemental Table 1). Midazolam, the probe substrate, was prepared at 10x the final concentration (2 to 3 μM, corresponding to K_M in HLM and HHEP, respectively) in either potassium phosphate buffer or WEM, for HLM or HHEP, respectively. The final total solvent in the incubations was ≤1%. The incubation was initiated with the addition of drug stock immediately followed by the probe substrate. After a 4-minute incubation in HLM or a 10-minute incubation in HHEP, the reaction was terminated by the addition of either two or four volumes of acetonitrile containing internal standard (100 ng/ml [$^2H_4$]1'-hydroxymidazolam) for HLM and HHEP incubations, respectively. All reactions were carried out at 37°C, at a final volume of 200 μl, in duplicate. Samples were vortexed and centrifuged for 5 minutes at approximately 2300 x *g* at room temperature. The supernatant was mixed with an equal volume of water containing 0.2% formic acid and analyzed directly by LC-MS/MS (methods described below). A standard curve (0.250–250 nM) and inhibitor quality control (iQC, 50 nM) of 1'-hydroxymidazolam was prepared in duplicate at the final protein concentration in the assay for either HLM or HHEP. The inhibitor concentration included in the iQC was determined based on the highest concentration tested in the assay.

Standards and iQC samples were processed in the same manner as the incubation samples.

Time-Dependent Inhibition in Human Liver Microsomes

TDI of CYP3A was measured in HLM (0.3 mg/ml) supplemented with $MgCl_2$ (3.3 mM) and NADPH (1.3 mM) in potassium phosphate buffer (100 mM, pH 7.4). Drug stock solutions, at incrementing concentrations up to 300 μM (final), were prepared at 100 times the final incubation concentration in a mixture of organic and aqueous solvents, usually acetonitrile and water (Supplemental Table 1). The final total solvent in the primary incubations was ≤1%. The incubation was initiated with the addition of drug stock to the microsomal mixture. At various time points, generally up to 40 minutes, an aliquot of the mixture was transferred to an activity incubation mixture containing midazolam (20.9 μM, 10-fold K_M), $MgCl_2$ (3.3 mM), and NADPH (1.3 mM) in potassium phosphate buffer (100 mM, pH 7.4), generally resulting in a 20-fold dilution. After 6 minutes, the activity reaction was terminated by the addition of two volumes of acetonitrile containing internal standard (100 ng/ml [$^2H_4$] 1'-hydroxymidazolam). All reactions were carried out at 37°C, at a final volume of 200 μl, in duplicate. Samples were vortexed and centrifuged for 5 minutes at approximately 2300 x *g* at room temperature. The supernatant was mixed with an equal volume of water containing 0.2% formic acid and analyzed directly by LC-MS/MS (methods described below). A standard curve (0.250–250 nM) and inhibitor quality control (iQC, 50 nM) of 1'-hydroxymidazolam was prepared in duplicate at the final protein concentration in the activity assay. The inhibitor concentration included in the iQC was determined based on the highest concentration tested in the assay divided by the fold-dilution of the primary to secondary incubation. Standards and iQC samples were processed in the same manner as the incubation samples. For several drugs, assay conditions were modified due to rapid inactivation or potent inhibition at the initial time point. Modifications to the incubation conditions can be found in Supplemental Table 1.

Time-Dependent Inhibition in Suspension Human Hepatocytes

TDI of CYP3A was measured in HHEP in a manner similar to that described by Chen et al., 2011. Drug stock solutions, at concentrations up to 300 μM (final), were prepared at 10-times the final incubation concentration in a mixture of organic and aqueous solvents, usually acetonitrile and water (Supplemental Table 1). The incubation was initiated with the addition of drug stock to HHEP (0.45 million hepatocytes/ml) suspended in WEM supplemented with L-glutamine and HEPES (50 mM), in a total volume of 50 μl. At various time points (typically up to 120 minutes unless otherwise stated), a 200 μl aliquot of the activity incubation mixture consisting of midazolam (final concentration 30 μM, approximately 10-fold K_M) in media was added to the incubation wells, resulting in a 5-fold dilution of the primary incubation. After a 20-minute activity reaction, the incubation was terminated by the addition of two volumes of acetonitrile containing internal standard (100 ng/ml [$^2H_4$]1'-hydroxymidazolam). All reactions were carried out at 37°C in a humidified incubator (75% relative humidity, 5% CO_2) in duplicate. The final total solvent in the primary incubations was ≤1%. Samples were vortexed and centrifuged for 5 minutes at approximately 2300 x *g* at room temperature. The supernatant was mixed with an equal volume of water containing 0.2% formic acid and analyzed directly by LC-MS/MS (methods described below). A standard curve (0.58–1000 nM) and inhibitor quality control (iQC, 100 nM) of 1'-hydroxymidazolam was prepared in duplicate at the final protein concentration in the activity assay. The inhibitor concentration included in the iQC was determined based on the highest concentration tested in the assay divided by the fold-dilution of the primary to secondary incubation. Standards and iQC samples were processed in the same manner as the incubation samples. For several drugs, assay conditions were modified due to rapid inactivation or solubility limitations of the test drug. Modifications to the incubation conditions can be found in Supplemental Table 1.

LC-MS/MS Methodology for the Quantitation of 1'-Hydroxymidazolam

LC-MS/MS analysis was conducted on either a Sciex 5500 or 6500 triple quadrupole mass spectrometer (Framingham, MA) fitted with an electrospray ion source operated in positive ion mode using multiple reaction monitoring. An Agilent 1290 binary pump (Santa Clara, CA) with a CTC Leap autosampler (Leap Technology, Carrboro, NC) was programmed to inject 10 μl of sample on a Halo 2.7 μm C18 2.1x30 mm column (Advanced Materials Technology, Wilmington, DE). A binary gradient was employed using 0.1% (v/v) formic acid in water (mobile phase A) and 0.1% (v/v) formic acid in acetonitrile (mobile phase B) at a flow rate of 0.5 ml/min. Mass-to-charge transitions for analytes 1'-hydroxymidazolam and [$^2H_4$]1'-hydroxymidazolam were 342.2 → 324.2 and 346.2 → 328.2, respectively. Analytes were quantified against a standard curve using Analyst software (Sciex). A linear regression with either a weighting of 1/x or $1/x^2$ was used. Standards and iQCs were accepted if the calculated concentrations were ±25% of their nominal concentration. Acceptance of the iQC demonstrates that the inhibitor did not interfere with 1'-hydroxymidazolam signal on the MS.

Data Analysis

Estimation of K_i. Percent activity remaining of the CYP3A enzyme was determined by normalizing the concentration of 1'-hydroxymidazolam in the presence of varying concentrations of test drug to the concentration of 1'-hydroxymidazolam in the solvent control. The concentration of inhibitor corresponding to a 50% decrease in activity (IC_{50}) was generated using GraphPad Prism 8 (La Jolla, CA). Since inhibition experiments were conducted at the K_M of midazolam, K_i was estimated as IC_{50} divided by two ($IC_{50}/2$) assuming competitive inhibition (Cheng and Prusoff, 1973). Free K_i was determined by correcting K_i with the free fraction determined in microsomes ($f_{u,mic}$) or $K_{p,uu}$ for HLM or HHEP experiments, respectively.

Estimation of K_I and k_{inact}. Data analysis methods previously described by Yates et al., 2012 were used for the estimation of k_{obs}, K_I, and k_{inact}. Briefly, k_{obs} was determined by normalizing the 1'-hydroxymidazolam concentration in each sample to that of the mean solvent control concentration in the initial time point, plotting the natural log of percent remaining activity versus preincubation time, and then calculating the slope of the line ($-k_{obs}$) using the initial linear portion of the curve. A statistical test was done at each concentration of test drug to determine whether k_{obs} was statistically different from the within-experiment solvent control, i.e., a parallel lines test, shown in eq. 2.

$$z = \frac{\left|k_{obs[I]} - k_{obs[0\mu M]}\right|}{\sqrt{SE^2_{k_{obs[I]}} + SE^2_{k_{obs[0\mu M]}}}} \quad (2)$$

Here, $k_{obs[I]}$, $k_{obs[0\mu M]}$, and S.E. represent the inactivation rate for an inhibitor at a single concentration, inactivation rate with solvent control, and standard error, respectively. A statistically significant TDI is defined when the parallel lines test yields a P value of <0.05. When possible, K_I and k_{inact} parameters were determined using nonlinear regression of the three-parameter Michaelis-Menten equation below:

$$k_{obs} = k_{obs[0\mu M]} + \frac{k_{inact} \times [I]}{K_I + [I]} \quad (3)$$

[I] represents the concentrations of the test drug in the primary incubation, k_{inact} is the maximal inactivation rate, and K_I is the inactivator concentration at half k_{inact}.

For compounds where substrate inhibition was observed at the higher concentrations, nonlinear regression of a four-parameter substrate inhibition model (eq. 4) was used to fit the curve.

$$k_{obs} = k_{obs[0\mu M]} + \frac{k_{inact} \times [I]}{K_I + [I] \cdot \left(\frac{1+[I]}{K_s}\right)} \quad (4)$$

In the equation above, K_s is a dissociation constant for binding, enabling a better fit of the data.

In six instances, the relationship between k_{obs} and [I] did not yield enough of a hyperbola to reliably estimate values for K_I and k_{inact}. For these, a composite slope of the initial linear portion of the k_{obs} vs [I] curve was determined to represent the ratio of k_{inact}/K_I. The static model equations and Simcyp require individual parameters as input values. To accomplish this, $K_{I,u}$ was arbitrarily set at a high value of 1 mM, and the slope was used to calculate k_{inact}. This value for k_{inact} along with the value of 1 mM for $K_{I,u}$ were then used as input values for DDI projections, under the reasonable assumption that $[I]_{in\ vivo} \ll 1$ mM. For compounds where K_I could be determined, $K_{I,u}$ was determined by correcting K_I with $f_{u,mic}$ or $K_{p,uu}$ for HLM or HHEP experiments, respectively. Analyses were performed using Microsoft Excel (Redmond, WA) and GraphPad Prism 8.

Predicting Magnitude of DDIs. The magnitude of DDI (AUCR) can be described as a ratio of the area under the concentration versus time curve when coadministered with an inhibitor divided by AUC when administered alone. Mathematical models to determine the extent of DDI while incorporating

competitive inhibition and time-dependent inactivation in the liver and gut have been extensively described (Rowland and Matin, 1973; Mayhew et al., 2000; Wang et al., 2004; Obach et al., 2006, 2007; Fahmi et al., 2008) and are summarized in the equation below (eq. 5).

$$AUCR = \frac{AUC_i}{AUC} = \frac{1}{\left(\left(\frac{1}{1+\frac{[I]_h}{K_i}} \times \frac{1}{1+\left(\frac{k_{inact}\times[I]_h}{(K_I+[I]_h)\times k_{deg,CYP3A,h}}\right)}\right) \times f_{m(CYP3A)}\right) + \left(1 - f_{m(CYP3A)}\right)} \times \frac{1}{\left(\left(\frac{1}{1+\frac{[I]_g}{K_i}} \times \frac{1}{1+\left(\frac{k_{inact}\times[I]_g}{(K_I+[I]_g)\times k_{deg,CYP3A,g}}\right)}\right) \times (1 - F_g)\right) + F_g} \quad (5)$$

In the above equation, k_{deg} represents the hepatic ($CYP3A_h$, 0.00032 $minute^{-1}$) and intestinal ($CYP3A_g$, 0.00050 $minute^{-1}$) degradation rates of the CYP3A enzyme (Obach et al., 2007; Rowland Yeo et al., 2011). The intestinal k_{deg} is based on a half-life of 23.1 hours, which is the natural turnover rate of enterocytes in vivo (Greenblatt et al., 2003). The hepatic k_{deg} is based on a half-life of 36 hours, which was derived from a clinical DDI study conducted by Fromm et al., 1996 (Obach et al., 2007). The fraction of the victim drug metabolized by the CYP3A enzyme is represented as $f_{m(CYP3A)}$. In this analysis, $f_{m(CYP3A)}$ for the victim drugs midazolam, buspirone, terfenadine, triazolam, and simvastatin are 0.93, 0.94, 0.74, 0.92, and 0.92, respectively (Obach et al., 2006; Yadav et al., 2018). The fraction of the victim drug escaping intestinal metabolism is represented by F_g. For the victim drugs midazolam, buspirone, terfenadine, triazolam, and simvastatin, F_g are 0.57, 0.21, 0.40, 0.75, and 0.66, respectively (Paine et al., 1996; Brown et al., 2005; Galetin et al., 2006, 2008, 2010; Gertz et al., 2008; Shou et al., 2008). The terms $[I]_h$ and $[I]_g$ represent inhibiting concentrations of the test drug in the liver and intestine, respectively. Unbound test drug concentrations (C_u) resulting in enzyme inhibition in the liver were estimated as unbound steady state maximum hepatic inlet concentration ($C_{max,hepatic\ inlet,u}$) using the equation below (eq. 6) (Kanamitsu et al., 2000) or unbound steady state maximum ($C_{max,systemic,u}$) or average ($C_{avg,systemic,u}$) systemic concentrations.

$$C_{max,hepatic\ \ inlet,u} = f_{u,p} \times \left(C_{max} + \frac{F_a \times F_g \times k_a \times Dose}{BPR \times Q_h}\right) \quad (6)$$

In the equation above, k_a is the oral absorption rate of the test drug (or 0.1 $minute^{-1}$), F_a is the fraction of test drug absorbed after oral administration (assume 1), F_g is the fraction of test drug escaping intestinal metabolism (assume 1), $f_{u,p}$ is the free fraction of the test drug in plasma, BPR is the blood-to-plasma ratio (assume 1), and Q_h is the liver blood flow [1617 ml/min (Yang et al., 2007a)].

Test drug concentrations resulting in enzyme inhibition in the intestine were estimated as total or free inhibiting concentrations in the enterocyte (I_g) as defined in eq. 7a by (Rostami-Hodjegan and Tucker, 2004), unbound steady state maximum portal vein concentration ($C_{max,portal,u}$, eq. 7b) or average portal vein concentration ($C_{avg,portal,u}$, eq. 7c).

$$[I]_g = \frac{F_a \times k_a \times Dose}{Q_{ent}} \quad (7a)$$

$$C_{max,portal,u} = f_{u,p} \times \left(C_{max} + \frac{F_a \times F_g \times k_a \times Dose}{BPR \times Q_{pv}}\right) \quad (7b)$$

$$C_{avg,portal,u} = f_{u,p} \times \left(C_{avg} + \frac{F_a \times F_g \times Dose}{\tau \times BPR \times Q_{pv}}\right) \quad (7c)$$

The parameters are the same as described above, with Q_{ent} representing the intestinal blood flow [300 ml/min (Yang et al., 2007b)], Q_{pv} represents the portal vein blood flow (1213 ml/min), which is approximated as 75% of hepatic blood flow, and τ is the dosing interval for the inhibitor. Free enterocyte inhibiting concentrations are calculated as $[I]_g$ corrected for $f_{u,plasma}$. Compound specific inputs can be found in Supplemental Table 4.

Simcyp Modeling. Simcyp version 19 release 1 (19.0; Certara, Princeton, NJ) was used to simulate the time courses of victim and perpetrator concentrations in plasma. Simulations were conducted using a design of 10 trials with 10 subjects using the age range of 20–50 years and 1:1 male to female ratio. Simulations were performed in a virtual population library of healthy volunteers supplied by Simcyp (Sim-Healthy Volunteers). The hepatic and intestinal CYP3A k_{deg} were 0.0193 $hour^{-1}$ ($t_{1/2}$ = 36 hours) and 0.03 $hour^{-1}$ ($t_{1/2}$ = 23.1 hours), respectively, consistent with those used in static modeling. The intestinal concentrations were the enterocyte exit concentration (portal vein) with $f_{u,gut} = f_{u,plasma}$, whereas liver concentrations were the liver exit concentration. A summary of the trial designs for all simulations are listed in Table 1. In the DDI studies, the fold-increase in AUCR (e.g., $AUC_{infinity}$ ratios in the single-dose studies and AUC_τ ratios in the multiple-dose studies) was calculated from the ratios of the simulated values in treatment groups relative to control groups. Geometric means of pharmacokinetic parameters generated from Simcyp simulations were compared with the clinically observed geometric mean parameters. For perpetrator drugs clarithromycin, diltiazem, erythromycin, paroxetine, simvastatin, and verapamil, compound files were qualified by Simcyp. Azithromycin Simcyp file was developed by Certara using Simcyp V14 and published in Simcyp Global Health Repository. To maintain consistency with the use of input parameters generated internally (i.e., $f_{u,p}$, K_I, k_{inact}, etc.), the steady-state volume of distribution (V_{ss}) and oral clearance were adjusted to adequately recover the clinically observed AUC and C_{max} at the dose used in the DDI study. In predicting the inhibitory effect of diltiazem administration, we have incorporated the inhibitory effects of its primary metabolite (MA). Sim-desmethyldiltiazem (MA) was qualified by Simcyp and used without adjusting V_{ss} and CL. Input parameters of 23 perpetrators are summarized in Supplemental Tables 5–27. Briefly, physicochemical properties (p*K*a, log P) are obtained from in silico software (www.acdlabs.com; www.biobyte.com). Plasma binding ($f_{u,p}$) was obtained from internal experimental data (Supplemental Table 3). The apparent permeability values used were either default values included as part of the qualified Simcyp files (https://members.simcyp.com/account/libraryFiles) or calculated from in silico models (Keefer et al., 2013) and extrapolated to effective permeability in human. k_a, V_{ss}, and oral clearance were fitted manually to adequately recover the clinically observed results at the doses used in the DDI studies (Supplemental Table 38). These values were internally consistent with those used in static projections (model 4).

For victim drugs, Sim-midazolam, SV-triazolam, and SV-simvastatin, Simcyp library compound files were qualified by Simcyp and used without modification. The terfenadine compound file was developed by Simcyp for QT prolongation prediction and was adjusted to reasonably recover the clinical $f_{m(CYP3A)}$ and F_g. The buspirone Simcyp model was developed based on physicochemical properties, plasma binding, distribution, and elimination obtained from literature (Kivisto et al., 1997, 1999; Mahmood and Sahajwalla, 1999). The buspirone model could reasonably recover both PK and $f_{m(CYP3A)}$. Using this model, the predicted AUCR after coadministration of itraconazole are in reasonable agreement with the observed values. Input parameters for the victim drugs are summarized in Supplemental Tables 28-33.

Confusion Matrix Analyses. To determine the success of predicting DDI, contingency tables were analyzed separately for HLM and HHEP results. Cutoff values of AUCR were defined prospectively as ≥1.25-fold (bioequivalence) or ≥2-fold. As an example, in the pairing of clinical and predicted AUCR ≥1.25-fold, true positives (TP) were defined as drugs which resulted in an observed clinical AUCR ≥1.25-fold and were predicted to have an AUCR ≥1.25-fold. True negative (TN) drugs were those that resulted in an observed clinical AUCR <1.25 and were predicted to have an AUCR <1.25-fold. False positive (FP) drugs were defined as observed clinical AUCR <1.25-fold, but were predicted to have an AUCR ≥1.25-fold, whereas false negative (FN) drugs were those where an observed clinical AUCR was ≥1.25-fold, but the predicted AUCR was <1.25-fold.

Additional assessments of probability to describe model success included sensitivity, specificity, positive predictive value (PPV), negative predictive value (NPV), positive predictive error (PPE), and negative predictive error (NPE). The sensitivity value describes the ability of the model to correctly identify observed positive DDIs (eq. 8), whereas the specificity value describes the ability of the model to correctly identify observed negative DDIs (eq. 9). The PPV is the portion of studies that were predicted to have an interaction in the clinic and a clinical interaction was observed (eq. 10). Conversely, the NPV represents the portion of studies that were predicted to not have an interaction in the clinic and a clinical interaction was not observed (eq. 11). The PPE describes the portion of studies that were predicted to have an interaction in the clinic, but a clinical interaction was not observed (eq. 12). Lastly, NPE describes the

TABLE 2

Total and free inhibition parameters determined in human liver microsomes

Drug Name	Reversible Inhibition			Time-Dependent Inhibition				
	K_i[a] μM	$f_{u,mic}$ at 0.01 mg/ml[d]	$K_{i,u}$ μM	K_I (S.E.) μM	$f_{u,mic}$ (%CV) at 0.3 mg/ml	$K_{I,u}$ μM	k_{inact} (S.E.) min^{-1}	$k_{inact}/K_{I,u}$ $ml \cdot min^{-1} \cdot \mu mol^{-1}$
Azithromycin	>50.0	0.982	>49.1	NR	0.650 (9)	NR	NR	0.025
Boceprevir	11.9	0.990	11.8	13.8 (1.7)	0.766 (12)	10.6	0.304 (0.010)	28.8
Carfilzomib	2.19	0.964	2.11	1.18 (0.22)	0.473[b]	0.558	0.107 (0.007)	192
Clarithromycin	43.9	0.982	43.1	55.9 (13.4)	0.647 (16)	36.2	0.0812 (0.0086)	2.25
Conivaptan	4.14	0.929	3.84	1.04 (0.16)	0.303 (4)	0.315	0.329 (0.013)	1040
Diltiazem	20.3	0.986	20.0	1.90 (0.28)	0.696 (9)	1.32	0.0109 (0.0004)	8.24
N-desmethyl Diltiazem[c]	ND	ND	ND	0.961 (0.115)	ND	0.961	0.00954 (0.00027)	9.94
Disulfiram[c]	1.18	ND	1.18	16.4 (5.2)	ND	16.4	0.129 (0.012)	7.87
Eplerenone	>50.0	0.991	>49.5	202 (58)	0.779 (10)	157	0.0223 (0.0029)	0.142
Erythromycin	32.0	0.979	31.3	23.3 (3.3)	0.613 (38)	14.3	0.0557 (0.0025)	3.90
Imatinib	28.9	0.974	28.2	16.4 (4.9)	0.560 (15)	9.18	0.0348 (0.0029)	3.79
Midostaurin	2.79	0.267	0.740	0.360 (0.120)	0.0118 (29)	0.00425	0.0207 (0.0015)	4870
Nelfinavir	1.46	0.561	0.816	1.44 (0.45)	0.0408 (21)	0.0588	0.510 (0.057)	8680
Nitrendipine	1.37	0.960	1.32	10.4 (3.1)	0.444 (22)	4.62	0.0266 (0.0020)	5.76
Panobinostat	4.99	0.971	4.84	30.3 (6.8)	0.530 (9)	16.1	0.0436 (0.0027)	2.71
Paroxetine	13.4	0.833	11.2	49.4 (22.0)	0.143 (17)	7.06	0.0277 (0.0084)	3.92
Propiverine	8.05	0.961	7.74	1.71 (0.23)	0.451 (25)	0.771	0.0298 (0.0012)	38.7
Propranolol	>50.0	0.978	>48.9	No TDI	0.594 (3)	No TDI	No TDI	No TDI
Simvastatin	0.146	0.651	0.095	NR	0.0585 (12)	NR	NR	0.195
Tabimorelin	8.30	0.973	8.08	1.98 (0.31)	0.547 (12)	1.08	0.0652 (0.0023)	60.2
Tadalafil	8.55	0.990	8.46	13.0 (1.7)	0.776 (4)	10.1	0.143 (0.004)	14.2
Telaprevir	11.6	0.992	11.5	0.644 (0.109)	0.806 (9)	0.519	0.108 (0.004)	208
Terfenadine	0.218	0.559	0.122	9.32 (5.85)	0.0405 (3)	0.377	0.0276 (0.0111)	73.2
Verapamil	12.9	0.979	12.6	2.80 (0.54)	0.610 (23)	1.71	0.0487 (0.0023)	28.5

%CV, percent coefficient of variation; ND, not determined (assume 1); NR, not reported (see data analysis section for the estimation of $k_{inact}/K_{I,u}$).
[a]Calculated as measured $IC_{50}/2$.
[b]Based on in silico modeling.
[c]Total values were reported since unbound fractions were not determined.
[d]$f_{u,mic}$ was calculated from $f_{u,mic}$ measured at 0.3 mg/ml (n = 3 to 4) using equation from (Austin et al., 2002).

TABLE 3

Total and free inhibition parameters determined in human hepatocytes

Drug Name	Reversible Inhibition			Time-Dependent Inhibition			
	K_i[a] μM	$K_{p,uu}$[b] %CV	$K_{i,u}$ μM	K_I (S.E.) μM	$K_{I,u}$ μM	k_{inact} (S.E.) min^{-1}	$k_{inact}/K_{I,u}$ $ml \cdot min^{-1} \cdot \mu mol^{-1}$
Azithromycin	>25.0	5.70 (5)	>143	51.2 (17.3)	292	0.0327 (0.0032)	0.112
Boceprevir	10.8	0.190 (0.5)	2.04	25.9 (10.7)	4.92	0.0978 (0.0161)	19.9
Carfilzomib	1.71	0.0160 (33)	0.0300	7.76 (2.26)	0.126	0.0289 (0.0020)	229
Clarithromycin	13.8	0.600 (7)	8.25	7.45 (2.06)	4.47	0.0112 (0.0007)	2.51
Conivaptan	1.27	1.70 (8)	2.16	0.634 (0.124)	1.08	0.0182 (0.0010)	16.9
Diltiazem	13.0	0.253 (10)	3.28	35.4 (6.6)	8.96	0.0217 (0.0010)	2.42
N-desmethyl Diltiazem[c]	ND	ND	ND	2.96 (1.12)	2.96	0.0127 (0.0011)	4.29
Disulfiram	ND	ND	ND	ND	ND	ND	ND
Eplerenone	>25.0	0.141 (13)	>3.53	NR	NR	NR	0.0166
Erythromycin	16.9	0.328 (9)	5.06	27.1 (19.7)	8.13	0.0141 (0.0044)	1.73
Imatinib	22.5	1.00 (16)	22.5	29.4 (8.1)	29.4	0.0202 (0.0014)	0.687
Midostaurin	>25.0	0.005 (43)	>0.120	0.574 (0.165)	0.00276	0.00566 (0.00041)	2050
Nelfinavir	0.496	1.70 (12)	0.842	NR	NR	NR	6.24
Nitrendipine	ND	ND	ND	ND	ND	ND	ND
Panobinostat	>25.0	0.600 (11)	>15.0	26.0 (7.2)	15.6	0.00446 (0.00038)	0.286
Paroxetine	14.3	0.600 (14)	8.55	NR	NR	NR	0.113
Propiverine	7.50	0.500 (15)	3.75	1.38 (0.62)	0.690	0.0196 (0.0040)	28.4
Propranolol	ND	ND	ND	ND	ND	ND	ND
Simvastatin	ND	ND	ND	ND	ND	ND	ND
Tabimorelin	2.85	0.200 (18)	0.569	7.57 (2.62)	1.51	0.0148 (0.0013)	9.78
Tadalafil	12.9	0.600 (5)	7.71	4.26 (1.44)	2.56	0.028 (0.002)	11.0
Telaprevir	0.273	0.450 (17)	0.123	2.24 (0.95)	1.01	0.0112 (0.0011)	11.1
Terfenadine	2.17	1.40	3.04	NR	NR	NR	0.426
Verapamil	13.4	0.310 (20)	4.14	0.661 (0.143)	0.205	0.0172 (0.0010)	83.9

%CV, percent coefficient of variation; ND, not determined since no TDI was detected in a single concentration screen at 30 μM; NR, not reported see data analysis section for the estimation of $k_{inact}/K_{I,u}$.
[a]Calculated as measured $IC_{50}/2$.
[b]Calculated from K_p (n=3) and $f_{u,liver}$ reported in supplemental tables.
[c]Total value was reported since $K_{p,uu}$ was not determined.

TABLE 4

Numerical accuracy of DDI predictions determined from human liver microsomes and human hepatocytes using mechanistic static models

	Model 1	Model 2	Model 3	Model 4
Relevant $[I]_g$	entrance	entrance	exit	exit
Relevant $[I]_h$	entrance	entrance	exit	exit
	Fixed Input Parameters			
F_a	1			
CYP3A $k_{deg,g}$	0.00050 min^{-1}			
CYP3A $k_{deg,h}$	0.00032 min^{-1}			
Q_g	300 ml/min	300 ml/min	1213 ml/min	1213 ml/min
Q_h	1617 ml/min	1617 ml/min	NA	NA
	Varied Input Parameters			
k_a	0.1 min^{-1}	custom	custom	custom
$[I]_g$	Total Enterocyte[a]	Free Enterocyte[b]	$C_{max,portal,u}$[c]	$C_{avg,portal,u}$[d]
$[I]_h$	$C_{max,hepatic\ inlet,u}$[e]	$C_{max,hepatic\ inlet,u}$[e]	$C_{max,systemic,u}$	$C_{avg,systemic,u}$
$f_{u,gut}$	1	$f_{u,plasma}$	$f_{u,plasma}$	$f_{u,plasma}$
Performance	Human Liver Microsomes			
Bias ($CI_{90\%}$)	6.3 (4.8–8.1)	5.0 (3.8–6.5)	2.7 (2.2–3.4)	1.8 (1.5–2.3)
GMFE ($CI_{90\%}$)	6.3 (4.8–8.1)	5.1 (3.9–6.6)	2.8 (2.3–3.5)	2.0 (1.6–2.4)
RMSFE	7.38	6.09	3.37	2.42
% Within 2-fold	12	12	36	56
% Within 3-fold	16	28	48	80
% Outside 10-fold	24	16	4	0
Performance	Human Hepatocytes			
Bias ($CI_{90\%}$)	3.8 (2.9–4.9)	2.7 (2.0–3.4)	1.6 (1.2–2.1)	1.1 (0.88–1.4)
GMFE ($CI_{90\%}$)	3.8 (3.0–4.9)	2.7 (2.1–3.5)	2.0 (1.6–2.5)	1.7 (1.4–2.0)
RMSFE	4.70	3.49	2.52	2.04
% Within 2-fold	24	44	56	68
% Within 3-fold	36	60	76	84
% Outside 10-fold	12	4	0	0

CI_{90}%, 90% confidence interval; $C_{max,systemic,u}$, unbound maximum systemic concentration; $f_{u,gut}$, intestinal free fraction; $k_{deg,g}$, intestinal degradation rate; $k_{deg,h}$, hepatic degradation rate; NA, not applicable; Q_g, intestinal blood flow; Q_h, liver blood flow.

[a]As calculated per eq. 7a.

[b]As calculated per eq. 7a corrected for free fraction in plasma.

[c]As calculated per eq. 7b.

[d]As calculated per eq. 7c.

[e]As calculated per eq. 6.

portion of studies that were predicted to not have an interaction in the clinic, but a clinical interaction was observed (eq. 13).

$$Sensitivity = \frac{TP}{TP+FN} \times 100\% \quad (8)$$

$$Specificity = \frac{TN}{TN+FP} \times 100\% \quad (9)$$

$$PPV = \frac{TP}{TP+FP} \times 100\% \quad (10)$$

$$NPV = \frac{TN}{TN+FN} \times 100\% \quad (11)$$

$$PPE = (1 - PPV) \times 100\% \quad (12)$$

$$NPE = (1 - NPV) \times 100\% \quad (13)$$

Accuracy of Predictions. Accuracy of the various prediction models was assessed by the average fold error or bias (eq. 14). Precision of the predictions were evaluated using geometric mean absolute fold error (GMFE, eq. 15) and root mean square fold error (RMSFE, eq. 16).

$$AFE = 10^{\frac{\sum log\frac{predicted\ \ DDI}{actual\ \ DDI}}{N}} \quad (14)$$

$$GMFE = 10^{\frac{\sum \left|log\frac{predicted\ \ DDI}{actual\ \ DDI}\right|}{N}} \quad (15)$$

$$RMSFE = \sqrt{\frac{\left(log\frac{predicted\ \ DDI}{actual\ \ DDI}\right)^2}{N}} \quad (16)$$

where N is the total number of predictions.

Results

CYP3A TDI in Human Liver Microsomes and Hepatocytes. Among the 24 compounds evaluated (23 drugs and one metabolite), 23 and 20 demonstrated measurable inactivation kinetic parameters in HLM and HHEP, respectively. Values for K_I ranged from 0.360 to 202 μM in HLM and 0.574 to 51.2 μM in HHEP. These were corrected for unbound fraction prior to utilizing them in projection of DDI (see below). Since hepatocytes are intact cells that possess a membrane barrier, availability of the inhibitor to the P450 enzyme to cause inactivation may be limited, and this barrier is not present in HLM. By estimating the intracellular free drug concentration, inhibitor availability to the active site can be determined using $K_{p,uu}$. Therefore, application of $K_{p,uu}$ to HHEP K_I was deemed to be a reasonable estimate of HHEP $K_{I,u}$. For K_{inact}, values ranged from 0.00954 to 0.329 $minute^{-1}$ in HLM and 0.00446 to 0.0978 $minute^{-1}$ in HHEP. Values are listed in Tables 2 and 3, and the percent of control activity versus incubation time and k_{obs} versus [I] plots for each drug are shown in the Supplemental Figures. On average, (i.e., average fold error) the $K_{I,u}$, k_{inact}, and $k_{inact}/K_{I,u}$ values in HLM were 1.2-, 3.5-, and 3.2-fold greater than in HHEP (Fig. 1).

Projection of DDI from CYP3A TDI Data in Liver Microsomes and Hepatocytes: Static Method. The equations described above were used to make projections of DDI, based on AUCR. Although the in vitro kinetic parameters are measured experimentally, several input values needed for these projections cannot be measured experimentally and must be estimated (e.g., F_a, k_a, etc.). Furthermore,

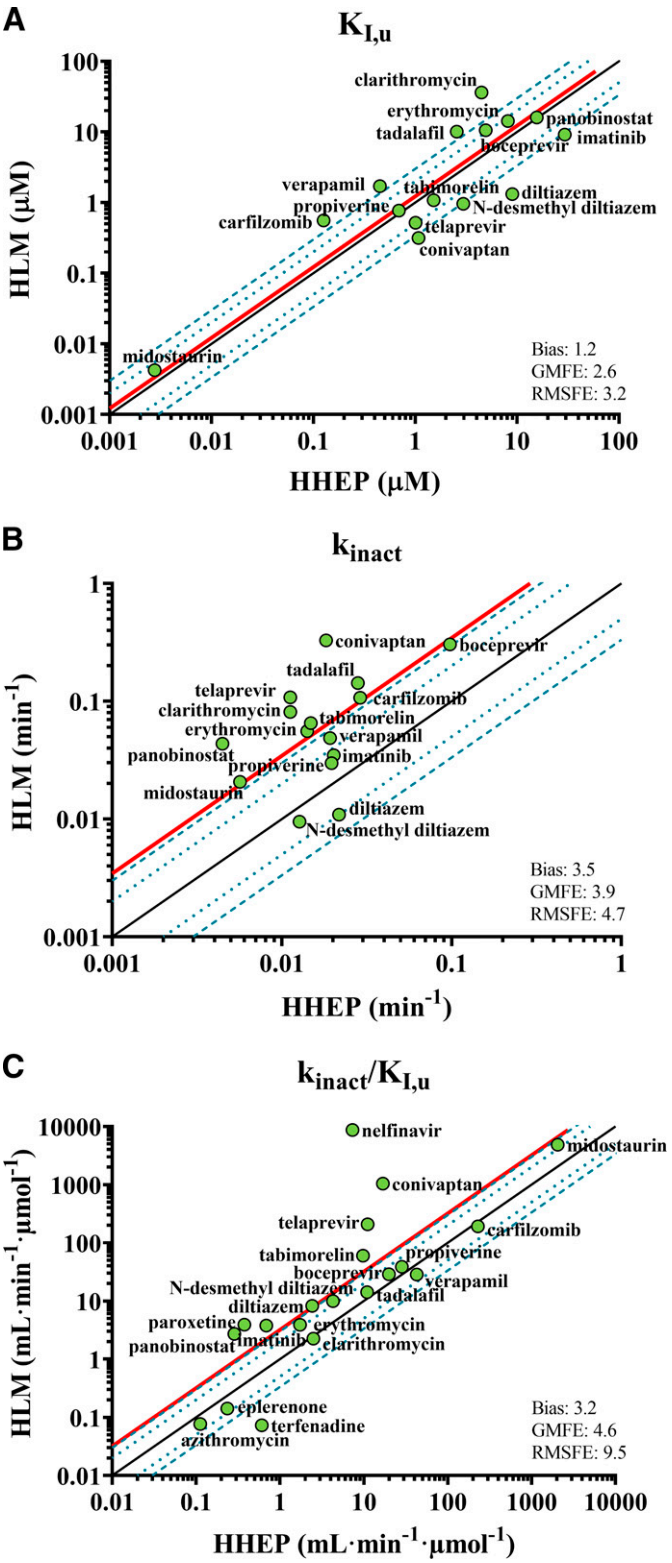

Fig. 1. Comparison of TDI parameters obtained in HLM versus HHEP). (A) $K_{I,u}$; (B) k_{inact}; and (C) $k_{inact}/K_{I,u}$. Solid black lines represent unity, dotted and dashed lines represent 2-fold and 3-fold deviation from unity, and solid red line represents bias. Azithromycin, nelfinavir, terfenadine, paroxetine, and eplerenone are not shown in (A) and (B) because individual K_I and k_{inact} were not able to be determined.

the correct in vivo concentrations of the inactivator in the liver and intestine are needed, and whether the best values to use are represented by maximum or average organ inlet or egress values is unknown. Based on the input parameters mentioned above, over 50 combinations of these values could be evaluated. These methods were narrowed down to three (referred to as Methods 2–4), selected because they represented internally consistent and physiologically meaningful combinations. That is, we did not further pursue random combinations that would make no sense or be illogically contradictory. These were also compared with the input parameters currently recommended in the United States Food and Drug Administration regulatory document on drug-drug interactions [referred to as Method 1; (FDA, 2020)].

When comparing the approaches, the input parameters of CYP3A degradation rates and organ flow rates were kept constant, as these are reasonably well established, and it was not an objective to test the validity of these values. Also, for many of the drugs used in the evaluation, their overall oral absorption is not known, and thus, a value of unity was used. This could be an overestimate for some of the drugs. The greatest source of variation in prediction methods lies in the selection of the most relevant in vivo concentrations of the perpetrator drug, in both liver and intestine. In these approaches, unbound concentrations were used, and the concentrations entering the organ (liver and intestine) were compared with concentrations exiting the organ. The concentrations entering the liver were considered as the hepatic inlet estimates ($C_{max,hepatic\ inlet,u}$), whereas the concentrations entering the intestine were estimated using the absorption rate constant and oral doses (eq. 7a). The concentrations exiting the liver and intestine were considered as the systemic concentrations ($C_{max,systemic,u}$ or $C_{avg,systemic,u}$) and estimated portal vein concentrations ($C_{max,portal,u}$, eq. 7b or $C_{avg,portal,u}$, eq. 7c), respectively. Calculated concentrations for $[I]_g$ and $[I]_h$ are listed in Supplemental Table 34.

A summary of performance characteristics of DDI prediction from TDI data are presented in Table 4. When using TDI data gathered in HLM in making estimates of DDI, the best input values for concentrations for the liver were the average organ exit values (i.e., $C_{avg,u}$), and the best input values for concentrations for the intestine were also the exit values described by the estimates of portal vein concentrations (Models 3 and 4). Model performance was somewhat better when employing estimated $C_{avg,u}$ values than unbound maximum concentration values. Model 4 had a GMFE of 2.0, indicating that, on average, projections of DDI from in vitro data were within about 2-fold of the actual values, in this case the 2-fold error favored an overprediction of DDI (Fig. 2A). Using organ entrance values for perpetrator concentrations (Models 1 and 2) yielded poorer performance and marked over-projections of DDI. The consideration of using the estimated free concentration in the intestine (Models 2–4) is an important one. Model 1, as recommended in regulatory guidance, uses a very rapid rate of absorption (proximate to the rate of gastric emptying) and essentially states that the concentration of the perpetrator drug in the enterocyte is equal to the concentration of the total dose dissolved in the luminal fluids. This yields poor performance and consistent over-projection of DDI from TDI data. Consideration of the free concentration in the enterocytes, along with more realistic absorption rates (Models 2–4), yields a considerable improvement in DDI projection over Model 1. Individual estimates are listed in Supplemental Table 35.

A similar trend among the use of various input values for in vivo perpetrator drug concentrations was observed when using TDI data from HHEP (Table 4). Again, Models 3 and 4, which use unbound exit concentrations for liver and intestine, yielded the most reliable projections of DDI (Fig. 2B, Model 4). Furthermore, use of HHEP TDI data offered nominal performance improvements in projections relative to HLM TDI data, with Model 4 yielding a GMFE of 1.7, as compared with 2.0 for HLM data. Overall, projections of DDI

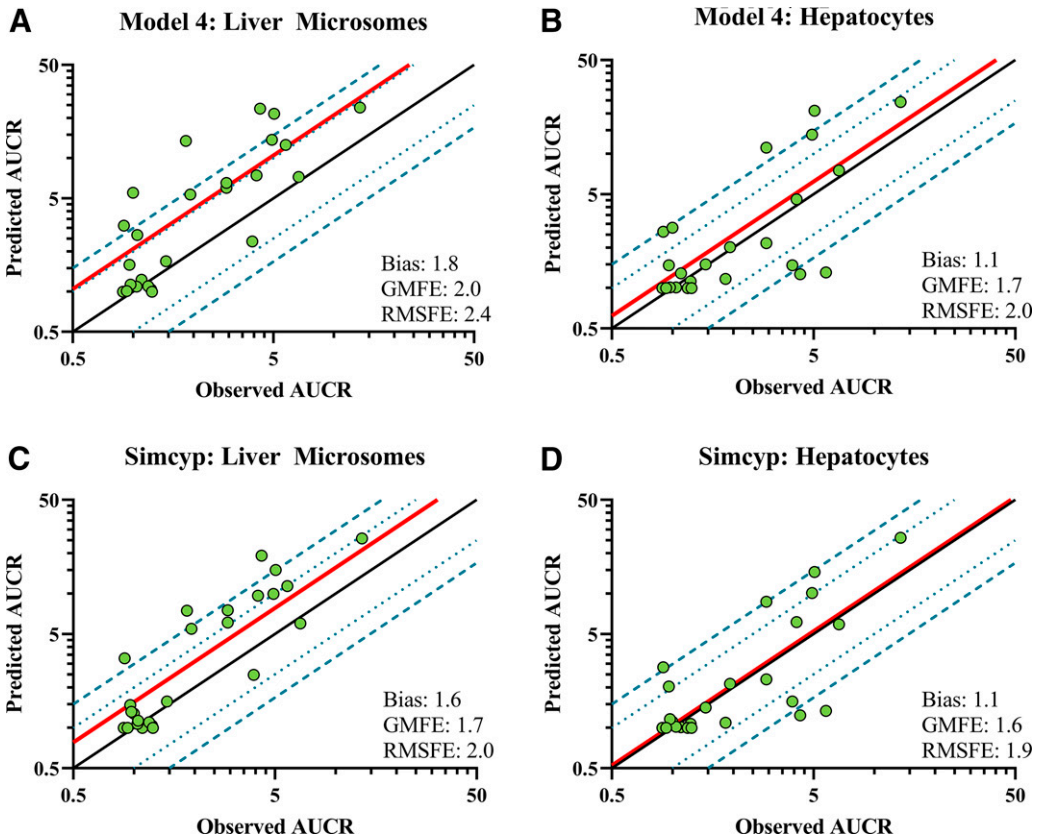

Fig. 2. Predicted versus observed AUC ratios from mechanistic static Model 4 (A and B) and Simcyp modeling (C and D). (A and C) are results using human liver microsome–generated inactivation parameters, and (B and D) are results human hepatocyte–generated inactivation parameters. Solid black lines represent unity, dotted lines represent 2-fold and 3-fold deviation from unity, and red solid lines represent the bias.

were still higher than those observed in vivo, especially if organ entrance values for perpetrator concentrations were employed (Models 1 and 2). Individual estimates are listed in Supplemental Table 36.

Evaluation of AUCR projections relative to the extent of observed clinical AUCR revealed no clear relationship with overpredictions above and below the 2-fold criteria (Fig. 3). Of particular interest is significant overpredictions with observed AUCR below 2-fold for several drugs (e.g., tadalafil, midostaurin) irrespective of whether the in vitro data generated in HLM or HHEP. Further mechanistic evaluation may be required to clarify contributing factors. Drugs with underprediction of DDI using data generated in HHEP were diltiazem (Simcyp only), nelfinavir, and conivaptan (static and dynamic modeling).

In addition to evaluating these approaches for numerical accuracy of projection of DDI, it is also useful to evaluate them using categorical criteria and cutoff values for what is defined as a DDI and what is not (i.e., a confusion matrix analysis). This analysis was conducted using two criteria for DDI: 1.25-fold, as defined by bioequivalence boundaries, and 2-fold. The latter is offered as a reasonable value for DDI that may actually be meaningful for clinical outcome. This will always be dependent on the therapeutic window for the affected drug, as some drugs are very safe, and marked increases in exposure can still be well tolerated, but others could be dosed at levels such that smaller increases in exposure can yield meaningful side effects. Nevertheless, very few drugs go from safe to toxic with a mere 2-fold increase in exposure, and thus, a 2-fold DDI cutoff criteria was deemed a useful one by which to evaluate these DDI projection methods.

TDI experiments performed in HLM offer very high sensitivity, however, specificity can be low, depending on the model employed. When using the data in this binary fashion, the ten drugs (Fig. 4) that cause a greater than 2-fold DDI are readily identified irrespective of the model used yielding 100% sensitivity (Table 5). However, this comes at a cost of a high rate of false positives especially when using Models 1 and 2 (organ entrance concentrations as input for in vivo [I]), as 13 of 15 drugs that cause DDI below 2-fold are actually identified as causing greater than 2-fold DDI. The PPE, i.e., the portion of DDI studies that are identified as needing to be conducted but actually are negative and would not need to be conducted, is high at 57%. This attribute improves to 33%–50% if Models 3 or 4 are employed in that a greater number of the negative drugs are properly identified as such and this does not come at the expense of any false negative drugs: all positive drugs are identified. Overall, the performance of the models using HLM data are similar when using either 1.25- or 2-fold as the defining cutoff for DDI. When using TDI data generated in HHEP, the PPE improves to a minor extent, decreasing to as low as 25%. However, this comes at a cost of 1–3 instances of false negative outcomes. Overall, the combination that yields the lowest PPE while not giving any false negative is the use of TDI data from HLM entered into Model 4, which uses the average organ exit concentrations for in vivo [I]. This observation is independent of the DDI cutoff applied (i.e., 1.25- or 2-fold).

Projection of DDI from CYP3A TDI Data in Liver Microsomes and Hepatocytes: Dynamic PBPK Method. These in vitro data were also used as input values for projecting DDI using Simcyp (individual estimates are listed in Supplement Table 37). In this case, various input parameters such as in vivo [I] values, absorption extent and rate values, and enzyme degradation rates are embedded in the

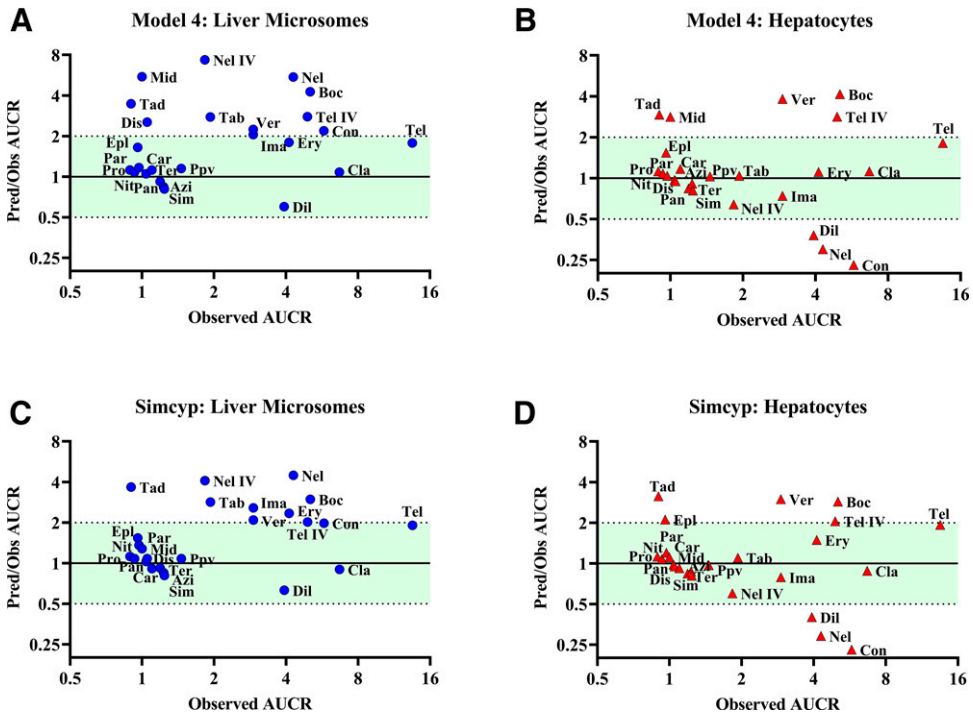

Fig. 3. Model performance versus observed AUCR from mechanistic static Model 4 (A and B) and Simcyp modeling (C and D). (A and C) are results using human liver microsome–generated inactivation parameters, and (B and D) are results using human hepatocyte–generated inactivation parameters. Shaded area represents 0.5- to 2-fold criteria. Azi, azithromycin; Boc, boceprevir; Car, carfilzomib; Cla, clarithromycin; Con, conivaptan; Dil, diltiazem; Dis, disulfiram; Epl, eplerenone; Ery, erythromycin; Ima, imatinib; Mid, midostaurin; Nel IV, nelfinavir (IV midazolam); Nit, nitrendipine; Pan, panobinostat; Par, paroxetine; Ppv, propiverine; Pro, propranolol; Sim, simvastatin; Tab, tabimorelin; Tad, tadalafil; Tel, telaprevir; Tel IV, telaprevir (IV midazolam); Ter, terfenadine; Ver, verapamil.

algorithms. The output DDI projections were evaluated as above for both numerical accuracy of DDI projections (Table 6) as well as categorical assignment of the potential for DDI using 1.25- and 2-fold boundaries (Table 7). Use of Simcyp yielded overall accuracy for projections of DDI from in vitro data with GMFE of 1.7 and 1.6 if data were from HLM or HHEP, respectively (Fig. 2, C and D). These performance characteristics are slightly better than the best of the static models (Model 4). When evaluated in a confusion matrix, Simcyp modeling performed very well with TDI data from HLM, with no instances of false negatives (i.e., 100% sensitivity) and with high specificity (PPE of only 24% and 23% when using 1.25-fold and 2-fold cutoff values for defining a DDI (Table 7). However, with TDI data obtained from HHEP, the performance of Simcyp suffered slightly with occurrences of false negatives that decreased sensitivity to about 70%–85% depending on cutoff criteria (Fig. 5).

Discussion

The projection of clinical DDI from in vitro TDI data is challenging. Considerable progress has been made, yet it is still commonplace to project DDI from in vitro data and then conduct a clinical study based on that projection, only to observe no DDI. In drug development, such an occurrence (i.e., a false positive from the in vitro data), while demonstrating that it will be acceptable to coadminister the two agents based on the clinical observation, expends effort on a clinical DDI study that really did not need to be conducted. Efforts and resources would be better expended on other clinical studies. Our exploration of different model input values, especially the application of projected organ egress concentrations instead of entry concentrations, improves the overall fidelity of predictions of DDI while still avoiding the occurrence of false negative outputs. Use of PBPK modeling (Simcyp) yielded excellent performance with data from HLM, with no false negative outputs. It is false negative outputs (i.e., projection of no DDI from in vitro data but actual DDI in the clinic) which must be avoided as this would result in a deleterious impact on patient safety.

It should be noted that in vitro TDI assays, using HLM or HHEP, are highly sensitive. If one considers the lower limit of statistically detectable k_{obs} values in vitro [0.002 minute^{-1} and 0.0015 minute^{-1} for HLM and HHEP, respectively; (Eng et al., 2021)] as compared with the estimate for the natural turnover rate for CYP3A in vivo (0.00032 minute^{-1}), then any drug demonstrating measurable TDI would be expected to cause at least a 12-fold decline in CYP3A activity at the inhibitor concentration that yielded the lower limit value of k_{obs}. That is, the rate of inactivation would exceed the natural rate of enzyme resynthesis by 12-fold. It should also be noted that varying values of $k_{deg,h}$ for CYP3A4 have been reported in the literature (Yang et al., 2008), and that the accuracy of projections of DDI from in vitro data will be dependent on the $k_{deg,h}$ value used. A value of 0.00032 minute^{-1} was selected for our static models to be consistent with the value embedded in the Simcyp algorithm.

The present efforts focused on three main objectives: 1) a comparison of in vitro TDI data generated in HLM and HHEP; 2) evaluation of different input values for estimates of in vivo concentrations of the inhibitor in static models for DDI prediction and identification of the best values; and 3) evaluation of the dynamic PBPK model Simcyp for prediction of DDI from TDI data. The in vitro dataset generated for these objectives represents the largest one reported using a fixed source of in vitro reagents and consistent methods run in one laboratory, paired with clinical DDI data gathered from the literature. Previously reported efforts had many fewer examples included (Mayhew et al., 2000; Obach et al., 2007; Mao et al., 2011; Kenny et al., 2012). CYP3A was the enzyme of focus, since the greatest number of TDI and DDI is known for this enzyme. Other P450 enzymes such as CYP2D6 or

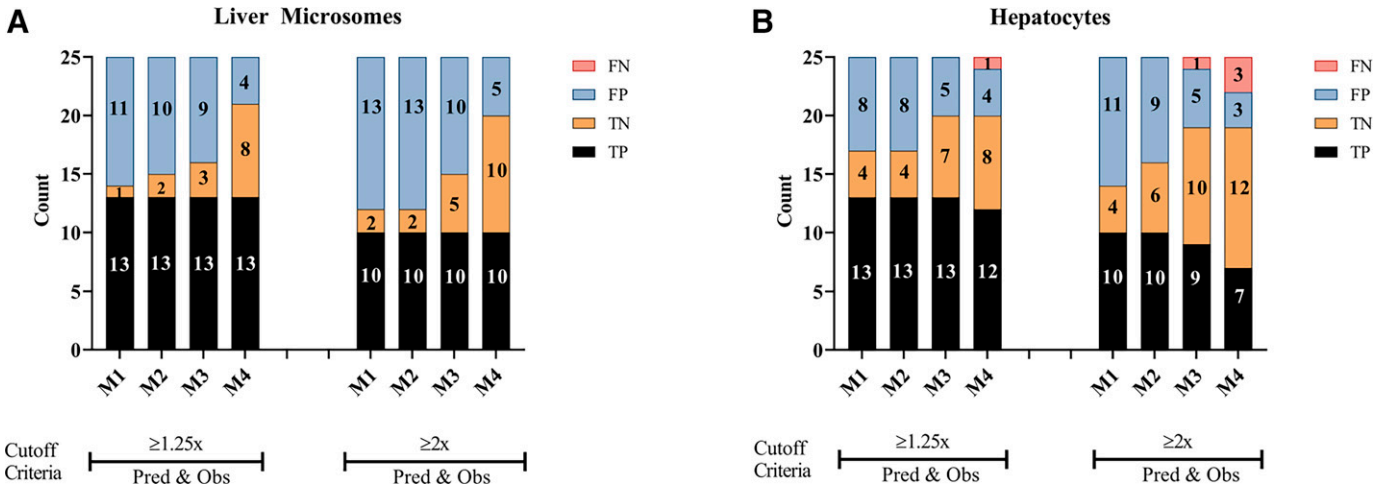

Fig. 4. Classification of predicted (Pred) AUCR versus observed (Obs) AUCR using 1.25- and 2-fold cutoff criteria in mechanistic static models 1–4. Values in each section of the bar graphs represent the number of drugs that were predicted to be TP, TN, FP, or FN using liver microsome (A) or hepatocyte- (B) generated parameters.

CYP1A2 have few examples of drugs that are TDI with corresponding clinical data for comparison and as such do not offer a large enough set of drugs from which conclusions could be drawn. It is proposed that the conclusions generated for CYP3A could be applicable to other enzymes. Also, compared with other P450s, the magnitude of CYP3A-based DDIs can be high for orally administered drugs because of the potential for inhibition of this enzyme not only in the liver but also in the small intestine during the absorption of the drugs after oral administration.

The data demonstrated that DDI are predictable from in vitro TDI data gathered in either in vitro system. Inactivation kinetic values in HLM were generally greater than in HHEP. In both cases, it was important to correct K_i and K_I values generated from nominal concentrations of the inhibitor added to the incubations by binding and partition factors. Inhibitor concentrations available to inactivate CYP3A may actually be lower than those added to the assay due to nonspecific binding (HLM and HHEP) and unequal concentrations of unbound drug inside and outside the cell (i.e., $K_{p,uu}$ in hepatocyte incubations). Most important is the selection of the most appropriate value for in vivo concentration of the inhibitor drug. Previous recommendations have advocated that the total concentration of drug in the lumen should be used for projection of DDI occurring in the intestine and unbound maximum concentrations estimated for the portal vein during absorption be used for projection of DDI occurring in the liver (Ito et al., 1998; Rostami-Hodjegan and Tucker, 2004; FDA, 2020). These are represented in Model 1, and lead to such marked over-projection of DDI (mean GMFE of 4–6, and high false positive rates) that the value of conducting in vitro TDI assays is essentially negated. The assay would be futile, as just about every drug tested will suggest the likelihood of DDI and the need for a clinical DDI study. However, moving to potentially more realistic values for in vivo [I] in intestine (enterocytes) and in liver greatly improves the accuracy of DDI projection. In Models 3 and 4, estimated unbound organ exit concentrations are used (i.e., free portal concentrations for intestine and free systemic concentrations for liver), and these may better reflect the concentrations of inhibitor available to affect the enzyme in these tissues. Use of $C_{avg,u}$ values were shown to be best. Mean GMFE values of 2.0 and 1.7 were calculated when using HLM and HHEP data, respectively (Table 4). Simcyp modeling, in which the relevant in vivo concentration values are embedded in the software, yielded mean GMFE values of 1.7 and 1.6 for HLM and HHEP, respectively (Table 6). Furthermore, a high degree of correlation ($r^2 > 0.9$) was observed when predicted AUCRs from HLM and

TABLE 5

Categorical accuracy of DDI predictions using mechanistic static models

DDI Cutoff	Matrix	Model	*N*	Sensitivity	Specificity	PPV	NPV	PPE	NPE
				%	%	%	%	%	%
Clinical ≥ 1.25-fold and prediction ≥ 1.25-fold	Human liver microsomes	1	25	100	8	54	100	46	0
		2	25	100	17	57	100	43	0
		3	25	100	25	59	100	41	0
		4	25	100	67	76	100	24	0
	Human hepatocytes	1	25	100	33	62	100	38	0
		2	25	100	33	62	100	38	0
		3	25	100	58	72	100	28	0
		4	25	92	67	75	89	25	11
Clinical ≥ 2-fold and prediction ≥ 2-fold	Human liver microsomes	1	25	100	13	43	100	57	0
		2	25	100	13	43	100	57	0
		3	25	100	33	50	100	50	0
		4	25	100	67	67	100	33	0
	Human hepatocytes	1	25	100	27	48	100	52	0
		2	25	100	40	53	100	47	0
		3	25	90	67	64	91	36	9
		4	25	70	80	70	80	30	20

TABLE 6
Numerical accuracy of DDI predictions using Simcyp

Performance	Human Liver Microsomes	Human Hepatocytes
Bias (CI_{90}%)	1.6 (1.3–1.9)	1.1 (0.85–1.3)
GMFE (CI_{90}%)	1.7 (1.5–2.0)	1.6 (1.4–1.8)
RMSFE	2.02	1.88
% Within 2-fold	64	68
% Within 3-fold	88	88
% Outside 10-fold	0	0

HHEP using Model 4 and Simcyp were compared (Fig. 6). These performance characteristics for both static and Simcyp modeling demonstrate that DDI can be projected from in vitro TDI data provided that appropriate input values are entered. Additionally, the use of HHEP generated TDI values with Simcyp modeling would provide an estimated AUCR with the highest degree of numerical accuracy compared with clinical observations.

A second manner in which in vitro TDI data may be used is in a binary decision making fashion. Thus, instead of seeking numerical accuracy in projecting DDI, the data are used to determine whether a clinical DDI study is needed or not. This depends on the cutoff used to define a DDI, and in this analysis, the data were evaluated using two cutoff criteria: 2-fold representing a minimum of what may cause a clinically meaningful DDI for many drugs and 1.25-fold representing a conservative bioequivalence boundary. Utilizing the data in this manner strives for minimizing false positives (i.e., running a clinical DDI study which shows no DDI) while not allowing for any false negatives (i.e., not running a clinical DDI study when one was actually needed). As with the aforementioned numerical accuracy findings, evaluating the data in this manner yielded similar conclusions with regard to the most appropriate input values used for in vivo [I]. If using organ entry concentrations, over-projection of the frequency of actual DDI was high, rendering the use of in vitro TDI essentially uninformative for such decision making (Table 5). This observation was similar irrespective of the cutoff values used (1.25- or 2-fold). However, when organ exit concentrations were employed, the sensitivity remained high, and the selectivity increased (fewer false positives). Method 4 with HLM data also yielded a mean GMFE of 2-fold. Thus, the overall conclusion for static models is that the use of TDI data from HLM along with $C_{avg,u}$ values for [I] (Model 4) is the recommendation for an optimal strategy when employing in vitro data for clinical study planning for CYP3A based DDI caused by TDI.

Similar observations were made from the data entered into Simcyp modeling (Tables 6 and 7). Simcyp modeling offers a more sophisticated approach than simple equations that assume a single static in vivo concentration of inhibitor and substrate when estimating DDI. In Simcyp, concentrations are correctly assumed to be changing over time, and this is accounted for when projecting the extent of CYP3A inactivation. Model performance characteristics for Simcyp were even better than Model 4. When performance was evaluated using the categorical criteria, Simcyp yielded no false negative outcomes for HLM TDI data, however, when employing TDI data from HHEP, there were instances of false negative outcomes (Table 7). Thus, the overall conclusion for Simcyp modeling for CYP3A DDI caused by TDI is that the best in vitro input data are from HLM.

Reasons behind why there are differences between TDI parameters generated in HHEP versus HLM, particularly k_{inact}, have not been determined. Corrections for $f_{u,mic}$ and $K_{p,uu}$ were made before making comparisons, removing these as possible factors. Various reasons can be speculated, such as the presence of conjugating enzyme activities present in HHEP but absent in HLM that could remove inactivating metabolites, or the existence of some unknown enzyme protection mechanism in HHEP that is absent in HLM. The catalytic cycle of P450 activity is complex and possesses steps wherein the process can be uncoupled, resulting in generation of reactive oxygen species without catalyzing metabolism of the substrate, and alteration of this cycle in one system versus the other could yield differences in enzyme inactivation. Furthermore, it has been proposed that there are multiple phases of inactivation in TDI experiments and that a more sophisticated method of deriving in vitro values from these experiments is needed as compared with the manner in which the present data were processed (Yadav et al., 2018, 2020). Preliminary data has been generated that shows that not only are k_{inact} values different in the two systems, but that partition coefficients also differ (data on file). The partition coefficient is a measure of the ratio of the molecules of substrate consumed per molecule of enzyme inactivated and is an inherent biochemical property of an enzyme-inactivator pair. Thus, there appears to be a difference in the manner in which CYP3A behaves in the intact hepatocyte system versus microsome incubations. Further efforts to understand these differences at a fundamental biochemical level are underway and will be reported in due course. The drugs assessed here have not been demonstrated to be clinical inducers. However, this does not preclude them from possessing in vitro induction potential. Although the current analysis excludes in vitro induction parameters, work is ongoing to determine how in vitro induction may play a role in aligning compounds for which over predictions were observed.

Lastly, from the simplest basic and static models to more sophisticated and complex PBPK models, there is always a level of uncertainty that arises from the assumptions required for various in vivo input parameters (e.g., k_{deg}, f_m, F_g, $[I]_{in\ vivo}$, $K_{p,uu\ in\ vivo}$) and conceptual simplifications needed for modeling. Regarding the latter, it is necessary to simplify that the target organs, liver and intestine, are homogeneous compartments as opposed to the complex multicompartment tissues that they truly are. Furthermore, subcellular distribution of the inactivators and substrates is likely heterogeneous, which cannot be currently measured. Absorption is a more complex kinetic process than what has been addressed in the present treatment, and further work is planned to evaluate the impact of more complex and multiphasic absorption

TABLE 7
Categorical accuracy of DDI predictions using Simcyp

DDI Cutoff	Matrix	N	Sensitivity %	Specificity %	PPV %	NPV %	PPE %	NPE %
Clinical ≥ 1.25-fold and prediction ≥ 1.25-fold	Human liver microsomes	25	100	67	76	100	24	0
	Human hepatocytes	25	85	83	85	83	15	17
Clinical ≥ 2-fold and prediction ≥ 2-fold	Human liver microsomes	25	100	80	77	100	23	0
	Human hepatocytes	25	70	80	70	80	30	20

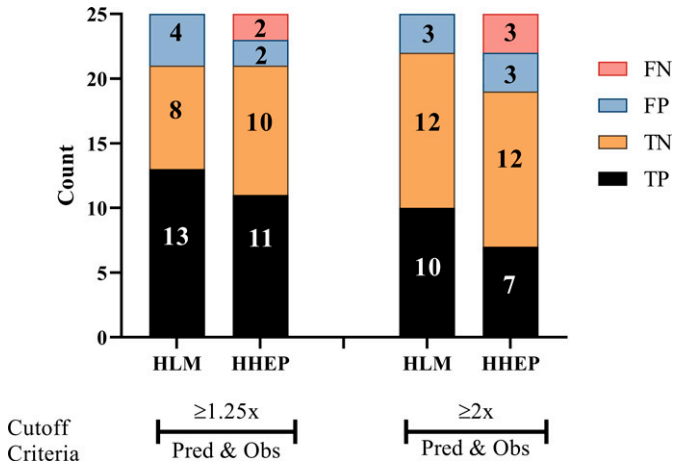

Fig. 5. Classification of predicted (Pred) AUCR versus observed (Obs) AUCR using 1.25- and 2-fold cutoff criteria using Simcyp. Values in each section of the bar graphs represent the number of drugs that were predicted to be TP, TN, FP, or FN using HLM or HHEP generated parameters.

models driving in vivo input concentrations (e.g., the Advanced Dissolution, Absorption, Metabolism (ADAM) model in Simcyp). Finally, it must be appreciated that there is uncertainty and variability in important input parameters like k_{deg} for CYP3A4 and F_g for midazolam and other substrates, among others, as well as the potential impact of the role for CYP3A5 in the metabolism of the substrates in vivo. As the science and knowledge around these factors continue to develop, re-evaluation and refinement of DDI prediction methods will be necessary. With the present state of knowledge, the approaches described here offer the best performance for predicting DDI for CYP3A time-dependent inactivators that can be currently achieved.

In conclusion, it has been demonstrated that TDI data for CYP3A generated in either HLM or HHEP can be used effectively to predict the magnitude of DDI and to make decisions regarding the need for clinical DDI studies. Data from HLM appears to perform better overall regarding not missing any DDI, whether using static or dynamic modeling, however, use of these data tended to yield more over-projection of DDI as compared with TDI data generated using HHEP. Key to the success in this endeavor is the selection of the most appropriate value for the in vivo concentration of the inactivator at the most important sites of action, the liver and intestine. Projected organ exit concentrations were best, and the use of maximum or average values can work depending on the reagent used to generate the in vitro TDI data. PBPK modeling using the Simcyp module, wherein concentrations of the substrate and inhibitor are changing over time, performed well in predicting DDI.

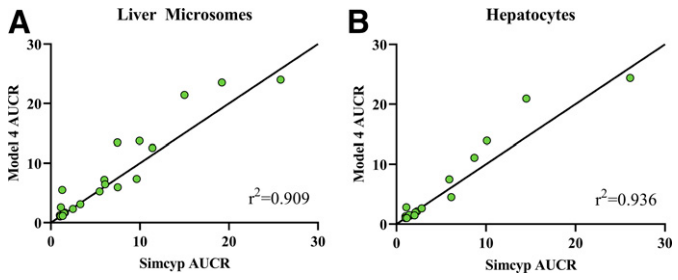

Fig. 6. Correlation of predicted AUC ratios (AUCR) from mechanistic static Model 4 and Simcyp modeling. (A) represents predictions using human liver microsome–generated inactivation parameters and (B) represents predictions using human hepatocyte–generated inactivation parameters. The solid black line represents unity.

Acknowledgments

We would like to thank Samantha Jordan and the scientists at York Bioanalytical Solutions for their contributions toward the generation of the binding data.

Authorship Contributions

Participated in research design: Tseng, Eng, Lin, Cerny, Goosen, Obach.

Conducted experiments: Tseng, Eng.

Performed data analysis: Tseng, Eng, Lin, Cerny, Tess, Goosen, Obach.

Wrote or contributed to the writing of the manuscript: Tseng, Eng, Lin, Cerny, Goosen, Obach.

References

Austin RP, Barton P, Cockroft SL, Wenlock MC, and Riley RJ (2002) The influence of nonspecific microsomal binding on apparent intrinsic clearance, and its prediction from physicochemical properties. *Drug Metab Dispos* **30**:1497–1503.

Backman JT, Olkkola KT, Aranko K, Himberg JJ, and Neuvonen PJ (1994) Dose of midazolam should be reduced during diltiazem and verapamil treatments. *Br J Clin Pharmacol* **37**:221–225.

Brown HS, Ito K, Galetin A, and Houston JB (2005) Prediction of in vivo drug-drug interactions from in vitro data: impact of incorporating parallel pathways of drug elimination and inhibitor absorption rate constant. *Br J Clin Pharmacol* **60**:508–518.

Chen Y, Liu L, Monshouwer M, and Fretland AJ (2011) Determination of time-dependent inactivation of CYP3A4 in cryopreserved human hepatocytes and assessment of human drug-drug interactions. *Drug Metab Dispos* **39**:2085–2092.

Cheng Y and Prusoff WH (1973) Relationship between the inhibition constant (K1) and the concentration of inhibitor which causes 50 per cent inhibition (I50) of an enzymatic reaction. *Biochem Pharmacol* **22**:3099–3108.

Cook CS, Berry LM, and Burton E (2004) Prediction of in vivo drug interactions with eplerenone in man from in vitro metabolic inhibition data. *Xenobiotica* **34**:215–228.

Di L, Breen C, Chambers R, Eckley ST, Fricke R, Ghosh A, Harradine P, Kalvass JC, Ho S, Lee CA, et al. (2017) Industry perspective on contemporary protein-binding methodologies: considerations for regulatory drug-drug interaction and related guidelines on highly bound drugs. *J Pharm Sci* **106**:3442–3452.

Dutreix C, Munarini F, Lorenzo S, Roesel J, and Wang Y (2013) Investigation into CYP3A4-mediated drug-drug interactions on midostaurin in healthy volunteers. *Cancer Chemother Pharmacol* **72**:1223–1234.

Einolf HJ, Lin W, Won CS, Wang L, Gu H, Chun DY, He H, and Mangold JB (2017) Physiologically based pharmacokinetic model predictions of panobinostat (LBH589) as a victim and perpetrator of drug-drug interactions. *Drug Metab Dispos* **45**:1304–1316.

Eng H, Tseng E, Cerny MA, Goosen TC, and Obach RS (2021) Cytochrome P450 3A time-dependent inhibition assays are too sensitive for identification of drugs causing clinically significant drug-drug interactions: a comparison of human liver microsomes and hepatocytes and definition of boundaries for inactivation rate constants. *Drug Metab Dispos* **49**:442–450.

Ernest 2nd CS, Hall SD, and Jones DR (2005) Mechanism-based inactivation of CYP3A by HIV protease inhibitors. *J Pharmacol Exp Ther* **312**:583–591.

Fahmi OA, Maurer TS, Kish M, Cardenas E, Boldt S, and Nettleton D (2008) A combined model for predicting CYP3A4 clinical net drug-drug interaction based on CYP3A4 inhibition, inactivation, and induction determined in vitro. *Drug Metab Dispos* **36**:1698–1708.

FDA (2005) *Drug approval package: Vaprisol (conivaptan). FDA application NDA 021697*, FDA Silver Springs, MD.

FDA (2011) *Drug approval package: Victrelis (boceprevir). FDA application NDA 202258*, FDA Silver Springs, MD.

FDA (2020) Clinical Drug Interaction Studies - Cytochrome P450 Enzyme- and Transporter-Mediated Drug Interactions Guidance for Industry. *Center for Drug Evaluation and Research (CDER), US Department of Health and Human Services Food and Drug Administration*.

Friedman EJ, Fraser IP, Wang YH, Bergman AJ, Li CC, Larson PJ, Chodakewitz J, Wagner JA, and Stoch SA (2011) Effect of different durations and formulations of diltiazem on the single-dose pharmacokinetics of midazolam: how long do we go? *J Clin Pharmacol* **51**:1561–1570.

Friedman H, Greenblatt DJ, Burstein ES, Scavone JM, Harmatz JS, and Shader RI (1988) Triazolam kinetics: interaction with cimetidine, propranolol, and the combination. *J Clin Pharmacol* **28**:228–233.

Fromm MF, Busse D, Kroemer HK, and Eichelbaum M (1996) Differential induction of prehepatic and hepatic metabolism of verapamil by rifampin. *Hepatology* **24**:796–801.

Galetin A, Burt H, Gibbons L, and Houston JB (2006) Prediction of time-dependent CYP3A4 drug-drug interactions: impact of enzyme degradation, parallel elimination pathways, and intestinal inhibition. *Drug Metab Dispos* **34**:166–175.

Galetin A, Gertz M, and Houston JB (2008) Potential role of intestinal first-pass metabolism in the prediction of drug-drug interactions. *Expert Opin Drug Metab Toxicol* **4**:909–922.

Galetin A, Gertz M, and Houston JB (2010) Contribution of intestinal cytochrome p450-mediated metabolism to drug-drug inhibition and induction interactions. *Drug Metab Pharmacokinet* **25**:28–47.

Garg V, Chandorkar G, Farmer HF, Smith F, Alves K, and van Heeswijk RP (2012) Effect of telaprevir on the pharmacokinetics of midazolam and digoxin. *J Clin Pharmacol* **52**:1566–1573.

Gertz M, Davis JD, Harrison A, Houston JB, and Galetin A (2008) Grapefruit juice-drug interaction studies as a method to assess the extent of intestinal availability: utility and limitations. *Curr Drug Metab* **9**:785–795.

Gorski JC, Jones DR, Haehner-Daniels BD, Hamman MA, O'Mara Jr EM, and Hall SD (1998) The contribution of intestinal and hepatic CYP3A to the interaction between midazolam and clarithromycin. *Clin Pharmacol Ther* **64**:133–143.

Greenblatt DJ, von Moltke LL, Harmatz JS, Chen G, Weemhoff JL, Jen C, Kelley CJ, LeDuc BW, and Zinny MA (2003) Time course of recovery of cytochrome p450 3A function after single doses of grapefruit juice. *Clin Pharmacol Ther* **74**:121–129.

Grimm SW, Einolf HJ, Hall SD, He K, Lim HK, Ling KH, Lu C, Nomeir AA, Seibert E, Skordos KW, et al. (2009) The conduct of in vitro studies to address time-dependent inhibition of drug-metabolizing enzymes: a perspective of the pharmaceutical research and manufacturers of America. *Drug Metab Dispos* **37**:1355–1370.

Guengerich FP(1995) Human Cytochrome P450 Enzymes, in: *Cytochrome P450: Structure, Mechanism, and Biochemistry (de Montellano PRO ed)*, pp 473-535, Springer US, Boston, MA.

Gurley B, Hubbard MA, Williams DK, Thaden J, Tong Y, Gentry WB, Breen P, Carrier DJ, and Cheboyina S (2006) Assessing the clinical significance of botanical supplementation on human cytochrome P450 3A activity: comparison of a milk thistle and black cohosh product to rifampin and clarithromycin. *J Clin Pharmacol* **46**:201–213.

Gurley BJ, Swain A, Hubbard MA, Hartsfield F, Thaden J, Williams DK, Gentry WB, and Tong Y (2008) Supplementation with goldenseal (Hydrastis canadensis), but not kava kava (Piper methysticum), inhibits human CYP3A activity in vivo. *Clin Pharmacol Ther* **83**:61–69.

Handel J, Ziegler G, Gemeinhardt A, Stuber H, Fischer C, and Klotz U (1988) Lack of effect of nitrendipine on the pharmacokinetics and pharmacodynamics of midazolam during steady state. *Br J Clin Pharmacol* **25**:243–250.

Ito K, Iwatsubo T, Kanamitsu S, Nakajima Y, and Sugiyama Y (1998) Quantitative prediction of in vivo drug clearance and drug interactions from in vitro data on metabolism, together with binding and transport. *Annu Rev Pharmacol Toxicol* **38**:461–499.

Jones DR, Gorski JC, Hamman MA, Mayhew BS, Rider S, and Hall SD (1999) Diltiazem inhibition of cytochrome P-450 3A activity is due to metabolite intermediate complex formation. *J Pharmacol Exp Ther* **290**:1116–1125.

Kanamitsu S, Ito K, and Sugiyama Y (2000) Quantitative prediction of in vivo drug-drug interactions from in vitro data based on physiological pharmacokinetics: use of maximum unbound concentration of inhibitor at the inlet to the liver. *Pharm Res* **17**:336–343.

Keefer CE, Kauffman GW, and Gupta RR (2013) Interpretable, probability-based confidence metric for continuous quantitative structure-activity relationship models. *J Chem Inf Model* **53**:368–383.

Kenny JR, Mukadam S, Zhang C, Tay S, Collins C, Galetin A, and Khojasteh SC (2012) Drug-drug interaction potential of marketed oncology drugs: in vitro assessment of time-dependent cytochrome P450 inhibition, reactive metabolite formation and drug-drug interaction prediction. *Pharm Res* **29**:1960–1976.

Kharasch ED, Hankins DC, Jubert C, Thummel KE, and Taraday JK (1999) Lack of single-dose disulfiram effects on cytochrome P-450 2C9, 2C19, 2D6, and 3A4 activities: evidence for specificity toward P-450 2E1. *Drug Metab Dispos* **27**:717–723.

Kirby BJ, Collier AC, Kharasch ED, Whittington D, Thummel KE, and Unadkat JD (2011) Complex drug interactions of HIV protease inhibitors 1: inactivation, induction, and inhibition of cytochrome P450 3A by ritonavir or nelfinavir. *Drug Metab Dispos* **39**:1070–1078.

Kivistö KT, Lamberg TS, Kantola T, and Neuvonen PJ (1997) Plasma buspirone concentrations are greatly increased by erythromycin and itraconazole. *Clin Pharmacol Ther* **62**:348–354.

Kivistö KT, Lamberg TS, and Neuvonen PJ (1999) Interactions of buspirone with itraconazole and rifampicin: effects on the pharmacokinetics of the active 1-(2-pyrimidinyl)-piperazine metabolite of buspirone. *Pharmacol Toxicol* **84**:94–97.

Kokudai M, Inui N, Takeuchi K, Sakaeda T, Kagawa Y, and Watanabe H (2009) Effects of statins on the pharmacokinetics of midazolam in healthy volunteers. *J Clin Pharmacol* **49**:568–573.

Lamberg TS, Kivistö KT, and Neuvonen PJ (1999) Lack of effect of terfenadine on the pharmacokinetics of the CYP3A4 substrate buspirone. *Pharmacol Toxicol* **84**:165–169.

Mahmood I and Sahajwalla C (1999) Clinical pharmacokinetics and pharmacodynamics of buspirone, an anxiolytic drug. *Clin Pharmacokinet* **36**:277–287.

Mao J, Johnson TR, Shen Z, and Yamazaki S (2013) Prediction of crizotinib-midazolam interaction using the Simcyp population-based simulator: comparison of CYP3A time-dependent inhibition between human liver microsomes versus hepatocytes. *Drug Metab Dispos* **41**:343–352.

Mao J, Mohutsky MA, Harrelson JP, Wrighton SA, and Hall SD (2011) Prediction of CYP3A-mediated drug-drug interactions using human hepatocytes suspended in human plasma. *Drug Metab Dispos* **39**:591–602.

Mao J, Mohutsky MA, Harrelson JP, Wrighton SA, and Hall SD (2012) Predictions of cytochrome P450-mediated drug-drug interactions using cryopreserved human hepatocytes: comparison of plasma and protein-free media incubation conditions. *Drug Metab Dispos* **40**:706–716.

Martin DE, Zussman BD, Everitt DE, Benincosa LJ, Etheredge RC, and Jorkasky DK (1997) Paroxetine does not affect the cardiac safety and pharmacokinetics of terfenadine in healthy adult men. *J Clin Psychopharmacol* **17**:451–459.

Mayhew BS, Jones DR, and Hall SD (2000) An in vitro model for predicting in vivo inhibition of cytochrome P450 3A4 by metabolic intermediate complex formation. *Drug Metab Dispos* **28**:1031–1037.

Mullins ME, Horowitz BZ, Linden DH, Smith GW, Norton RL, and Stump J (1998) Life-threatening interaction of mibefradil and beta-blockers with dihydropyridine calcium channel blockers. *JAMA* **280**:157–158.

O'Brien SG, Meinhardt P, Bond E, Beck J, Peng B, Dutreix C, Mehring G, Milosavljev S, Huber C, Capdeville R, et al. (2003) Effects of imatinib mesylate (STI571, Glivec) on the pharmacokinetics of simvastatin, a cytochrome p450 3A4 substrate, in patients with chronic myeloid leukaemia. *Br J Cancer* **89**:1855–1859.

Obach RS, Walsky RL, and Venkatakrishnan K (2007) Mechanism-based inactivation of human cytochrome p450 enzymes and the prediction of drug-drug interactions. *Drug Metab Dispos* **35**:246–255.

Obach RS, Walsky RL, Venkatakrishnan K, Gaman EA, Houston JB, and Tremaine LM (2006) The utility of in vitro cytochrome P450 inhibition data in the prediction of drug-drug interactions. *J Pharmacol Exp Ther* **316**:336–348.

Olkkola KT, Aranko K, Luurila H, Hiller A, Saarnivaara L, Himberg JJ, and Neuvonen PJ (1993) A potentially hazardous interaction between erythromycin and midazolam. *Clin Pharmacol Ther* **53**:298–305.

Paine MF, Shen DD, Kunze KL, Perkins JD, Marsh CL, McVicar JP, Barr DM, Gillies BS, and Thummel KE (1996) First-pass metabolism of midazolam by the human intestine. *Clin Pharmacol Ther* **60**:14–24.

Prueksaritanont T, Ma B, Tang C, Meng Y, Assang C, Lu P, Reider PJ, Lin JH, and Baillie TA (1999) Metabolic interactions between mibefradil and HMG-CoA reductase inhibitors: an in vitro investigation with human liver preparations. *Br J Clin Pharmacol* **47**:291–298.

Prueksaritanont T, Tatosian DA, Chu X, Railkar R, Evers R, Chavez-Eng C, Lutz R, Zeng W, Yabut J, Chan GH, et al. (2017) Validation of a microdose probe drug cocktail for clinical drug interaction assessments for drug transporters and CYP3A. *Clin Pharmacol Ther* **101**:519–530.

Quinney SK, Haehner BD, Rhoades MB, Lin Z, Gorski JC, and Hall SD (2008) Interaction between midazolam and clarithromycin in the elderly. *Br J Clin Pharmacol* **65**:98–109.

Riccardi K, Lin J, Li Z, Niosi M, Ryu S, Hua W, Atkinson K, Kosa RE, Litchfield J, and Di L (2017) Novel method to predict in vivo liver-to-plasma K_{puu} for OATP substrates using suspension hepatocytes. *Drug Metab Dispos* **45**:576–580.

Riccardi K, Ryu S, Lin J, Yates P, Tess D, Li R, Singh D, Holder BR, Kapinos B, Chang G, et al. (2018) Comparison of species and cell-type differences in fraction unbound of liver tissues, hepatocytes, and cell lines. *Drug Metab Dispos* **46**:415–421.

Ring BJ, Patterson BE, Mitchell MI, Vandenbranden M, Gillespie J, Bedding AW, Jewell H, Payne CD, Forgue ST, Eckstein J, et al. (2005) Effect of tadalafil on cytochrome P450 3A4-mediated clearance: studies in vitro and in vivo. *Clin Pharmacol Ther* **77**:63–75.

Rostami-Hodjegan A and Tucker G (2004) 'In silico' simulations to assess the 'in vivo' consequences of 'in vitro' metabolic drug-drug interactions. *Drug Discov Today Technol* **1**:441–448.

Rowland M and Matin SB (1973) Kinetics of drug-drug interactions. *J Pharmacokinet Biopharm* **1**:553–567.

Rowland Yeo K, Walsky RL, Jamei M, Rostami-Hodjegan A, and Tucker GT (2011) Prediction of time-dependent CYP3A4 drug-drug interactions by physiologically based pharmacokinetic modelling: impact of inactivation parameters and enzyme turnover. *Eur J Pharm Sci* **43**:160–173.

Shou M, Hayashi M, Pan Y, Xu Y, Morrissey K, Xu L, and Skiles GL (2008) Modeling, prediction, and in vitro in vivo correlation of CYP3A4 induction. *Drug Metab Dispos* **36**:2355–2370.

Tomalik-Scharte D, Jetter A, Kinzig-Schippers M, Skott A, Sörgel F, Klaassen T, Kasel D, Harlfinger S, Doroshyenko O, Frank D, et al. (2005) Effect of propiverine on cytochrome P450 enzymes: a cocktail interaction study in healthy volunteers. *Drug Metab Dispos* **33**:1859–1866.

Treyer A, Mateus A, Wiśniewski JR, Boriss H, Matsson P, and Artursson P (2018) Intracellular drug bioavailability: effect of neutral lipids and phospholipids. *Mol Pharm* **15**:2224–2233.

Treyer A, Walday S, Boriss H, Matsson P, and Artursson P (2019) A cell-free approach based on phospholipid characterization for determination of the cell specific unbound drug fraction ($f_{u,cell}$). *Pharm Res* **36**:178.

Wang YH, Jones DR, and Hall SD (2004) Prediction of cytochrome P450 3A inhibition by verapamil enantiomers and their metabolites. *Drug Metab Dispos* **32**:259–266.

Wang Z, Yang J, Kirk C, Fang Y, Alsina M, Badros A, Papadopoulos K, Wong A, Woo T, Bomba D, et al. (2013) Clinical pharmacokinetics, metabolism, and drug-drug interaction of carfilzomib. *Drug Metab Dispos* **41**:230–237.

Yadav J, Korzekwa K, and Nagar S (2018) Improved predictions of drug-drug interactions mediated by time-dependent inhibition of CYP3A. *Mol Pharm* **15**:1979–1995.

Yadav J, Paragas E, Korzekwa K, and Nagar S (2020) Time-dependent enzyme inactivation: numerical analyses of in vitro data and prediction of drug-drug interactions. *Pharmacol Ther* **206**:107449.

Yang J, Jamei M, Yeo KR, Rostami-Hodjegan A, and Tucker GT (2007a) Misuse of the well-stirred model of hepatic drug clearance. *Drug Metab Dispos* **35**:501–502.

Yang J, Jamei M, Yeo KR, Tucker GT, and Rostami-Hodjegan A (2007b) Prediction of intestinal first-pass drug metabolism. *Curr Drug Metab* **8**:676–684.

Yang J, Liao M, Shou M, Jamei M, Yeo KR, Tucker GT, and Rostami-Hodjegan A (2008) Cytochrome p450 turnover: regulation of synthesis and degradation, methods for determining rates, and implications for the prediction of drug interactions. *Curr Drug Metab* **9**:384–394.

Yates P, Eng H, Di L, and Obach RS (2012) Statistical methods for analysis of time-dependent inhibition of cytochrome p450 enzymes. *Drug Metab Dispos* **40**:2289–2296.

Yeates RA, Laufen H, and Zimmermann T (1996) Interaction between midazolam and clarithromycin: comparison with azithromycin. *Int J Clin Pharmacol Ther* **34**:400–405.

Zdravkovic M, Olsen AK, Christiansen T, Schulz R, Taub ME, Thomsen MS, Rasmussen MH, and Ilondo MM (2003) A clinical study investigating the pharmacokinetic interaction between NN703 (tabimorelin), a potential inhibitor of CYP3A4 activity, and midazolam, a CYP3A4 substrate. *Eur J Clin Pharmacol* **58**:683–688.

Zhang L, Reynolds KS, Zhao P, and Huang SM (2010) Drug interactions evaluation: an integrated part of risk assessment of therapeutics. *Toxicol Appl Pharmacol* **243**:134–145.

Zhou S, Chan E, Lim LY, Boelsterli UA, Li SC, Wang J, Zhang Q, Huang M, and Xu A (2004) Therapeutic drugs that behave as mechanism-based inhibitors of cytochrome P450 3A4. *Curr Drug Metab* **5**:415–442.

Zhou SF (2008) Drugs behave as substrates, inhibitors and inducers of human cytochrome P450 3A4. *Curr Drug Metab* **9**:310–322.

Zimmerlin A, Trunzer M, and Faller B (2011) CYP3A time-dependent inhibition risk assessment validated with 400 reference drugs. *Drug Metab Dispos* **39**:1039–1046.

Zimmermann T, Yeates RA, Laufen H, Scharpf F, Leitold M, and Wildfeuer A (1996) Influence of the antibiotics erythromycin and azithromycin on the pharmacokinetics and pharmacodynamics of midazolam. *Arzneimittelforschung* **46**:213–217.

Address correspondence to: Elaine Tseng, Pfizer Inc., Eastern Point Rd., Groton, CT 06340. elaine.tseng@pfizer.com; or R. Scott Obach, Pfizer Inc., Eastern Point Rd., Groton, CT 06340. Email: r.scott.obach@pfizer.com

SUPPLEMENTAL FIGURES

Static and Dynamic Projections of Drug-Drug Interactions Caused by Cytochrome P450 3A Time-Dependent Inhibitors Measured in Human Liver Microsomes and Hepatocytes

Elaine Tseng, Heather Eng, Jian Lin, Matthew A. Cerny, David A. Tess, Theunis C. Goosen, and R. Scott Obach

Supplemental Figure 1. Plot of percent activity remaining data and K_I and k_{inact} fitting for azithromycin.
The percent remaining activity is shown along with a regression where the slope represents $-k_{obs}$. These studies were conducted n=2. The figure inlay shows the k_{obs} vs inhibitor concentration K_I and k_{inact} fitting, where hollow symbols were excluded from the fit. The data generated in HLM are shown in panel A and the data generated in HHEP are shown in panel B. The K_I (SE) and k_{inact} (SE) for azithromycin were 0.025 (0.002) $mL \cdot min^{-1} \cdot \mu mol^{-1}$ (reported as k_{inact}/K_I (SE) composite slope) and 51.2 (17.3) µM and 0.0327 (0.0032) min^{-1} in HLM and HHEP, respectively.

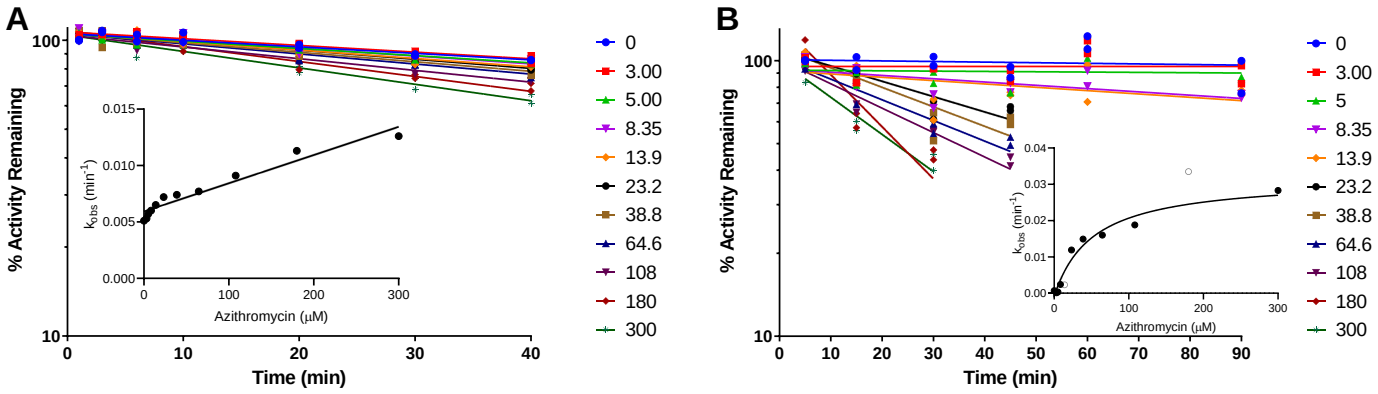

Supplemental Figure 2. Plot of percent activity remaining data and K_I and k_{inact} fitting for boceprevir.
The percent remaining activity is shown along with a regression where the slope represents $-k_{obs}$. These studies were conducted n=2. The figure inlay shows the k_{obs} vs inhibitor concentration K_I and k_{inact} fitting. The data generated in HLM are shown in panel A and the data generated in HHEP are shown in panel B. The K_I (SE) and k_{inact} (SE) for boceprevir were 13.8 (1.7) µM and 0.304 (0.010) min^{-1} and 25.9 (10.7) µM and 0.0978 (0.0161) min^{-1} in HLM and HHEP, respectively.

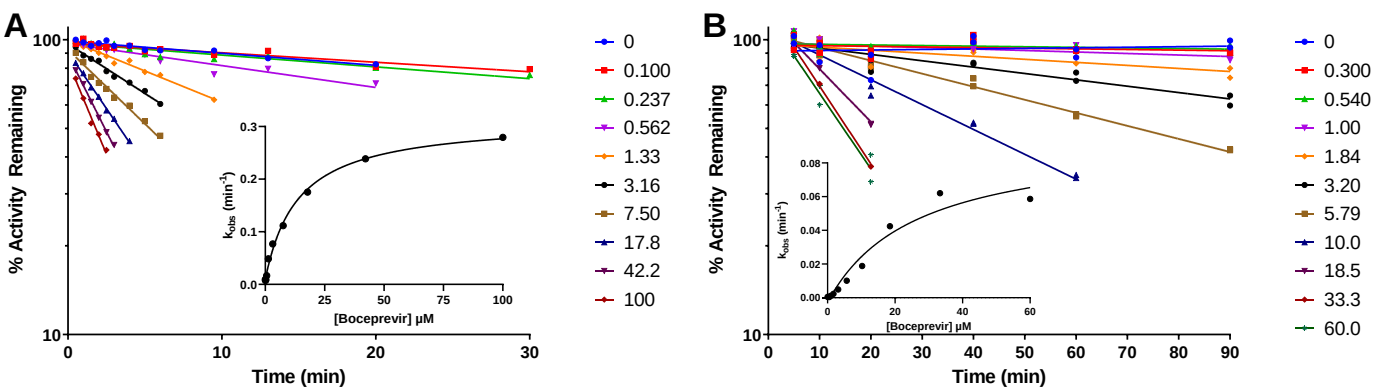

Supplemental Figure 3. Plot of percent activity remaining data and K_I and k_{inact} fitting for carfilzomib.
The percent remaining activity is shown along with a regression where the slope represents -k_{obs}. These studies were conducted n=2. The figure inlay shows the k_{obs} vs inhibitor concentration K_I and k_{inact} fitting. The data generated in HLM are shown in panel A and the data generated in HHEP are shown in panel B. The K_I (SE) and k_{inact} (SE) for carfilzomib were 1.18 (0.22) µM and 0.107 (0.007) min^{-1} and 7.76 (2.26) µM and 0.0289 (0.0020) min^{-1} in HLM and HHEP, respectively.

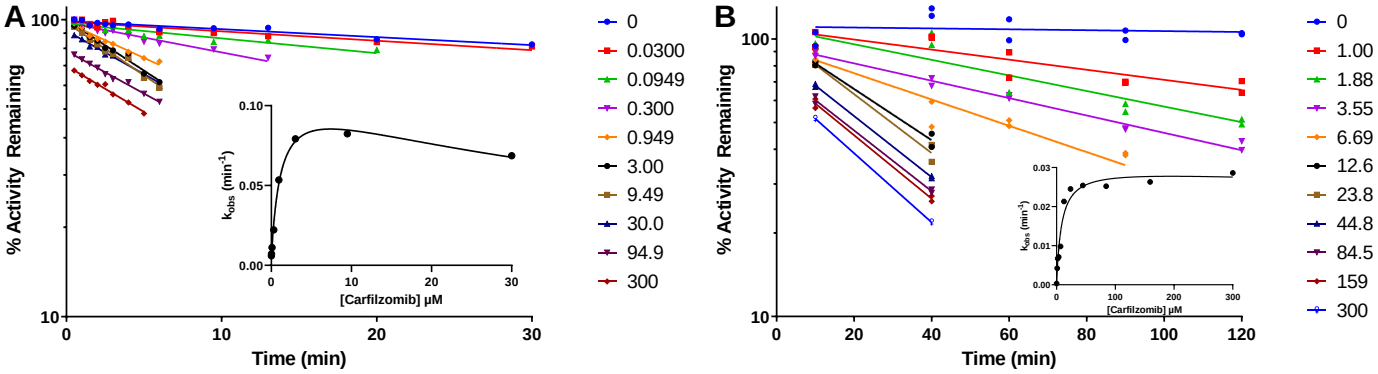

Supplemental Figure 4. Plot of percent activity remaining data and K_I and k_{inact} fitting for clarithromycin.
The percent remaining activity is shown along with a regression where the slope represents -k_{obs}. These studies were conducted n=2. The figure inlay shows the k_{obs} vs inhibitor concentration K_I and k_{inact} fitting. The data generated in HLM are shown in panel A and the data generated in HHEP are shown in panel B. The K_I (SE) and k_{inact} (SE) for clarithromycin were 55.9 (13.4) µM and 0.0812 (0.0086) min^{-1} and 7.45 (2.06) µM and 0.0112 (0.0007) min^{-1} in HLM and HHEP, respectively.

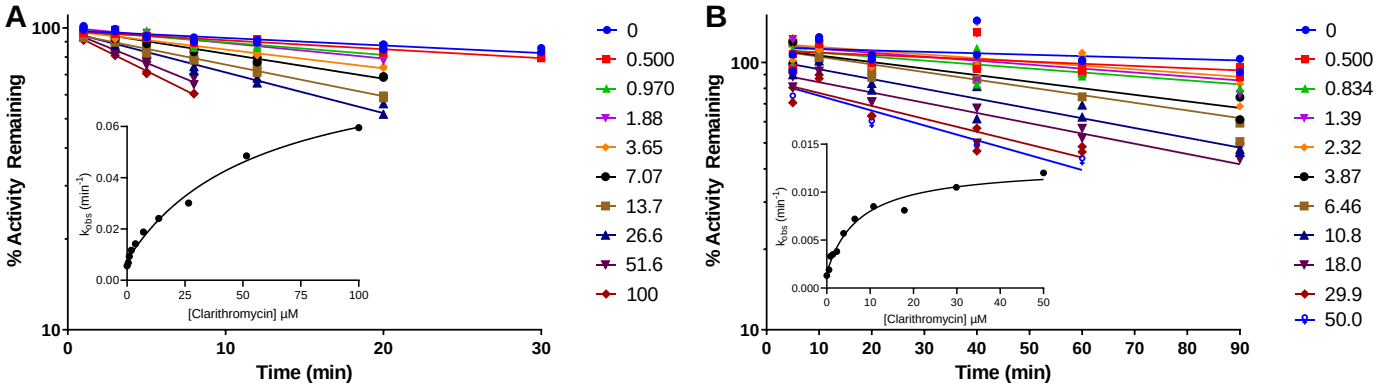

Supplemental Figure 5. Plot of percent activity remaining data and K_I and k_{inact} fitting for conivaptan.
The percent remaining activity is shown along with a regression where the slope represents $-k_{obs}$. These studies were conducted n=2. The figure inlay shows the k_{obs} vs inhibitor concentration K_I and k_{inact} fitting. The data generated in HLM are shown in panel A and the data generated in HHEP are shown in panel B. The K_I (SE) and k_{inact} (SE) for conivaptan were 1.04 (0.16) µM and 0.329 (0.013) min^{-1} and 0.634 (0.124) µM and 0.0182 (0.0010) min^{-1} in HLM and HHEP, respectively.

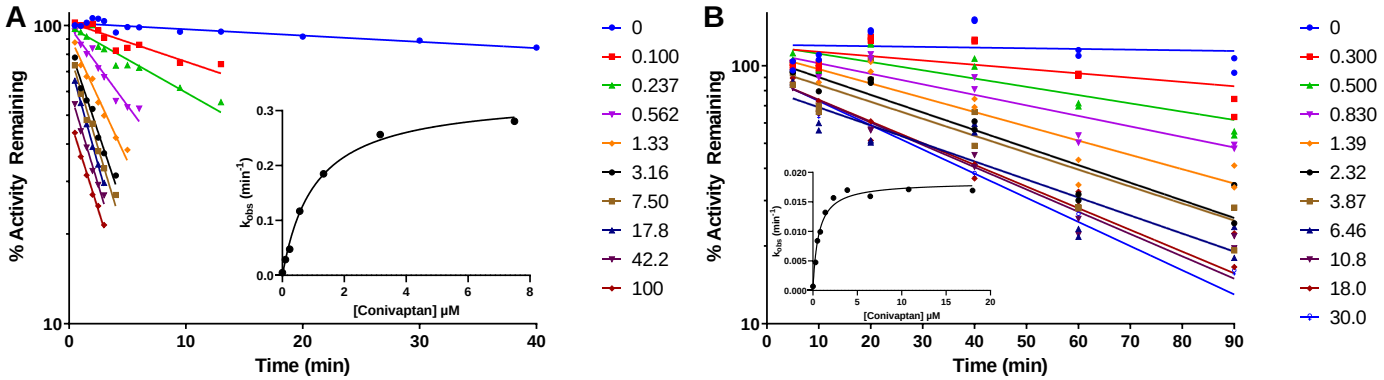

Supplemental Figure 6. Plot of percent activity remaining data and K_I and k_{inact} fitting for diltiazem.
The percent remaining activity is shown along with a regression where the slope represents $-k_{obs}$. These studies were conducted n=2. The figure inlay shows the k_{obs} vs inhibitor concentration K_I and k_{inact} fitting. The data generated in HLM are shown in panel A and the data generated in HHEP are shown in panel B. The K_I (SE) and k_{inact} (SE) for diltiazem were 1.90 (0.28) µM and 0.0109 (0.0004) min^{-1} and 35.4 (6.6) µM and 0.0217 (0.0010) min^{-1} in HLM and HHEP, respectively.

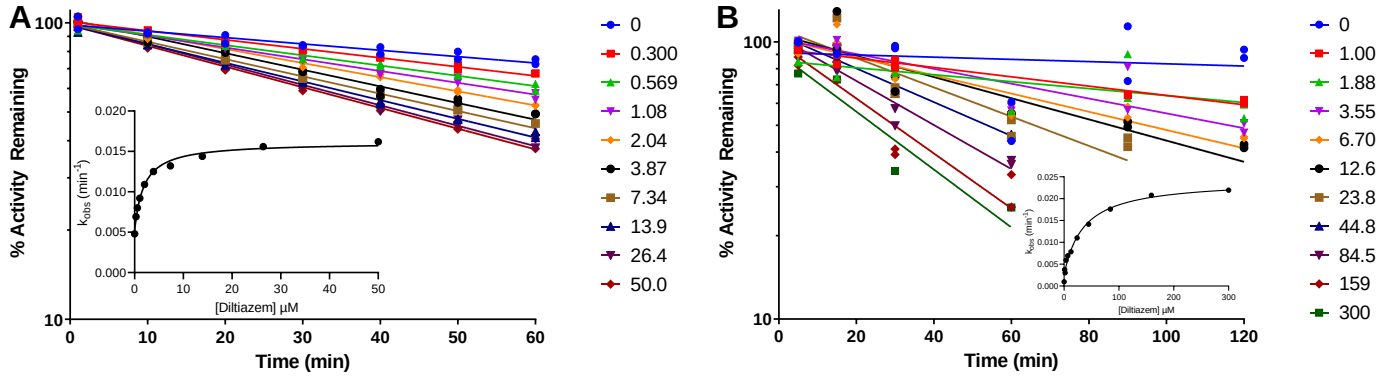

Supplemental Figure 7. Plot of percent activity remaining data and K_I and k_{inact} fitting for n-desmethyl diltiazem. The percent remaining activity is shown along with a regression where the slope represents $-k_{obs}$. These studies were conducted n=2. The figure inlay shows the k_{obs} vs inhibitor concentration K_I and k_{inact} fitting. The data generated in HLM are shown in panel A and the data generated in HHEP are shown in panel B. The K_I (SE) and k_{inact} (SE) for n-desmethyl diltiazem were 0.961 (0.115) µM and 0.00954 (0.00027) min^{-1} and 2.96 (1.12) µM and 0.0127 (0.0011) min^{-1} in HLM and HHEP, respectively.

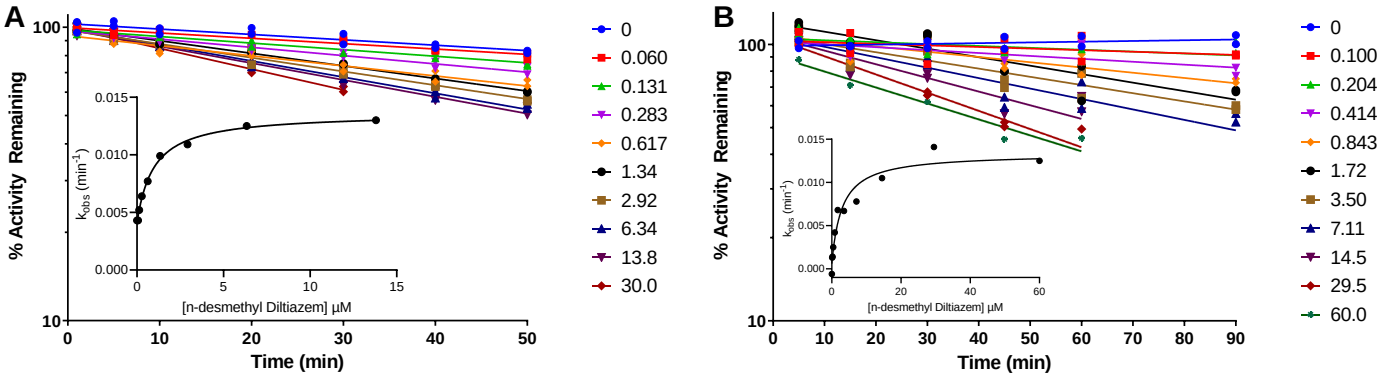

Supplemental Figure 8. Plot of percent activity remaining data and K_I and k_{inact} fitting for disulfiram. The percent remaining activity is shown along with a regression where the slope represents $-k_{obs}$. These studies were conducted n=2. The figure inlay shows the k_{obs} vs inhibitor concentration K_I and k_{inact} fitting. The HLM K_I (SE) and k_{inact} (SE) for disulfiram were 16.4 (5.2) µM and 0.129 (0.012) min^{-1}. No HHEP results are shown for disulfiram as it did not exhibit TDI in the HHEP test system.

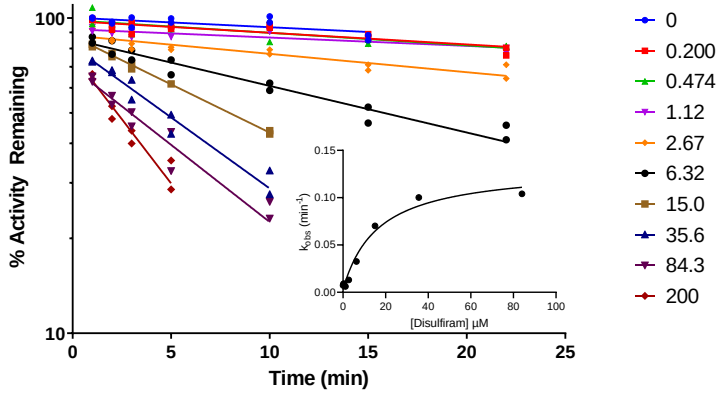

Supplemental Figure 9. Plot of percent activity remaining data and K_I and k_{inact} fitting for eplerenone.
The percent remaining activity is shown along with a regression where the slope represents $-k_{obs}$. These studies were conducted n=2. The figure inlay shows the k_{obs} vs inhibitor concentration K_I and k_{inact} fitting. The data generated in HLM are shown in panel A and the data generated in HHEP are shown in panel B. The K_I (SE) and k_{inact} (SE) for eplerenone were 202 (58) µM and 0.0223 (0.0029) min^{-1} and 0.0166 (0.0006) $mL \cdot min^{-1} \cdot \mu mol^{-1}$ (reported as k_{inact}/K_I composite slope) in HLM and HHEP, respectively.

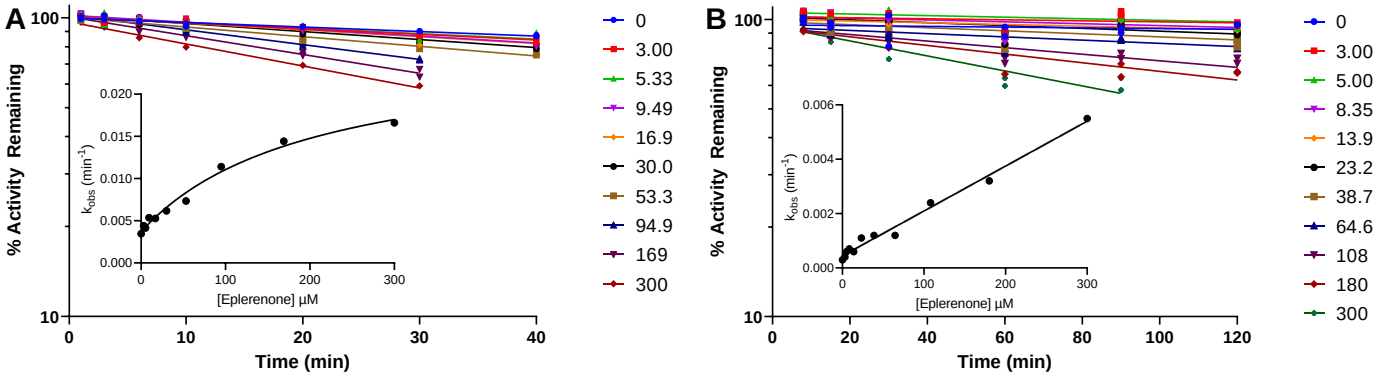

Supplemental Figure 10. Plot of percent activity remaining data and K_I and k_{inact} fitting for erythromycin.
The percent remaining activity is shown along with a regression where the slope represents $-k_{obs}$. These studies were conducted n=2. The figure inlay shows the k_{obs} vs inhibitor concentration K_I and k_{inact} fitting. The data generated in HLM are shown in panel A and the data generated in HHEP are shown in panel B. The K_I (SE) and k_{inact} (SE) for erythromycin were 23.3 (3.3) µM and 0.0557 (0.0025) min^{-1} and 27.1 (19.7) µM and 0.0141 (0.0044) min^{-1} in HLM and HHEP, respectively.

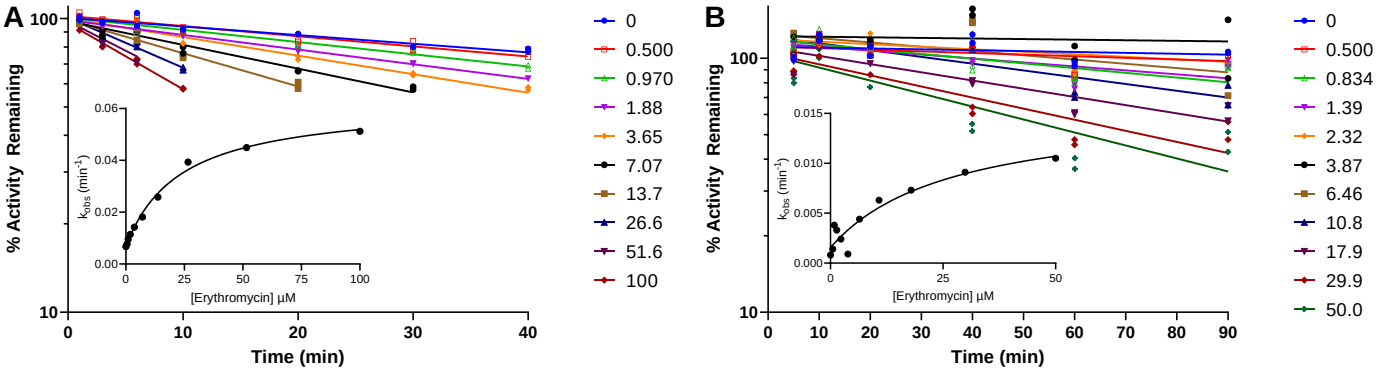

Supplemental Figure 11. Plot of percent activity remaining data and K_I and k_{inact} fitting for imatinib.
The percent remaining activity is shown along with a regression where the slope represents $-k_{obs}$. These studies were conducted n=2. The figure inlay shows the k_{obs} vs inhibitor concentration K_I and k_{inact} fitting. The data generated in HLM are shown in panel A and the data generated in HHEP are shown in panel B. The K_I (SE) and k_{inact} (SE) for imatinib were 16.4 (4.9) µM and 0.0348 (0.0029) min^{-1} and 29.4 (8.1) µM and 0.0202 (0.0014) min^{-1} in HLM and HHEP, respectively.

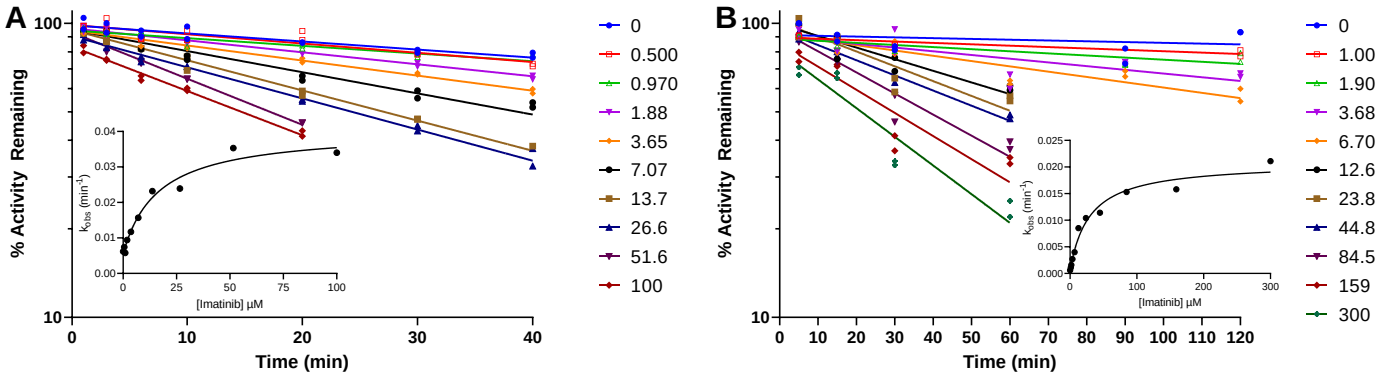

Supplemental Figure 12. Plot of percent activity remaining data and K_I and k_{inact} fitting for midostaurin.
The percent remaining activity is shown along with a regression where the slope represents $-k_{obs}$. These studies were conducted n=2. The figure inlay shows the k_{obs} vs inhibitor concentration K_I and k_{inact} fitting. The data generated in HLM are shown in panel A and the data generated in HHEP are shown in panel B. The K_I (SE) and k_{inact} (SE) for midostaurin were 0.360 (0.120) µM and 0.0207 (0.0015) min^{-1} and 0.574 (0.165) µM and 0.00566 (0.00041) min^{-1} in HLM and HHEP, respectively.

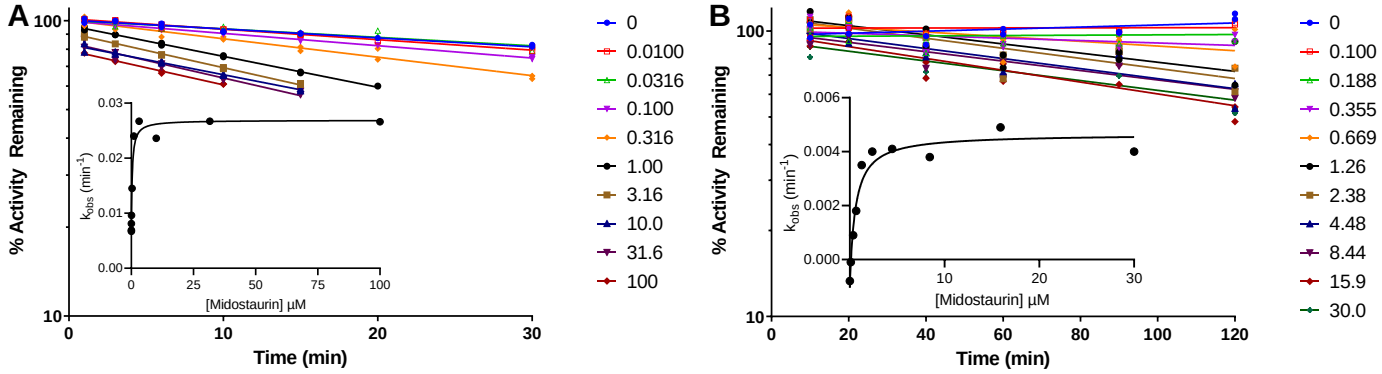

Supplemental Figure 13. Plot of percent activity remaining data and K_I and k_{inact} fitting for nelfinavir.
The percent remaining activity is shown along with a regression where the slope represents $-k_{obs}$. These studies were conducted n=2. The figure inlay shows the k_{obs} vs inhibitor concentration K_I and k_{inact} fitting. The data generated in HLM are shown in panel A and the data generated in HHEP are shown in panel B. The K_I (SE) and k_{inact} (SE) for nelfinavir were 1.44 (0.45) µM and 0.510 (0.057) min^{-1} and 6.24 (0.71) µM $mL \cdot min^{-1} \cdot \mu mol^{-1}$ (reported as k_{inact}/K_I composite slope) in HLM and HHEP, respectively. There was visual precipitate observed in HHEP concentrations ≥ 6.46 µM and they were excluded from the k_{inact}/K_I fit.

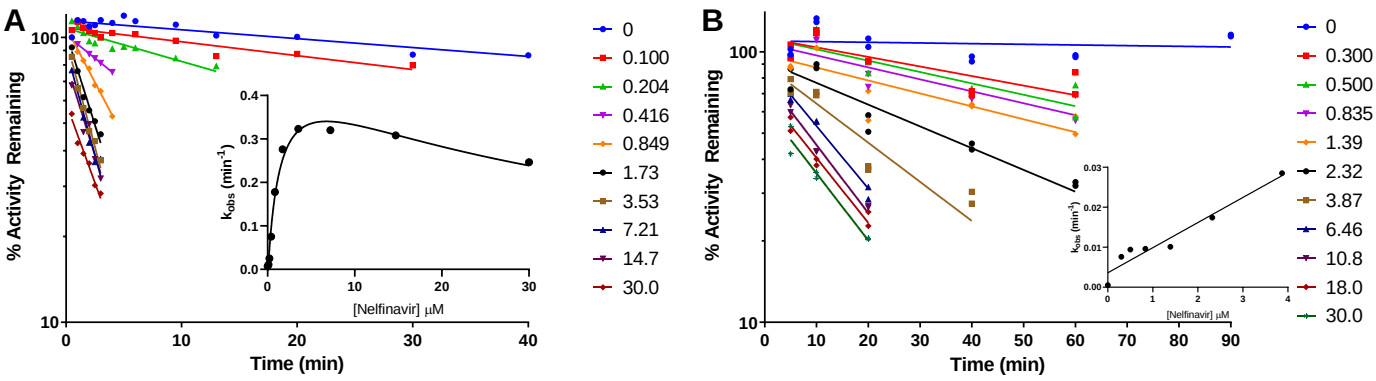

Supplemental Figure 14. Plot of percent activity remaining data and K_I and k_{inact} fitting for nitrendipine.
The percent remaining activity is shown along with a regression where the slope represents $-k_{obs}$. These studies were conducted n=2. The figure inlay shows the k_{obs} vs inhibitor concentration K_I and k_{inact} fitting. The HLM K_I (SE) and k_{inact} (SE) for nitrendipine were 10.4 (3.1) µM and 0.0266 (0.0020) min^{-1}. No HHEP results are shown for nitrendipine as it did not exhibit TDI in the HHEP test system.

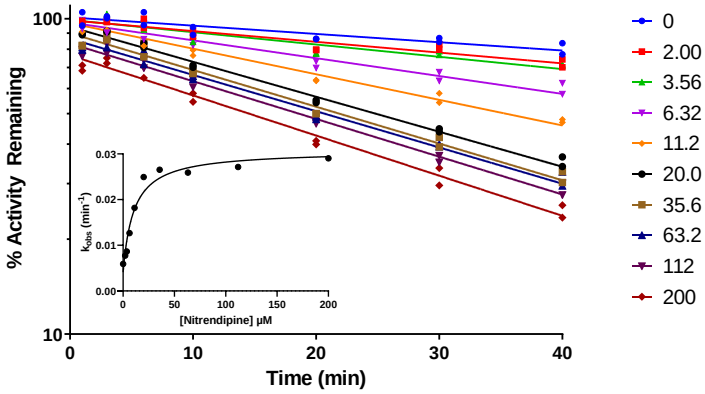

Supplemental Figure 15. Plot of percent activity remaining data and K_I and k_{inact} fitting for panobinostat.
The percent remaining activity is shown along with a regression where the slope represents $-k_{obs}$. These studies were conducted n=2. The figure inlay shows the k_{obs} vs inhibitor concentration K_I and k_{inact} fitting. The data generated in HLM are shown in panel A and the data generated in HHEP are shown in panel B. The K_I (SE) and k_{inact} (SE) for panobinostat were 30.3 (6.8) µM and 0.0436 (0.0027) min^{-1} and 26.0 (7.2) µM and 0.00446 (0.00038) min^{-1} in HLM and HHEP, respectively.

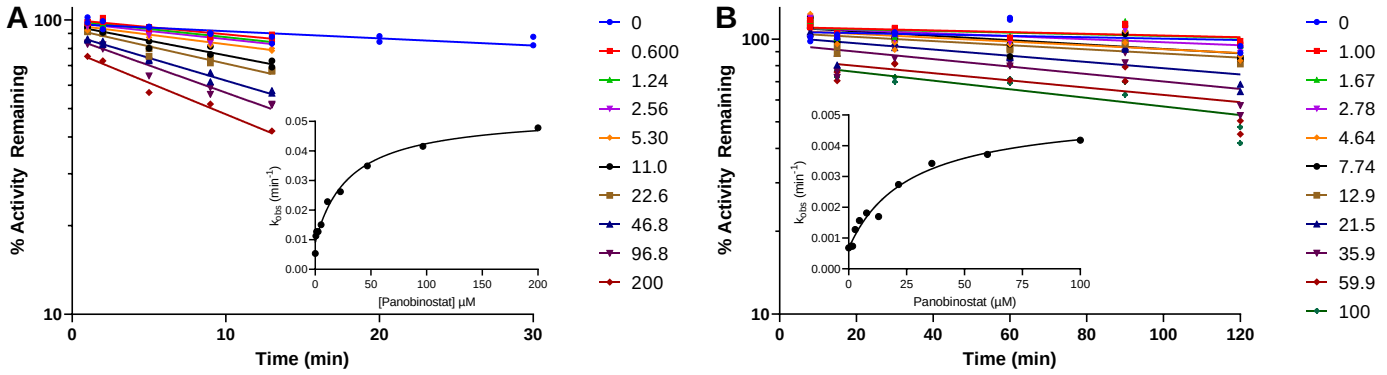

Supplemental Figure 16. Plot of percent activity remaining data and K_I and k_{inact} fitting for paroxetine.
The percent remaining activity is shown along with a regression where the slope represents $-k_{obs}$. These studies were conducted n=2. The figure inlay shows the k_{obs} vs inhibitor concentration K_I and k_{inact} fitting. The data generated in HLM are shown in panel A and the data generated in HHEP are shown in panel B. The K_I (SE) and k_{inact} (SE) for paroxetine were 49.4 (22.0) µM and 0.0277 (0.0084) min^{-1} and 0.113 (0.011) $mL \cdot min^{-1} \cdot \mu mol^{-1}$ (reported as k_{inact}/K_I composite slope) in HLM and HHEP, respectively.

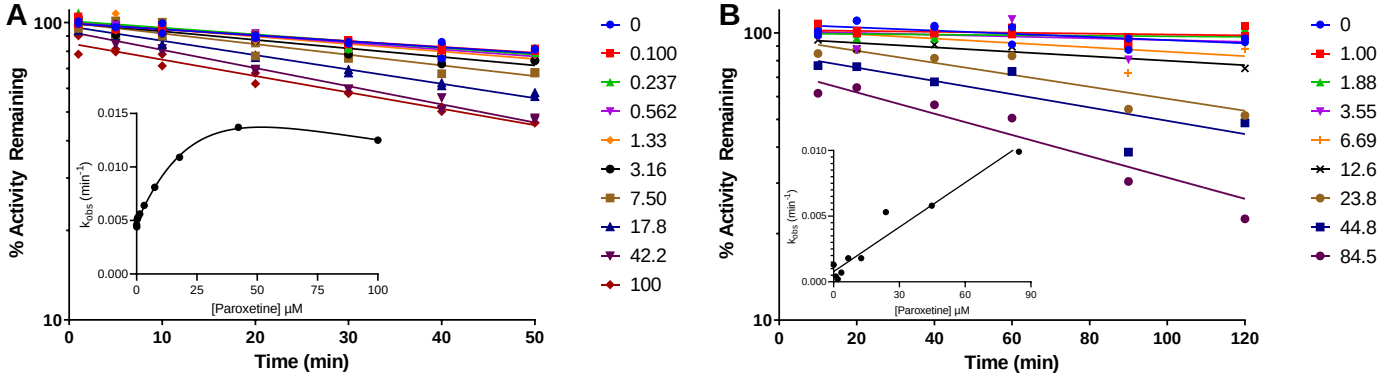

Supplemental Figure 17. Plot of percent activity remaining data and K_I and k_{inact} fitting for propiverine.
The percent remaining activity is shown along with a regression where the slope represents $-k_{obs}$. These studies were conducted n=2. The figure inlay shows the k_{obs} vs inhibitor concentration K_I (SE) and k_{inact} (SE) fitting. The data generated in HLM are shown in panel A and the data generated in HHEP are shown in panel B. The K_I and k_{inact} for propiverine were 1.71 (0.23) µM and 0.0298 (0.0012) min^{-1} and 1.38 (0.62) µM and 0.0196 (0.0040) min^{-1} in HLM and HHEP, respectively.

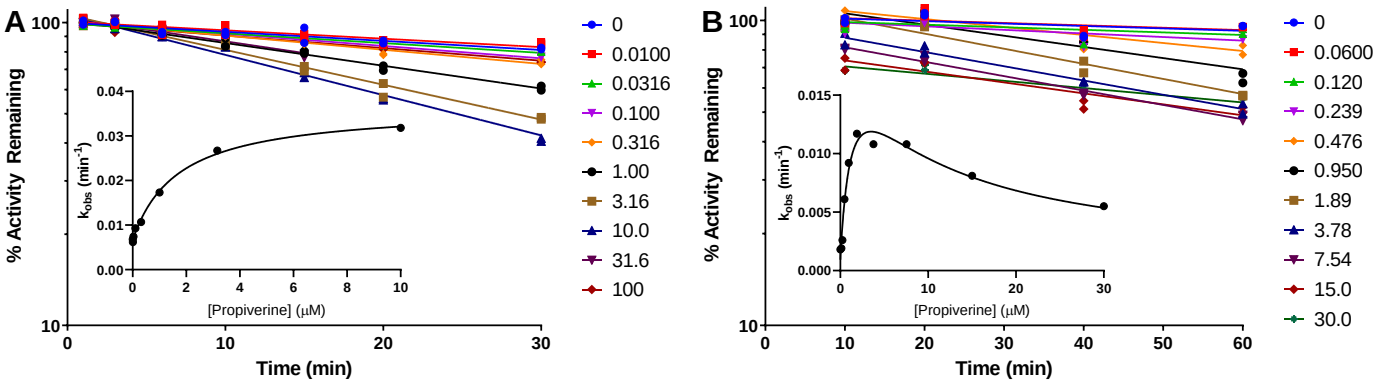

Supplemental Figure 18. Plot of percent activity remaining data and K_I and k_{inact} fitting for simvastatin.
The percent remaining activity is shown along with a regression where the slope represents $-k_{obs}$. These studies were conducted n=2. The figure inlay shows the k_{obs} vs inhibitor concentration K_I and k_{inact} fitting. The HLM K_I (SE) and k_{inact} (SE) for simvastatin was 0.195 (0.021) $mL \cdot min^{-1} \cdot \mu mol^{-1}$ (reported as k_{inact}/K_I composite slope). No HHEP results are shown for simvastatin as it did not exhibit TDI in the HHEP test system.

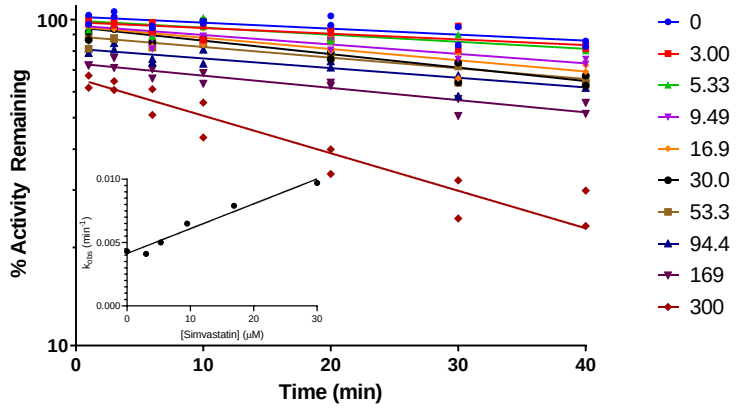

Supplemental Figure 19. Plot of percent activity remaining data and K_I and k_{inact} fitting for tabimorelin.
The percent remaining activity is shown along with a regression where the slope represents $-k_{obs}$. These studies were conducted n=2. The figure inlay shows the k_{obs} vs inhibitor concentration K_I and k_{inact} fitting. The data generated in HLM are shown in panel A and the data generated in HHEP are shown in panel B. The K_I (SE) and k_{inact} (SE) for tabimorelin were 1.98 (0.31) µM and 0.0652 (0.0023) min^{-1} and 7.57 (2.62) µM and 0.0148 (0.0013) min^{-1} in HLM and HHEP, respectively.

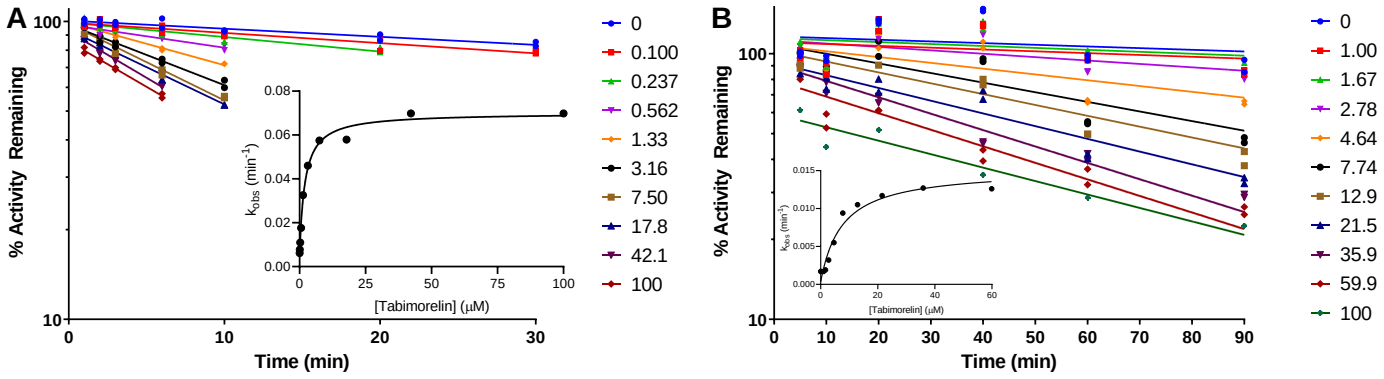

Supplemental Figure 20. Plot of percent activity remaining data and K_I and k_{inact} fitting for tadalafil.
The percent remaining activity is shown along with a regression where the slope represents $-k_{obs}$. These studies were conducted n=2. The figure inlay shows the k_{obs} vs inhibitor concentration K_I and k_{inact} fitting. The data generated in HLM are shown in panel A and the data generated in HHEP are shown in panel B. The K_I (SE) and k_{inact} (SE) for tadalafil were 13.0 (1.7) µM and 0.143 (0.004) min^{-1} and 4.26 (1.44) µM and 0.028 (0.002) min^{-1} in HLM and HHEP, respectively.

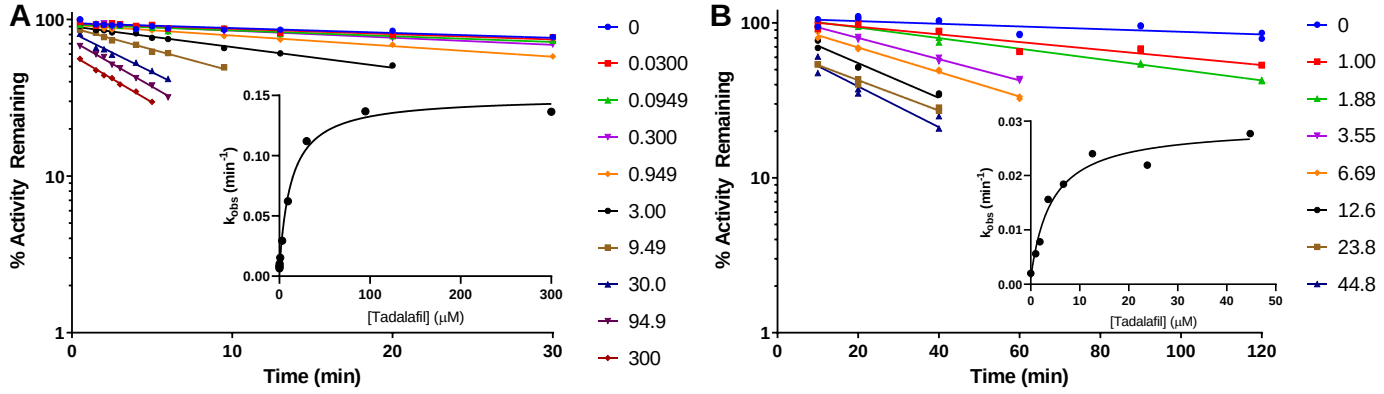

Supplemental Figure 21. Plot of percent activity remaining data and K_I and k_{inact} fitting for telaprevir.
The percent remaining activity is shown along with a regression where the slope represents $-k_{obs}$. These studies were conducted n=2. The figure inlay shows the k_{obs} vs inhibitor concentration K_I and k_{inact} fitting. The data generated in HLM are shown in panel A and the data generated in HHEP are shown in panel B. The K_I (SE) and k_{inact} (SE) for telaprevir were 0.644 (0.109) µM and 0.108 (0.004) min^{-1} and 2.24 (0.95) µM and 0.0112 (0.0011) min^{-1} in HLM and HHEP, respectively.

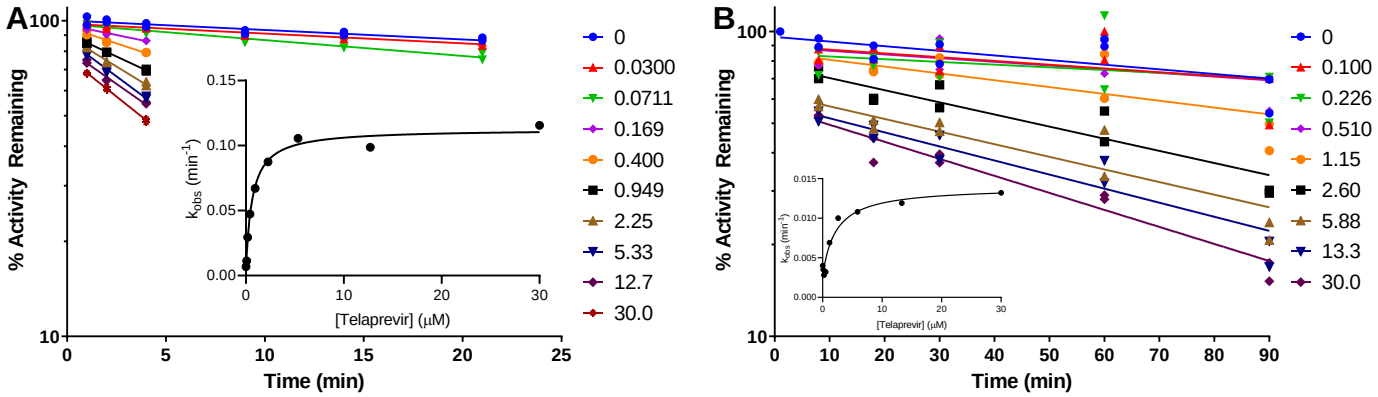

Supplemental Figure 22. Plot of percent activity remaining data and K_I and k_{inact} fitting for terfenadine.
The percent remaining activity is shown along with a regression where the slope represents $-k_{obs}$. These studies were conducted n=2. The figure inlay shows the k_{obs} vs inhibitor concentration K_I and k_{inact} fitting. The data generated in HLM are shown in panel A and the data generated in HHEP are shown in panel B. The K_I (SE) and k_{inact} (SE) for terfenadine were 9.32 (5.85) µM and 0.0276 (0.0111) min^{-1} and 0.426 (0.021) $mL \cdot min^{-1} \cdot \mu mol^{-1}$ (reported as k_{inact}/K_I composite slope) in HLM and HHEP, respectively.

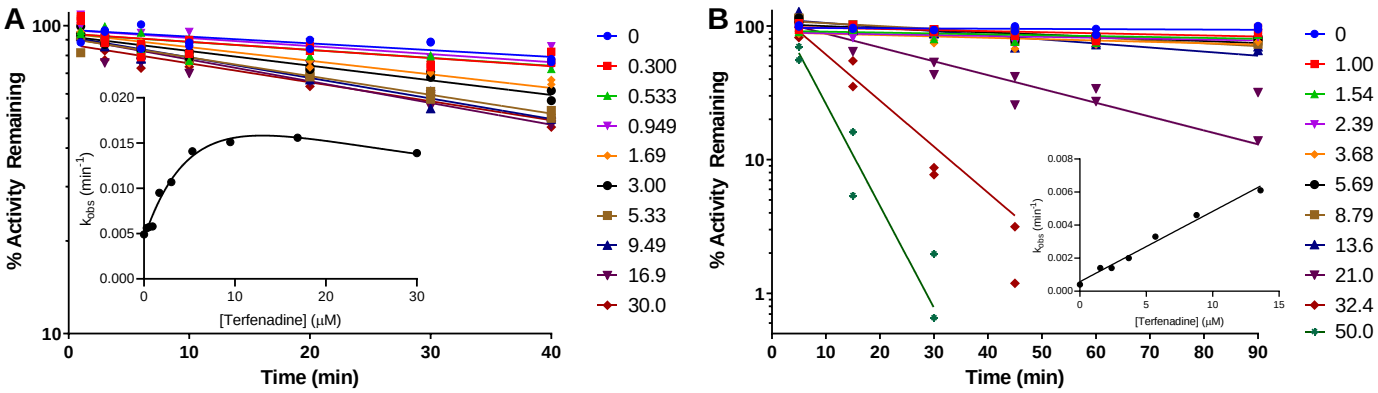

Supplemental Figure 23. Plot of percent activity remaining data and K_I and k_{inact} fitting for verapamil.
The percent remaining activity is shown along with a regression where the slope represents -k_{obs}. These studies were conducted n=2. The figure inlay shows the k_{obs} vs inhibitor concentration K_I and k_{inact} fitting, where the hollow symbol was excluded from the fit. The data generated in HLM are shown in panel A and the data generated in HHEP are shown in panel B. The K_I (SE) and k_{inact} (SE) for verapamil were 2.80 (0.540) µM and 0.0487 (0.0023) min^{-1} and 0.661 (0.143) µM and 0.0172 (0.0010) min^{-1} in HLM and HHEP, respectively.

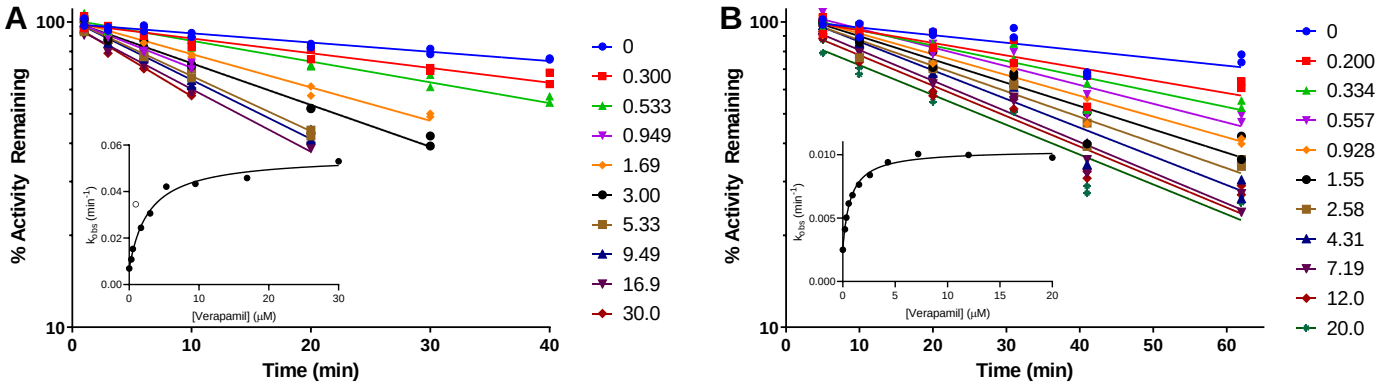

SUPPLEMENTAL TABLES

Static and Dynamic Projections of Drug-Drug Interactions Caused by Cytochrome P450 3A Time-Dependent Inhibitors Measured in Human Liver Microsomes and Hepatocytes

Elaine Tseng, Heather Eng, Jian Lin, Matthew A. Cerny, David A. Tess, Theunis C. Goosen, and R. Scott Obach

List of Supplemental Tables

Supplemental Table 1. Inhibitor Drug Concentration Range Used in Time Dependent Inhibition Studies

	Human Liver Microsomes				Human Hepatocytes			
Drug Name	Concentration Range Tested	Dilution Scheme[a]	Final Solvent in incubation (%)	Incubation Time (min)	Concentration Range Tested (μM)	Drug Concentration Stock[b]	Final Solvent in incubation (%)	Incubation Time (min)
Azithromycin	3-300[c]	1:20	0.9 MeCN	40	3-300	100x	0.9 MeOH	90
Boceprevir	0.1-100	1:40	0.5 MeCN	30	0.3-60	10x	0.5 MeCN	90
Carfilzomib	0.03-300[d]	1:40	0.45 MeCN/0.45 MeOH	30	1-300	100x	0.45 MeCN/0.45 MeOH	120
Clarithromycin	0.5-100	1:20	0.9 MeCN	30	0.5-50	10x	0.9 MeOH	90
Conivaptan	0.1-100	1:40	0.5 MeCN	40	0.3-30	10x	0.5 MeCN	90
Diltiazem	0.3-50	1:20	0.5 MeCN	60	1-300	10x	0.5 MeCN	120
n-desmethyl Diltiazem	0.06-30	1:20	0.9 MeCN	50	0.01-60	100x	0.9 MeCN	90
Disulfiram	0.2-200	1:40	0.5 MeCN	22	ND	ND	ND	ND
Eplerenone	3-300	1:20	0.9 MeCN	40	3-300[d]	100x	0.9 MeCN	120
Erythromycin	0.5-100	1:20	0.9 MeCN	40	0.5-50	10x	0.9 MeCN	90
Imatinib	0.5-100	1:20	0.9 MeCN	40	1-300	10x	0.5 MeCN	120
Midostaurin	0.010-100	1:20	0.45 MeCN/0.45 MeOH	30	0.1-30	100x	0.45 MeCN/0.45 MeOH	120
Nelfinavir	0.1-30[c]	1:80	0.5 MeCN	40	0.3-30[d]	100x	0.5 MeCN	90
Nitrendipine	2-200	1:40	0.9 MeCN	40	ND	ND	ND	ND
Panobinostat	0.6-200	1:40	0.8 MeCN	30	1-100	100x	0.45 MeCN/0.45 MeOH	120
Paroxetine	0.1-100	1:40	0.5 MeCN	50	1-100[d]	10x	0.5 MeCN	120
Propiverine	0.01-100	1:40	0.45 MeCN/0.45 MeOH	30	0.06-30[d]	100x	0.45 MeCN/0.45 MeOH	60
Propranolol	3-300	1:20	0.5 MeCN/0.4 MeOH	40	ND	ND	ND	ND
Simvastatin	3-300[c]	1:100	0.9 MeCN	40	ND	ND	ND	ND
Tabimorelin	0.1-100	1:20	0.5 MeCN	30	1-100	10x	0.5 MeCN	90
Tadalafil	0.03-300	1:40	0.45 MeCN/0.45 MeOH	30	1-100	100x	0.45 MeCN/0.45 MeOH	120
Telaprevir	0.03-30	1:20	0.9 MeCN	22	0.1-30	10x	0.9 MeCN	90
Terfenadine	0.3-30	1:60	0.9 MeCN	40	1-50[c]	100x	0.9 MeCN	90
Verapamil	0.3-30	1:20	0.9 MeCN	40	0.2-20	10x	0.5 MeOH	60

[a]primary incubation to secondary incubation dilution scheme
[b]drug stock dilution scheme due to compound solubility limitations
[c]results were fitted with linear regression due to unsaturable kinetics
[d]results were fitted to substrate inhibition model
MeCN, acetonitrile; MeOH, methanol; ND, not determined

Supplemental Table 2. LC-MS/MS Methods

	Q1	Q3	DP	CE	CXP	LC Conditions: %B(min)	Column & Mobile Phase
Azithromycin	749.6	591.4	50	37	20	10(0.5)-95(1.5)-95(1.8)-10(1.81)-10 (2.0)	A
Boceprevir	520.4	421.2	17	37	15	5(0.4)-95(0.8)-95(1.6)-5(1.7)-5 (2.0)	B
Carfilzomib	720.4	702.5	80	47	15	5(0.6)-95(1.2)-95(1.6)-5(1.61)-5 (2.0)	A
Clarithromycin	748.4	158.1	30	40	15	5(0.6)-95(1.2)-95(1.6)-5(1.61)-5 (2.0)	A
Conivaptan	499.2	181.0	105	60	15	5(0.6)-95(1.2)-95(1.6)-5(1.61)-5 (2.0)	A
Diltiazem	415.0	177.7	80	35	15	5(0.6)-95(1.2)-95(1.6)-5(1.61)-5 (2.0)	A
Disulfiram	297.0	116.1	40	15	15	5(0.6)-95(1.2)-95(1.6)-5(1.61)-5 (2.0)	A
Eplerenone	415.1	163.2	50	29	6	10(0.5)-95(1.5)-95(1.8)-10(1.81)-10 (2.0)	A
Erythromycin	734.5	158.1	62	43	15	5(0.6)-95(1.2)-95(1.6)-5(1.61)-5 (2.0)	A
Imatinib	494.3	394.1	40	35	15	5(0.6)-95(1.2)-95(1.6)-5(1.61)-5 (2.0)	A
Midostaurin	571.2	436.2	60	21	15	5(0.6)-95(1.2)-95(1.6)-5(1.61)-5 (2.0)	A
Nelfinavir	568.5	134.9	50	80	15	5(0.6)-95(1.2)-95(1.6)-5(1.61)-5 (2.0)	A
Nitrendipine	361.0	314.9	50	17	15	10(0.3)-90(1.0)-90(2.0)-10(2.05)-10(3.0)	C
Panobinostat	350.2	158.1	50	27	8	10(0.5)-95(1.5)-95(1.8)-10(1.81)-10 (2.0)	A
Paroxetine	330.6	192.4	25	30	15	10(0.5)-95(1.5)-95(1.8)-10(1.81)-10 (2.0)	A
Propiverine	368.6	183.2	80	38	15	5(0.6)-95(1.2)-95(1.6)-5(1.61)-5 (2.0)	A
Propranolol	260.3	116.0	85	24	15	10(0.3)-90(1.0)-90(2.0)-10(2.05)-10(3.0)	C
Simvastatin	419.3	285.1	60	30	15	5(0.6)-95(1.2)-95(1.6)-5(1.61)-5 (2.0)	A
Tabimorelin	529.4	280.2	60	18	15	5(0.6)-95(1.2)-95(1.6)-5(1.61)-5 (2.0)	A
Tadalafil	390.2	268.2	60	17	15	5(0.6)-95(1.2)-95(1.6)-5(1.61)-5 (2.0)	A
Telaprevir	680.7	322.7	40	20	15	5(0.4)-95(0.8)-95(1.6)-10(1.7)-5 (2.0)	B
Terfenadine	472.5	436.4	120	45	13	10(0.5)-95(1.5)-95(1.8)-10(1.81)-10 (2.0)	A
Verapamil	455.1	164.9	70	50	15	5(0.6)-95(1.2)-95(1.6)-5(1.61)-5 (2.0)	A
Indomethacin	358.1	139.0	60	45	13	10(0.5)-95(1.5)-95(1.8)-10(1.81)-10 (2.0)	A
Diclofenac (IS)	296.2	214.0	70	22	14	10(0.5)-95(1.5)-95(1.8)-10(1.81)-10 (2.0)	A

A. Halo C_{18} 2.1x30 mm 2.7 µm & mobile phase A = water with 0.1% formic acid and mobile phase B = acetonitrile with 0.1% formic acid
B. Waters BEH 2.1x50 mm 1.7 µm & mobile phase A = water with 0.1% ammonium hydroxide and mobile phase B = acetonitrile with 0.1% ammonium hydroxide
C. Kinetex C_{18} XB 3x50 mm 2.6 µm & mobile phase A = 5 mM ammonium acetate with 0.075% formic acid and mobile phase B = acetonitrile with 0.1% formic acid
IS, internal standard

Supplemental Table 3. Measured In Vitro Parameters

Drug Name	HLM IC_{50} (95%CI) (µM)	HHEP IC_{50} (95%CI) (µM)	K_p[e] (%CV)	$f_{u,liver}$ (%CV)	$f_{u,plasma}$ (%CV)
Azithromycin	>100 (NR)	>50.0 (NR)	31.7 (5%)	0.181 (8%)	0.690 (5%)
Boceprevir	23.8 (16.7 to 34.3)	21.5[a] (6.5 to 19.6, 19.7 to 69.6)	4.06 (0%)	0.0458 (16%)	0.695 (6%)
Carfilzomib	4.37 (2.32 to 8.14)	3.42[a] (3.47 to 4.94, 2.14 to 3.40)	18.5 (33%)	8.84E-04 (13%)	0.004[f]
Clarithromycin	87.8 (64.4 to 122)	27.5[a,b] (8.2 to 132.4, 4.5 to 50755)	9.99 (7%)	0.0595 (11%)	0.347 (5%)
Conivaptan	8.27 (4.39 to 15.9)	2.54[a] (1.73 to 3.58, 1.52 to 4.60)	491 (8%)	0.00338 (4%)	0.022 (6%)
Diltiazem	40.5 (24.5 to 68.3)	25.9[a] (7.7 to 83.7, 21.3 to 62.1)	15.3 (10%)	0.0165 (5%)	0.362 (5%)
Disulfiram	2.35 (1.95 to 2.82)	ND	ND	ND	0.205[g]
Eplerenone	>100 (NR)	>50.0 (NR)	0.530 (13%)	0.267 (11%)	0.621 (6%)
Erythromycin	64.0 (37.8 to 114)	33.7[a] (25.8 to 75.7, 13.3 to 107.5)	1.51 (9%)	0.218 (10%)	0.402 (10%)
Imatinib	57.8 (22.3 to 188)	44.9[a,c] (10.8 to 19022, 30.8 to 496.1)	134 (16%)	0.0073 (11%)	0.120 (6%)
Midostaurin	5.57 (2.23 to 14.78)	>50.0 (NR)	277 (43)	1.74E-05 (26%)	1.28E-04 (21%)
Nelfinavir	2.91 (2.28 to 3.71)	0.991[a] (0.469 to 0.972, 0.475 to 3.807)	2440 (12%)	3.8E-04 (8%)	0.00235 (10%)
Nitrendipine	2.74 (2.45 to 3.06)	ND	ND	0.00231 (9%)	0.0227 (15%)
Panobinostat	9.97 (9.04 to 11.0)	>50.0 (NR)	88.5 (11%)	0.00719 (13%)	0.346 (16%)
Paroxetine	26.8 (11.5 to 63.5)	28.5 (24.2 to 34.6)	649 (14%)	9.50E-04 (11%)	0.0840 (10%)
Propiverine	16.1 (9.2 to 28.3)	15.0[a] (9.8 to 22.6, 12.5 to 18.9)	453 (15)	0.00107 (8%)	0.0274 (7%)
Propranolol	>100 (NR)	ND	ND	0.00476 (14%)	0.290 (2%)
Simvastatin	0.292 (0.277 to 0.307)	ND	ND	4.81E-04 (13%)	0.00389 (16%)
Tabimorelin	16.6 (9.4 to 29.6)	5.69[a] (3.79 to 6.86, 2.53 to 18.34)	15.3 (18%)	0.0153 (5%)	0.255 (5%)
Tadalafil	17.1 (11.3 to 26.0)	25.7[a] (22.0 to 32.6, 20.0 to 32.1)	25.7 (5%)	0.0229 (5%)	0.0967 (2%)
Telaprevir	23.2 (7.2 to 89.5)	0.546[a] (0.338 to 1.328, 0.234 to 0.743)	35.5 (17%)	0.0126 (5%)	0.563 (2%)
Terfenadine	0.435 (0.368 to 0.513)	4.34 (3.10 to 6.07)	2670 (42%)	2.14E-04 (8%)	0.0057 (11%)
Verapamil	25.8 (14.1 to 47.9)	26.7[a,d] (11.0 to 1311, 4.6 to 282.4)	80.4 (20%)	0.00386 (12%)	0.234 (17%)

[a]reported as the average of two calculated IC_{50}s
[b]approximately 50% inhibition was observed at the 16.9 µM test concentration
[c]approximately 50% inhibition was observed at the 50.0 µM test concentration
[d]approximately 50% inhibition was observed between the 16.9 and 50.0 µM test concentrations
[e]additional factors used for the calculation of $K_{p,uu}$ include hepatocyte volume dilution factor = 54.5; $f_{u,cell} = f_{u,liver}$; $f_{u,media}$=1
[f]in silico prediction
[g]value obtained from Johansson et al. (Johansson, 1990)
ND,not determined; NR, not reported since IC_{50} could not be determined; 95%CI, 95% confidence interval; %CV,% coefficient of variation, n=3 or 4

Supplemental Table 4. Static Model Inputs Used for DDI Predictions

Drug Name	MW (g/mol)	D_{po} (mg)	f_a	k_a[c] (min^{-1})	C_{max} (µM)	C_{ave} (µM)	Victim Drug	Victim $f_{m,CYP3A}$[a]	Victim F_g[a]	Reference
Azithromycin	749	500	1	0.0275	0.720	0.323	Midazolam	0.93	0.57	(FDA, 2006)
Boceprevir	519	800	1	0.0283	3.32	1.30	Midazolam	0.93	0.57	(FDA, 2011b)
Carfilzomib	720	50[d]	1	NA[d]	7.99	0.105	Midazolam	0.93	0.57	(Wang et al., 2013)
Clarithromycin	748	500	1	0.0283	3.69	2.25	Midazolam	0.93	0.57	(Chu et al., 1993)
Conivaptan	498	40	1	0.0688	0.481	0.197	Midazolam	0.93	0.57	(FDA, 2005a)
Diltiazem	415	60	1	0.1000	0.169	0.088	Midazolam	0.93	0.57	(Friedman et al., 2011)
Disulfiram	297	500	1	0.0183	0.240	0.155	Midazolam	0.93	0.57	(McCance-Katz et al., 2014)
Eplerenone	414	100	1	0.0288	4.94	1.59	Midazolam	0.93	0.57	(FDA, 2003)
Erythromycin	734	500	1	0.0417	3.45	1.12	Midazolam	0.93	0.57	(Brannan et al., 1995)
Imatinib	494	400	1	0.0183	5.26	3.77	Simvastatin	0.92	0.66	(Peng et al., 2005)
Midostaurin	571	100	1	0.0357	4.08	2.09	Midazolam	0.93	0.57	(Dutreix et al., 2013)
Nelfinavir	568	1250	1	0.0200	7.04	3.88	Midazolam	0.93	0.57	(FDA, 2005b)
Nitrendipine	360	20	1	0.0385	0.0220	0.00369	Midazolam	0.93	0.57	(Soons et al., 1991)
Panobinostat	349	20	1	0.0533	0.0630	0.0208	Midazolam	0.93	0.57	(Van Veggel et al., 2018)
Paroxetine	329	20	1	0.1583	0.145	0.103	Terfenadine	0.74[b]	0.40[b]	(Calvo et al., 2004)
Propiverine	367	15	1	0.0250	0.178	0.158	Midazolam	0.93	0.57	(May et al., 2008)
Propranolol	259	40	1	0.0172	0.181	0.0964	Triazolam	0.92	0.75	(Stoschitzky et al., 1992)
Simvastatin	419	10	1	0.0238	0.0337	0.00428	Midazolam	0.93	0.57	(Desager and Horsmans, 1996)
Tabimorelin	529	210	1	0.0217	0.248	0.0627	Midazolam	0.93	0.57	(Agerso et al., 2001)
Tadalafil	389	10	1	0.0310	0.619	0.395	Midazolam	0.93	0.57	(Forgue et al., 2006)
Telaprevir	680	750	1	0.0145	5.16	4.10	Midazolam	0.93	0.57	(FDA, 2011a)
Terfenadine	472	120	1	0.0633	0.00303	0.000519	Buspirone	0.94	0.21	(Stern et al., 1998)
Verapamil	454	80	1	0.0442	0.403	0.214	Midazolam	0.93	0.57	(McTavish and Sorkin, 1989)

[a] (Obach et al., 2006)
[b](Yadav et al., 2018)
[c]k_a was calculated as $0.693/(t_{max,in\ vivo}/5)$ assuming rate of absorption equals rate of elimination at T_{max} and absorption is >90% complete after 5 absorption half-lives (Holford, 2016).
[d]drug administered as IV dose
D_{po}, oral dose; fa, fraction absorbed; ka, absorption rate constant; $f_{m,CYP3A}$, fraction of victim drug metabolized by CYP3A; F_g, fraction of victim drug escaping intestinal metabolism; NA, not applicable since dosed IV

Supplemental Table 5. Azithromycin Input Parameters Used in Simcyp Model for DDI Predictions

Parameter (units)	**Azithromycin (Pfizer modified value)**	**Source (modification)**
Physiochemical Properties		
Molecular weight (g/mol)	749.9	-
log P	4.02	Simcyp default
Compound type	Base	
pKa	8.70	Simcyp default
Blood/plasma ratio	1	Assumed
$f_{u,p}$	0.690	Simcyp default (none, same as measured In-house value)
Absorption-first order		
f_a	1	Assumed
k_a (hr^{-1})	0.5	Simcyp default
$f_{u,gut}$	1 (0.690)	Simcyp default (assumed to equal $f_{u,p}$)
$P_{eff,man}$ (10^{-4} cm/s)	6.50	Simcyp default
P_{app} (10^{-6} cm/s)	50.0	Simcyp default
Distribution		
V_{ss} (L/kg)	33.6	Simcyp default
Elimination		
Biliary CL_{int}	9.25 µL/min/million	Fitted manually to recover the $f_{m,CYP3A}$ and f_g
CL_R (L/hr)	8.67	Observed clinical mean value
Note	Azithromycin Simcyp file is a published compound file downloaded from Simcyp Global Health Repository (Simcyp) which has not been verified by Certara. File was used with modifications ($f_{u,g}$, K_i, K_I, k_{inact}).	

Supplemental Table 6. Boceprevir Input Parameters Used in Simcyp Model for DDI Predictions

Parameter (units)	Boceprevir	Source
Physiochemical Properties		
Molecular weight (g/mol)	520.0	-
log P	3.34	In silico (BioByte)
Compound type	Neutral	-
Blood/plasma ratio	1	Assumed
$f_{u,p}$	0.695	Measured In-house
Absorption-first order		
f_a	1	Assumed
k_a (hr^{-1})	1.7	Fitted to manually predict T_{max}
$f_{u,gut}$	0.695	Assumed to equal $f_{u,p}$
$P_{eff,man}$ (10^{-4} cm/s)	0.55	Predicted by P_{app}
P_{app} (10^{-6} cm/s)	3.32	In silico (Keefer et al., 2013)
Distribution		
V_{ss} (L/kg)	1.50	Fitted to manually predict C_{max}
Elimination		
CL_{po} (L/hr)	161	Fitted to manually predict C_{max} and AUC
Note	Internal Pfizer model, V_{ss} and CL fitted manually to adequately recover AUC and C_{max} at the dose used in the DDI study	

Supplemental Table 7. Carfilzomib Input Parameters Used in Simcyp Model for DDI Predictions

Parameter (units)	Carfilzomib	Source
Physiochemical Properties		
Molecular weight (g/mol)	719.9	-
log P	6.40	In silico (BioByte)
Compound type	Base	-
pKa	5.14	In silico (ACD/pKa)
Blood/plasma ratio	1	Assumed
$f_{u,p}$	0.00424	Measured In-house
Distribution		
V_{ss} (L/kg)	1.2	Fitted to manually predict C_{max}
Elimination		
CL_{IV} (L/hr)	136	Fitted to manually predict C_{max} and AUC
Note	Internal Pfizer model, V_{ss} and CL fitted manually to adequately recover AUC and C_{max} at the dose used in the DDI study	

Supplemental Table 8. Clarithromycin Input Parameters Used in Simcyp Model for DDI Predictions

Parameter (units)	Clarithromycin (Pfizer modified value)	Source (modification)
Physiochemical Properties		
Molecular weight (g/mol)	748.0	-
log P	1.70	Simcyp default
Compound type	Base	-
pKa	8.99	Simcyp default
Blood/plasma ratio	1	Simcyp default
$f_{u,p}$	0.18 (0.347)	Simcyp default (measured in-house)
Absorption-first order		
f_a	1	Simcyp default
k_a (hr^{-1})	2.4	Simcyp default
Lag time (hr)	0.26	Simcyp default
$f_{u,gut}$	1 (0.347)	Simcyp default (assumed to equal $f_{u,p}$)
$P_{eff,man}$ (10^{-4} cm/s)	2.11	Simcyp default
P_{app} (10^{-6} cm/s)	3.84	Simcyp default
Distribution		
V_{ss} (L/kg)	1.75	Simcyp default
Elimination		
CL_{po} (L/hr)	$V_{max,3A4:}$ 10.4 pmol/min/pmol $K_{m,3A4}$: 22.3 µM (30)	Simcyp default (fitted to manually predict C_{max} and AUC)
CL_R (L/hr)	8.05	Observed clinical mean value
Note	SV- Clarithromycin Simcyp compound file (Simcyp) with modifications ($f_{u,p}$, $f_{u,g}$, K_i, K_I, $k_{inact,}$ CL_{po})	

Supplemental Table 9. Conivaptan Input Parameters of in Simcyp Model for DDI Predictions

Parameter (units)	Conivaptan	Source
Physiochemical Properties		
Molecular weight (g/mol)	498.6	-
log P	5.00	In silico (BioByte)
Compound type	Base	-
pKa	7.32	In silico (ACD/pKa)
Blood/plasma ratio	1	Assumed
$f_{u,p}$	0.022	Measured In-house
Absorption-first order		
f_a	1	Assumed
k_a (hr^{-1})	2.0	Fitted to manually predict T_{max}
$f_{u,gut}$	0.022	Assumed to equal $f_{u,p}$
$P_{eff,man}$ (10^{-4} cm/s)	0.79	Predicted by P_{app}
P_{app} (10^{-6} cm/s)	6.32	In silico (Keefer et al., 2013)
Distribution		
V_{ss} (L/kg)	1.3	Fitted to manually predict C_{max}
Elimination		
CL_{po} (L/hr)	34	Fitted to manually predict C_{max} and AUC
Note	Internal Pfizer model developed based on (Burnier et al., 1999)	

Supplemental Table 10. Diltiazem Input Parameters Used in Simcyp Model for DDI Predictions

Parameter (units)	**Diltiazem (Pfizer modified value)**	**Source (modification)**
Physiochemical Properties		
Molecular weight (g/mol)	414.5	-
log P	2.80	Simcyp default
Compound type	Base	-
pKa	8.06	Simcyp default
Blood/plasma ratio	0.963	Simcyp default
$f_{u,p}$	0.25 (0.362)	Simcyp default (measured in-house)
Absorption-first order		
f_a	1	Simcyp default
k_a (hr^{-1})	6.0	Simcyp default
$f_{u,gut}$	0.25 (0.362)	Simcyp default (assumed to equal $f_{u,p}$)
$P_{eff,man}$ (10^{-4} cm/s)	5.30	Simcyp default
P_{app} (10^{-6} cm/s)	41.3	Simcyp default
Distribution		
V_{ss} (L/kg)	3.09	Simcyp default
Elimination		
CL_{int}	$V_{max,3A4}$: 1881 pmoL/min/mg, $K_{m,3A4}$: 50 µM; $CL_{int,1A2}$: 2.4 µL/min/mg; $CL_{int,HLM}$: 109 µL/min/mg	Simcyp default
CL_R (L/hr)	2.88	Simcyp default
Note	Sim-Diltiazem Simcyp compound file (Simcyp) with modifications ($f_{u,p}$, $f_{u,g}$, K_i, K_I, k_{inact})	

Supplemental Table 11. Disulfiram Input Parameters Used in Simcyp Model for DDI Predictions

Parameter (units)	Disulfiram	Source
Physiochemical Properties		
Molecular weight (g/mol)	297.0	-
log P	3.88	In silico (BioByte)
Compound type	Neutral	-
Blood/plasma ratio	1	Assumed
$f_{u,p}$	0.205	Measured In-house
Absorption-first order		
f_a	1	Assumed
k_a (hr^{-1})	2.0	Fitted to manually predict T_{max}
$f_{u,gut}$	0.205	Assumed to equal $f_{u,p}$
$P_{eff,man}$ (10^{-4} cm/s)	3.10	Predicted by P_{app}
P_{app} (10^{-6} cm/s)	24.1	In silico (Keefer et al., 2013)
Distribution		
V_{ss} (L/kg)	4.9	Fitted to manually predict C_{max}
Elimination		
CL_{po} (L/hr)	1086	Fitted to manually predict C_{max} and AUC
Note	Internal Pfizer model, V_{ss} and CL fitted manually to adequately recover AUC and C_{max} at the dose used in the DDI study	

Supplemental Table 12. Eplerenone Input Parameters Used in Simcyp Model for DDI Predictions

Parameter (units)	Eplerenone	Source
Physiochemical Properties		
Molecular weight (g/mol)	414.5	-
log P	0.93	In silico (BioByte)
Compound type	Neutral	-
Blood/plasma ratio	1	Assumed
$f_{u,p}$	0.621	Measured In-house
Absorption-first order		
f_a	1	Assumed
k_a (hr^{-1})	2.0	Fitted to manually predict T_{max}
$f_{u,gut}$	0.621	Assumed to equal $f_{u,p}$
$P_{eff,man}$ (10^{-4} cm/s)	2.20	Predicted by P_{app}
P_{app} (10^{-6} cm/s)	17.2	In silico (Keefer et al., 2013)
Distribution		
V_{ss} (L/kg)	0.5	Fitted to manually predict C_{max}
Elimination		
CL_{po} (L/hr)	9	Fitted to manually predict C_{max} and AUC
Note	Internal Pfizer model, V_{ss} and CL fitted manually to adequately recover AUC and C_{max} at the dose used in the DDI study	

Supplemental Table 13. Erythromycin Input Parameters Used in Simcyp Model for DDI Predictions

Parameter (units)	Erythromycin (Pfizer modified value)	Source (modification)
Physiochemical Properties		
Molecular weight (g/mol)	733.9	-
log P	2.50	Simcyp default
Compound type	Base	-
pKa	8.80	Simcyp default
Blood/plasma ratio	0.854	Simcyp default
$f_{u,p}$	0.31 (0.402)	Simcyp default (measured in-house)
Absorption-first order		
f_a	1	Simcyp default
k_a (hr^{-1})	3.6 (2.5)	Simcyp default (modified to be consistent with static model)
$f_{u,gut}$	1 (0.402)	Simcyp default (assumed to equal $f_{u,p}$)
$P_{eff,man}$ (10^{-4} cm/s)	0.21	Predicted by P_{app}
P_{app} (10^{-6} cm/s)	1.70	Simcyp default
Distribution		
V_{ss} (L/kg)	0.75 (1.5)	Fitted to manually predict C_{max}
Elimination		
CL_{po} (L/hr)	$V_{max,3A4:}$ 1.45 pmol/min/pmol $K_{m,3A4}$: 14.7 µM $V_{max,3A5:}$ 1.25 pmol/min/pmol $K_{m,3A5}$: 30.7 µM $CL_{int,HLM}$: 13 µL/min/mg (62)	Simcyp default (fitted to manually predict C_{max} and AUC)
CL_R (L/hr)	3.13	Simcyp default
Note	SV-Erythromycin_EC Simcyp compound file (Simcyp) with modifications ($f_{u,p}$, $f_{u,g}$, K_i, K_I, k_{inact}, V_{ss}, CL_{PO})	

Supplemental Table 14. Imatinib Input Parameters Used in Simcyp Model for DDI Predictions

Parameter (units)	Imatinib	Source
Physiochemical Properties		
Molecular weight (g/mol)	493.6	-
log P	4.53	In silico (BioByte)
Compound type	Base	-
pKa	7.55	In silico (ACD/pKa)
Blood/plasma ratio	0.732	Observed (Adiwidjaja et al., 2019)
$f_{u,p}$	0.12	Measured In-house
Absorption-first order		
f_a	1	Assumed
k_a (hr^{-1})	1.1	Fitted to manually predict T_{max}
$f_{u,gut}$	0.120	Assumed to equal $f_{u,p}$
$P_{eff,man}$ (10^{-4} cm/s)	1.20	Predicted by P_{app}
P_{app} (10^{-6} cm/s)	7.63	In silico (Keefer et al., 2013)
Distribution		
V_{ss} (L/kg)	1.5	Fitted to manually predict C_{max}
Elimination		
CL_{po} (L/hr)	13.8	Fitted to manually predict C_{max} and AUC
CL_R (L/hr)	0.5	Observed clinical mean value (Adiwidjaja et al., 2019)
Note	Internal Pfizer model, V_{ss} and CL fitted manually to adequately recover AUC and C_{max} at the dose used in the DDI study	

Supplemental Table 15. Midostaurin Input Parameters Used in Simcyp Model for DDI Predictions

Parameter (units)	Midostaurin	Source
Physiochemical Properties		
Molecular weight (g/mol)	570.6	-
log P	5.49	In silico (BioByte)
Compound type	Neutral	-
Blood/plasma ratio	1	Assumed
$f_{u,p}$	0.000128	Measured In-house
Absorption-first order		
f_a	1	Assumed
k_a (hr^{-1})	2.4	Fitted to manually predict T_{max}
$f_{u,gut}$	0.000128	Assumed to equal $f_{u,p}$
$P_{eff,man}$ (10^{-4} cm/s)	1.10	Predicted by P_{app}
P_{app} (10^{-6} cm/s)	6.86	In silico (Keefer et al., 2013)
Distribution		
V_{ss} (L/kg)	0.5	Fitted to manually predict C_{max}
Elimination		
CL_{po} (L/hr)	6.8	Fitted to manually predict C_{max} and AUC
Note	Internal Pfizer model, V_{ss} and CL fitted manually to adequately recover AUC and C_{max} at the dose used in the DDI study	

Supplemental Table 16. Nelfinavir Input Parameters Used in Simcyp Model for DDI Predictions

Parameter (units)	Nelfinavir	Source
Physiochemical Properties		
Molecular weight (g/mol)	567.8	-
log P	5.84	In silico (BioByte)
Compound type	Base	-
pKa	6.21	In silico (ACD/pKa)
Blood/plasma ratio	1	Assumed
$f_{u,p}$	0.00235	Measured In-house
Absorption-first order		
f_a	1	Assumed
k_a (hr^{-1})	1.2	Fitted to manually predict T_{max}
$f_{u,gut}$	0.00235	Assumed to equal $f_{u,p}$
$P_{eff,man}$ (10^{-4} cm/s)	0.320	Predicted by P_{app}
P_{app} (10^{-6} cm/s)	2.56	In silico (Keefer et al., 2013)
Distribution		
V_{ss} (L/kg)	2.0	Fitted to manually predict C_{max}
Elimination		
CL_{po} (L/hr)	50	Fitted to manually predict C_{max} and AUC
Note	Internal Pfizer model, V_{ss} and CL fitted manually to adequately recover AUC and C_{max} at the dose used in the DDI study	

Supplemental Table 17. Nitrendipine Input Parameters Used in Simcyp Model for DDI Predictions

Parameter (units)	Nitrendipine	Source
Physiochemical Properties		
Molecular weight (g/mol)	360.4	-
log P	3.73	In silico (BioByte)
Compound type	Neutral	-
Blood/plasma ratio	1	Assumed
$f_{u,p}$	0.0227	Measured In-house
Absorption-first order		
f_a	1	Assumed
k_a (hr^{-1})	2	Fitted to manually predict T_{max}
$f_{u,gut}$	0.0227	Assumed to equal $f_{u,p}$
$P_{eff,man}$ (10^{-4} cm/s)	2.90	Predicted by P_{app}
P_{app} (10^{-6} cm/s)	23.4	In silico (Keefer et al., 2013)
Distribution		
V_{ss} (L/kg)	3.9	Fitted to manually predict C_{max}
Elimination		
CL_{po} (L/hr)	500	Fitted to manually predict C_{max} and AUC
Note	Internal Pfizer model, V_{ss} and CL fitted manually to adequately recover AUC and C_{max} at the dose used in the DDI study	

Supplemental Table 18. Panobinostat Input Parameters Used in Simcyp Model for DDI Predictions

Parameter (units)	Panobinostat	Source
Physiochemical Properties		
Molecular weight (g/mol)	349.4	-
log P	2.64	In silico (BioByte)
Compound type	Base	-
pKa	9.29	In silico (ACD/pKa)
Blood/plasma ratio	1	Assumed
$f_{u,p}$	0.346	Measured In-house
Absorption-first order		
f_a	1	Assumed
k_a (hr^{-1})	2	Fitted to manually predict T_{max}
$f_{u,gut}$	0.346	Assumed to equal $f_{u,p}$
$P_{eff,man}$ (10^{-4} cm/s)	0.210	Predicted by P_{app}
P_{app} (10^{-6} cm/s)	1.71	In silico (Keefer et al., 2013)
Distribution		
V_{ss} (L/kg)	4.5	Fitted to manually predict C_{max}
Elimination		
CL_{po} (L/hr)	150	Fitted to manually predict C_{max} and AUC
Note	Internal Pfizer model, V_{ss} and CL fitted manually to adequately recover AUC and C_{max} at the dose used in the DDI study	

Supplemental Table 19. Paroxetine Input Parameters Used in Simcyp Model for DDI Predictions

Parameter (units)	**Paroxetine (Pfizer modified value)**	**Source (modification)**
Physiochemical Properties		
Molecular weight (g/mol)	329.4	-
log P	3.55	Simcyp default
Compound type	Base	-
pKa	9.66	Simcyp default
Blood/plasma ratio	1.26	Simcyp default
$f_{u,p}$	0.05 (0.084)	Simcyp default (measured in-house)
Absorption-first order		
f_a	0.94	Simcyp default
k_a (hr^{-1})	1.08	Simcyp default
$f_{u,gut}$	1 (0.084)	Simcyp default (assumed to equal $f_{u,p}$)
$P_{eff,man}$ (10^{-4} cm/s)	2.50	Simcyp default
P_{app} (10^{-6} cm/s)	17.0	Simcyp default
Distribution		
V_{ss} (L/kg)	12.5 (10.0)	Simcyp default (fitted to manually predict C_{max})
Elimination		
CL_{po} (L/hr)	$V_{max,1A2:}$ 0.27 pmol/min/pmol $K_{m,1A2}$: 8.8 µM $V_{max,2C19:}$ 0.6 pmol/min/pmol $K_{m,2C19}$: 26 µM $V_{max,2D6:}$ 7.2 pmol/min/pmol $K_{m,2D6}$: 0.028 µM $V_{max,3A4:}$ 1.2 pmol/min/pmol $K_{m,3A5}$: 13.3 µM $V_{max,3A5:}$ 0.38 pmol/min/pmol $K_{m,3A4}$: 108 µM $CL_{int,HLM}$: 62 µL/min/mg (24.6)	Simcyp default (fitted to manually predict C_{max} and AUC)
CL_R (L/hr)	0.5	Simcyp default
Note	SV-Paroxetine Simcyp compound file (Simcyp) with modifications ($f_{u,p}$, $f_{u,g}$, K_i, K_I, k_{inact}, V_{ss}, CL_{po})	

Supplemental Table 20. Propiverine Input Parameters Used in Simcyp Model for DDI Predictions

Parameter (units)	Propiverine	Source
Physiochemical Properties		
Molecular weight (g/mol)	367.5	-
log P	3.79	In silico (BioByte)
Compound type	Base	-
pKa	7.76	In silico (ACD/pKa)
Blood/plasma ratio	1	Assumed
$f_{u,p}$	0.0274	Measured In-house
Absorption-first order		
f_a	1	Assumed
k_a (hr^{-1})	1	Fitted to manually predict T_{max}
$f_{u,gut}$	0.0274	Assumed to equal $f_{u,p}$
$P_{eff,man}$ (10^{-4} cm/s)	2.50	Predicted by P_{app}
P_{app} (10^{-6} cm/s)	15.0	In silico (Keefer et al., 2013)
Distribution		
V_{ss} (L/kg)	3.0	Fitted to manually predict C_{max} and AUC
Elimination		
CL_{po} (L/hr)	32	Fitted to manually predict C_{max} and AUC
Note	Internal Pfizer model, V_{ss} and CL fitted manually to adequately recover AUC and C_{max} at the dose used in the DDI study	

Supplemental Table 21. Propranolol Input Parameters Used in Simcyp Model for DDI Predictions

Parameter (units)	Propranolol	Source
Physiochemical Properties		
Molecular weight (g/mol)	259.3	-
log P	2.75	In silico (BioByte)
Compound type	Base	-
pKa	9.5	In silico (ACD/pKa)
Blood/plasma ratio	1	Assumed
$f_{u,p}$	0.29	Measured In-house
Absorption-first order		
f_a	1	Assumed
k_a (hr^{-1})	2.0	Fitted to manually predict T_{max}
$f_{u,gut}$	0.29	Assumed to equal $f_{u,p}$
$P_{eff,man}$ (10^{-4} cm/s)	2.00	Predicted by P_{app}
P_{app} (10^{-6} cm/s)	16.2	In silico (Keefer et al., 2013)
Distribution		
V_{ss} (L/kg)	3	Fitted to manually predict C_{max}
Elimination		
CL_{po} (L/hr)	300	Fitted to manually predict C_{max} and AUC
Note	Internal Pfizer model, V_{ss} and CL fitted manually to adequately recover AUC and C_{max} at the dose used in the DDI study	

Supplemental Table 22. Simvastatin Input Parameters Used in Simcyp Model for DDI Predictions

Parameter (units)	Simvastatin (Pfizer modified value)	Source (modification)
Physiochemical Properties		
Molecular weight (g/mol)	418.6	-
log P	4.68	Simcyp default
Compound type	Neutral	-
Blood/plasma ratio	1	Simcyp default
$f_{u,p}$	0.02 (0.00389)	Simcyp default (measured in-house)
Absorption-first order		
f_a	1	A Simcyp default
k_a (hr^{-1})	1.43	Simcyp default
Lag time (hr)	0.25	Simcyp default
$f_{u,gut}$	1 (0.00389)	Simcyp default (assumed to equal $f_{u,p}$)
$P_{eff,man}$ (10^{-4} cm/s)	1.60	Simcyp default
P_{app} (10^{-6} cm/s)	6.80	Simcyp default
Distribution		
V_{ss} (L/kg)	1.5	Simcyp default
Elimination		
CL_{po} (L/hr)	$CL_{int,3A4}$: 2284 µL/min/mg $CL_{int,HLM}$: 254 µL/min/mg (232)	Simcyp default (fitted to manually predict C_{max} and AUC)
Note	SV-Simvastatin Simcyp compound file (Simcyp) with modifications ($f_{u,p}$, $f_{u,g}$, K_i, K_I, k_{inact}, CL_{PO})	

Supplemental Table 23. Tabimorelin Input Parameters Used in Simcyp Model for DDI Predictions

Parameter (units)	Tabimorelin	Source
Physiochemical Properties		
Molecular weight (g/mol)	528.7	-
log P	3.76	In silico (BioByte)
Compound type	Base	-
pKa	9.48	In silico (ACD/pKa)
Blood/plasma ratio	1	Assumed
$f_{u,p}$	0.255	Measured In-house
Absorption-first order		
f_a	1	Assumed
k_a (hr^{-1})	1.5	Fitted to manually predict T_{max}
$f_{u,gut}$	0.255	Assumed to equal $f_{u,p}$
$P_{eff,man}$ (10^{-4} cm/s)	0.52	Predicted by P_{app}
P_{app} (10^{-6} cm/s)	4.20	In silico (Keefer et al., 2013)
Distribution		
V_{ss} (L/kg)	4	Fitted to manually predict C_{max}
Elimination		
CL_{po} (L/hr)	264	Fitted to manually predict C_{max} and AUC
Note	Internal Pfizer model, V_{ss} and CL fitted manually to adequately recover AUC and C_{max} at the dose used in the DDI study	

Supplemental Table 24. Tadalafil Input Parameters Used in Simcyp Model for DDI Predictions

Parameter (units)	Tadalafil	Source
Physiochemical Properties		
Molecular weight (g/mol)	389.4	-
log P	2.58	In silico (BioByte)
Compound type	Neutral	-
Blood/plasma ratio	1	Assumed
$f_{u,p}$	0.0967	Measured In-house
Absorption-first order		
f_a	1	Assumed
k_a (hr^{-1})	1.73	Fitted to manually predict T_{max}
$f_{u,gut}$	0.0967	Assumed to equal $f_{u,p}$
$P_{eff,man}$ (10^{-4} cm/s)	2.10	Predicted by P_{app}
P_{app} (10^{-6} cm/s)	12.1	In silico (Keefer et al., 2013)
Distribution		
V_{ss} (L/kg)	1	Fitted to manually predict C_{max}
Elimination		
CL_{po} (L/hr)	2.7	Fitted to manually predict C_{max} and AUC
Note	Internal Pfizer model, V_{ss} and CL fitted manually to adequately recover AUC and C_{max} at the dose used in the DDI study	

Supplemental Table 25. Telaprevir Input Parameters Used in Simcyp Model for DDI Predictions

Parameter (units)	Telaprevir	Source
Physiochemical Properties		
Molecular weight (g/mol)	679.8	-
log P	5.35	In silico (BioByte)
Compound type	Neutral	-
pKa		In silico (ACD/pKa)
Blood/plasma ratio	0.65	(Kimoto et al., 2019)
$f_{u,p}$	0.563	Measured In-house
Absorption-first order		
f_a	1	Assumed
k_a (hr^{-1})	0.8	Fitted to manually predict T_{max}
$f_{u,gut}$	0.563	Assumed to equal $f_{u,p}$
$P_{eff,man}$ (10^{-4} cm/s)	0.13	Predicted by P_{app}
P_{app} (10^{-6} cm/s)	1.08	In silico (Keefer et al., 2013)
Distribution		
V_{ss} (L/kg)	2	Fitted to manually predict C_{max}
Elimination		
CL_{po} (L/hr)	32	Fitted to manually predict C_{max} and AUC
Note	Published model with modifications ($f_{u,p}$, $f_{u,g}$, K_i, K_I, k_{inact}, CL_{PO}) (Kimoto et al., 2019)	

Supplemental Table 26. Input Parameters of Terfenadine Used in Simcyp Model for DDI Predictions

Parameter (units)	Terfenadine	Source
Physiochemical Properties		
Molecular weight (g/mol)	471.7	-
log P	5.69	(Wisniowska and Polak, 2016)
Compound type	Base	-
pKa	9.5	(Wisniowska and Polak, 2016)
Blood/plasma ratio	1	Assumed
$f_{u,p}$	0.0057	Measured In-house
Absorption-first order		
f_a	0.787	(Wisniowska and Polak, 2016)
k_a (hr^{-1})	0.52	(Wisniowska and Polak, 2016)
$f_{u,gut}$	0.0057	Assumed to equal $f_{u,p}$
$P_{eff,man}$ (10^{-4} cm/s)	1.26	(Wisniowska and Polak, 2016)
Distribution		
V_{ss} (L/kg)	3	Fitted to manually predict C_{max}
Elimination		
CL_{po} (L/hr)	20408	Fitted to manually predict C_{max} and AUC
Note	Published model with modifications (V_{ss} and CL_{PO}) (Wisniowska and Polak, 2016)	

Supplemental Table 27. Input Parameters of Verapamil Used in Simcyp Model for DDI Predictions

Parameter (units)	Verapamil (Pfizer modified value)	Source (modification)
Physiochemical Properties		
Molecular weight (g/mol)	454.6	-
log P	4.46	Simcyp default
Compound type	Base	-
pKa	8.78	Simcyp default
Blood/plasma ratio	0.709	Simcyp default
$f_{u,p}$	0.09 (0.234)	Simcyp default (measured in-house)
Absorption-first order		
f_a	1	Simcyp default
k_a (hr^{-1})	2.65	Simcyp default
Lag time (hr)		Simcyp default (assumed to equal $f_{u,p}$)
$f_{u,gut}$	1 (0.234)	Simcyp default
$P_{eff,man}$ (10^{-4} cm/s)	6.10	Simcyp default
P_{app} (10^{-6} cm/s)	149	Simcyp default
Distribution		
V_{ss} (L/kg)	5.3 (4)	Simcyp default (fitted to manually predict C_{max})
Elimination		
CL_{po} (L/hr)	$CL_{int,2C8}$: 3.0 µL/min/pmol $CL_{int,3A4}$: 3.0 µL/min/pmol $CL_{int,3A5}$: 3.5 µL/min/pmol (sum of 2 pathways) CL_{intHLM}: 79.6 µL/min/mg (102)	Simcyp default (fitted to manually predict C_{max} and AUC)
CL_R (L/hr)	2.52	Simcyp default
Note	SV-Verapamil Simcyp compound file (Simcyp) with modifications ($f_{u,p}$, $f_{u,g}$, K_i ,K_I, k_{inact}, V_{ss}, CL_{PO})	

Supplemental Table 28. Input Parameters of Victim Drug Terfenadine Used in Simcyp Model for DDI Predictions

Parameter (units)	Terfenadine	Source
Physiochemical Properties		
Molecular weight (g/mol)	471.7	-
log P	5.69	(Wisniowska and Polak, 2016)
Compound type	Base	-
pKa	9.50	(Wisniowska and Polak, 2016)
Blood/plasma ratio	1	Assumed
$f_{u,p}$	0.03	(Wisniowska and Polak, 2016)
Absorption-first order		
f_a	0.787	(Wisniowska and Polak, 2016)
k_a (hr^{-1})	0.52	(Wisniowska and Polak, 2016)
$f_{u,gut}$	0.03	Assumed to equal $f_{u,p}$
$P_{eff,man}$ (10^{-4} cm/s)	1.26	(Wisniowska and Polak, 2016)
Distribution		
V_{ss} (L/kg)	4.4	(Wisniowska and Polak, 2016)
Elimination		
CL_{int}	$CL_{int,3A4}$: 64 µL/min/pmol $CL_{int,3D6}$: 160 µL/min/pmol $CL_{int,HLM}$: 200 µL/min/mg $CL_{int,HIM}$: 700 µL/min/mg	Fitted manually to recover the $f_{m,CYP3A}$ and f_g
Note	Published model with modifications (CL_{int}) (Wisniowska and Polak, 2016)	

Supplemental Table 29. Input Parameters of Victim Drug Buspirone Used in Simcyp Model for DDI Predictions

Parameter (units)	Buspirone	Source
Physiochemical Properties		
Molecular weight (g/mol)	385.5	-
log P	2.19	In silico (BioByte)
Compound type	Base	-
pKa	7.72[d]	In silico (ACD/pKa)
Blood/plasma ratio	1	Assumed
$f_{u,p}$	0.05	Kivisto et al 1999
Absorption-first order		
f_a	1.00	Assumed
k_a (hr^{-1})	5.00	Fitted to manually predict T_{max}
$f_{u,gut}$	1	Assumed
$P_{eff,man}$ (10^{-4} cm/s)	3.6	Predicted by P_{app}
P_{app} (10^{-6} cm/s)	28.6[k]	In silico (Keefer et al., 2013)
Distribution		
V_{ss} (L/kg)	5.02	Fitted to manually predict C_{max}
Elimination		
CL_{int}	$CL_{int,3A4}$: 10.3 µL/min/pmol $CL_{int,HLM}$: 69.8 µL/min/mg 30 L/hr (additional system clearance)	Fitted to manually predict C_{max} and AUC
Note	Published model (Kivisto et al., 1997; Kivisto et al., 1999; Mahmood and Sahajwalla, 1999)	

Supplemental Table 30. Input Parameters of Victim Drug Midazolam Used in Simcyp Model for DDI Predictions

Parameter (units)	Sim-Midazolam	Source
Physiochemical Properties		
Molecular weight (g/mol)	325.8	Simcyp default
log P	3.53	Simcyp default
Compound type	Base	Simcyp default
pKa	6.00	Simcyp default
Blood/plasma ratio	0.603	Simcyp default
$f_{u,p}$	0.032	Simcyp default
Absorption-first order		
f_a	1.0	Simcyp default
k_a (hr^{-1})	3.0	Simcyp default
$f_{u,gut}$	1.0	Simcyp default
$P_{eff,man}$ (10^{-4} cm/s)	6	Simcyp default
P_{app} (10^{-6} cm/s)	213	Simcyp default
Distribution		
V_{ss} (L/kg)	0.88	Simcyp default
V_{sac} (L/kg)	0.23	
K_{in} (hr^{-1})	0.2	
K_{out} (hr^{-1})	0.25	
Elimination		
CL_{int}	$V_{max,1\text{-}OH,3A4}$: 5.23 pmol/min/pmol $K_{m,1\text{-}OH,3A4}$: 2.16 µM $V_{max,1\text{-}OH,3A5}$: 19.7 pmol/min/pmol $K_{m,1\text{-}OH,3A5}$: 4.16 µM $V_{max,4\text{-}OH,3A4}$: 5.2 pmol/min/pmol $K_{m,4\text{-}OH,3A4}$: 31.8 µM $V_{max,4\text{-}OH,3A5}$: 4 pmol/min/pmol $K_{m,4\text{-}OH,3A5}$: 38.4 µM $V_{max,UGT1A4}$: 445 pmol/min/mg $K_{m,UGT1A4}$: 40.3 µM	Simcyp default
CL_R (L/hr)	0.085	Simcyp default
Note	Simcyp compound file (Simcyp) without modification	

Supplemental Table 31. Input Parameters of Victim Drug Triazolam Used in Simcyp Model for DDI Predictions

Parameter (units)	SV-Triazolam	Source
Physiochemical Properties		
Molecular weight (g/mol)	343.2	Simcyp default
log P	2.03	Simcyp default
Compound type	Base	Simcyp default
pKa	3.6	Simcyp default
Blood/plasma ratio	0.62	Simcyp default
$f_{u,p}$	0.179	Simcyp default
Absorption-first order		
f_a	1.00	Simcyp default
k_a (hr^{-1})	1.1	Simcyp default
$f_{u,gut}$	1	Simcyp default
$P_{eff,man}$ (10^{-4} cm/s)	9.5	Simcyp default
Distribution		
V_{ss} (L/kg)	0.658	Simcyp default
Elimination		
CL_{int}	$V_{max,1\text{-}OH,3A4}$: 2.11 pmol/min/pmol $K_{m,1\text{-}OH,3A4}$: 15.6 µM $V_{max,1\text{-}OH,3A5}$: 3.97 pmol/min/pmol $K_{m,1\text{-}OH,3A5}$: 23.8 µM $V_{max,4\text{-}OH,3A4}$: 5.59 pmol/min/pmol $K_{m,4\text{-}OH,3A4}$: 176 µM $V_{max,4\text{-}OH,3A5}$: 6 pmol/min/pmol $K_{m,4\text{-}OH,3A5}$: 142 µM	Simcyp default
CL_R (L/hr)	0.274	Simcyp default
Note	Simcyp compound file (Simcyp) without modification	

Supplemental Table 32. Input Parameters of Victim Drug Simvastatin Used in Simcyp Model for DDI Predictions

Parameter (units)	SV-Simvastatin	Source
Physiochemical Properties		
Molecular weight (g/mol)	418.6	Simcyp default
log P	4.68	Simcyp default
Compound type	Neutral	Simcyp default
Blood/plasma ratio	1	Simcyp default
$f_{u,p}$	0.02	Simcyp default
Absorption-first order		
f_a	1.00	Simcyp default
k_a (hr^{-1})	1.43	Simcyp default
$f_{u,gut}$	1	Simcyp default
$P_{eff,man}$ (10^{-4} cm/s)	1.6	Simcyp default
P_{app} (10^{-6} cm/s)	6.8	Simcyp default
Distribution		
V_{ss} (L/kg)	1.5	Simcyp default
Elimination		
CL_{int}	$CL_{int,3A4}$: 2284 µL/min/mg $CL_{int,HLM}$: 254 µL/min/mg	Simcyp default
Note	Simcyp compound file (Simcyp) without modification	

Supplemental Table 33. Mean $f_{m,CYP3A}$ and F_g for Victim Drugs

	Static Model		PBPK model (n=100)	
Victim Drug	$f_{m,CYP3A}$	F_g	$f_{m,CYP3A4}$[a]	F_g[a]
Midazolam	0.93	0.57	0.876	0.6
Simvastatin	0.92	0.66	0.88	0.12
Buspirone	0.94	0.21	0.95	0.27
Terfenadine	0.74	0.4	0.7	0.39
Triazolam	0.92	0.75	0.9	0.75

[a] $f_{m,cyp3A4}$ and F_g are reported as arithmetic mean

Supplemental Table 34. Calculated $[I]_g$ and $[I]_h$ Concentrations Used in Calculation of AUCR for Mechanistic Static Models 1-4

	Model 1		Model 2		Model 3		Model 4	
Drug Name	$[I]_g$ (μM) Total Enterocyte k_a=0.1 min^{-1}	$[I]_h$ (μM) Hepatic inlet $C_{max,u}$	$[I]_g$ (μM) Free Enterocyte k_a=custom	$[I]_h$ (μM) Hepatic inlet $C_{max,u}$	$[I]_g$ (μM) Portal $C_{max,u}$ k_a=custom	$[I]_h$ (μM) Systemic $C_{max,u}$ NA	$[I]_g$ (μM) Portal $C_{avg,u}$ k_a=custom	$[I]_h$ (μM) Systemic $C_{avg,u}$ NA
Azithromycin	223	29.0	42.2	8.33	10.9	0.497	0.487	0.223
Boceprevir	513	68.5	101	21.1	27.3	2.31	2.74	0.906
Carfilzomib	NA	0.0491	NA	0.0327	NA	0.0320	NA	0.000420
Clarithromycin	223	15.6	21.9	5.34	6.70	1.28	1.05	0.781
Conivaptan	26.8	0.120	0.405	0.0858	0.111	0.0106	0.00636	0.00433
Diltiazem	48.2	3.30	17.5	3.30	4.38	0.0612	0.122	0.0320
Disulfiram	562	21.4	21.1	3.96	5.26	0.0492	0.230	0.0318
Eplerenone	80.4	12.3	14.4	5.74	6.63	3.07	1.07	0.984
Erythromycin	227	18.3	38.0	8.44	10.8	1.39	0.919	0.449
Imatinib	270	6.64	5.94	1.73	2.10	0.631	0.508	0.452
Midostaurin	58.4	0.00191	0.00267	0.00102	0.00118	0.000522	0.000280	0.000267
Nelfinavir	734	0.336	0.345	0.0805	0.102	0.0165	0.0150	0.00911
Nitrendipine	18.5	0.0784	0.162	0.0305	0.0405	0.000499	0.000805	0.0000838
Panobinostat	19.1	1.25	3.52	0.675	0.892	0.0218	0.0128	0.00718
Paroxetine	20.3	0.328	2.69	0.512	0.679	0.0122	0.0116	0.00865
Propiverine	13.6	0.0741	0.0932	0.0222	0.0280	0.00493	0.00561	0.00433
Propranolol	51.4	2.82	2.56	0.528	0.687	0.0525	0.0536	0.0280
Simvastatin	7.96	0.00588	0.00877	0.00176	0.00230	0.000132	0.0000699	0.0000166
Tabimorelin	132	6.33	7.32	1.42	1.87	0.0632	0.0740	0.0160
Tadalafil	8.56	0.214	0.257	0.108	0.123	0.0600	0.0396	0.0382
Telaprevir	368	41.3	30.0	8.47	10.3	2.91	3.38	2.31
Terfenadine	84.8	0.0897	0.306	0.0568	0.0757	0.0000171	0.000833	0.00000296
Verapamil	58.7	2.64	6.07	1.22	1.59	0.0936	0.121	0.0501

$[I_g]$, inhibitor concentration in the gut; $[I_h]$, inhibitor concentration in the liver; $C_{max,u}$, maximum unbound concentration; $C_{avg,u}$, average unbound concentration; k_a, absorption rate constant; NA, not applicable

Supplemental Table 35. Observed Clinical DDIs and Predicted DDIs from HLM-generated Inhibition Parameters Using Mechanistic Static Models 1-4

Drug Name	Observed Clinical Interaction (AUCR)	Model 1		Model 2		Model 3		Model 4	
		Predicted	Predicted/ Observed	Predicted	Predicted/ Observed	Predicted	Predicted/ Observed	Predicted	Predicted/ Observed
Azithromycin	1.23[a]	6.85	5.57	2.80	2.27	1.31	1.07	1.04	0.84
Boceprevir	5.05	25.0	4.95	24.9	4.92	23.5	4.65	21.5	4.26
Carfilzomib	1.10	9.77	8.88	8.55	7.77	8.48	7.71	1.23	1.12
Clarithromycin	6.69[a]	22.2	3.32	18.4	2.75	10.5	1.57	7.25	1.08
Conivaptan	5.76	24.0	4.16	23.6	4.10	18.0	3.13	12.6	2.19
Diltiazem	3.93[a]	17.1	4.35	17.0	4.32	3.86	0.98	2.38	0.60
Disulfiram	1.05	25.0	23.8	24.1	23.0	3.69	3.51	2.66	2.54
Eplerenone	0.96	8.95	9.32	5.02	5.23	3.19	3.32	1.59	1.65
Erythromycin	4.12	23.1	5.60	21.5	5.22	14.0	3.39	7.43	1.80
Imatinib	2.92	15.8	5.41	11.7	4.02	7.61	2.61	5.99	2.05
Midostaurin	1.00	15.4	15.4	12.1	12.1	8.82	8.82	5.51	5.51
Nelfinavir	4.29	24.9	5.80	24.7	5.76	24.1	5.63	23.5	5.49
Nelfinavir[b]	1.83	14.2	7.75	14.1	7.70	13.8	7.52	13.5	7.35
Nitrendipine	0.93	4.01	4.31	2.15	2.31	1.18	1.27	1.01	1.08
Panobinostat	1.04	12.6	12.2	8.73	8.40	1.85	1.78	1.09	1.05
Paroxetine	0.97	6.04	6.23	6.41	6.60	2.23	2.30	1.13	1.17
Propiverine	1.46	10.2	7.01	4.88	3.34	2.16	1.48	1.69	1.15
Propranolol	0.89	1.21	1.36	1.02	1.15	1.00	1.13	1.00	1.12
Simvastatin	1.24	1.86	1.50	1.06	0.85	1.01	0.82	1.00	0.81
Tabimorelin	1.93	24.0	12.5	22.8	11.8	12.0	6.21	5.35	2.77
Tadalafil	0.90	11.0	12.3	6.97	7.74	4.64	5.16	3.12	3.47
Telaprevir	13.5	24.8	1.84	24.5	1.81	24.1	1.79	24.0	1.78
Telaprevir[b]	4.92	14.2	2.88	14.0	2.84	13.8	2.80	13.7	2.79
Terfenadine	1.19	52.5	44.1	40.8	34.3	3.90	3.27	1.10	0.92
Verapamil	2.92	22.4	7.68	21.0	7.18	9.96	3.41	6.54	2.24

[a]average AUCR weighted by number of subjects per study
[b]clinical IV midazolam studies

Supplemental Table 36. Observed Clinical DDIs and Predicted DDIs from HHEP-generated Inhibition Parameters Using Mechanistic Static Models 1-4

Drug Name	Observed Clinical Interaction (AUCR)	Model 1		Model 2		Model 3		Model 4	
		Predicted	Predicted/ Observed	Predicted	Predicted/ Observed	Predicted	Predicted/ Observed	Predicted	Predicted/ Observed
Azithromycin	1.23[a]	11.9	9.70	5.52	4.49	1.69	1.37	1.12	0.91
Boceprevir	5.05	25.0	4.95	24.9	4.94	23.6	4.66	21.0	4.15
Carfilzomib	1.10	12.0	10.9	10.8	9.80	10.7	9.74	1.29	1.17
Clarithromycin	6.69[a]	21.5	3.22	17.7	2.64	10.6	1.58	7.52	1.12
Conivaptan	5.76	8.69	1.51	6.84	1.19	2.26	0.39	1.31	0.23
Diltiazem	3.93[a]	18.6	4.74	18.6	4.73	2.47	0.63	1.48	0.38
Disulfiram	1.05	1.00	0.95	1.00	0.95	1.00	0.95	1.00	0.95
Eplerenone	0.96	8.84	9.21	4.65	4.84	2.89	3.01	1.48	1.54
Erythromycin	4.12	23.0	5.57	20.6	5.00	10.3	2.49	4.59	1.11
Imatinib	2.92	11.1	3.81	5.35	1.83	2.89	0.99	2.16	0.74
Midostaurin	1.00	9.42	9.42	6.59	6.59	4.57	4.57	2.82	2.82
Nelfinavir	4.29	11.1	2.59	3.98	0.93	1.78	0.42	1.27	0.30
Nelfinavir[b]	1.83	6.33	3.46	2.50	1.36	1.32	0.72	1.17	0.64
Nitrendipine	0.93	1.00	1.08	1.00	1.08	1.00	1.08	1.00	1.08
Panobinostat	1.04	3.37	3.24	2.25	2.16	1.21	1.16	1.01	0.97
Paroxetine	0.97	2.63	2.71	1.80	1.85	1.15	1.19	1.01	1.04
Propiverine	1.46	8.67	5.94	4.01	2.74	1.89	1.29	1.50	1.03
Propranolol	0.89	1.00	1.12	1.00	1.12	1.00	1.12	1.00	1.12
Simvastatin	1.24	1.00	0.81	1.00	0.81	1.00	0.81	1.00	0.81
Tabimorelin	1.93	24.4	12.6	21.5	11.2	4.78	2.48	2.02	1.04
Tadalafil	0.90	9.32	10.4	5.75	6.39	3.85	4.28	2.63	2.93
Telaprevir	13.5	25.0	1.85	24.9	1.85	24.6	1.82	24.4	1.81
Telaprevir[b]	4.92	14.3	2.90	14.2	2.89	14.0	2.85	13.9	2.83
Terfenadine	1.19	5.43	4.56	1.40	1.17	1.07	0.90	1.00	0.84
Verapamil	2.92	21.6	7.40	20.4	6.99	14.3	4.89	11.1	3.82

[a]average AUCR weighted by number of subjects per study
[b]clinical IV midazolam studies
[c]predicted AUCR=1 compound is not a TDI in hepatocytes

Supplemental Table 37. Observed Clinical DDIs and Predicted DDIs Using Simcyp

Drug Name	Observed Clinical Interaction (AUCR)	Liver Microsomes		Hepatocytes	
		Predicted AUCR[d]	Predicted/ Observed	Predicted AUCR[d]	Predicted/ Observed
Azithromycin	1.23[a]	1.04	0.85	1.07	0.87
Boceprevir	5.05	15.0	2.97	14.5	2.87
Carfilzomib	1.10	1.00	0.91	1.01	0.92
Clarithromycin	6.69[a]	6.00	0.90	5.91	0.88
Conivaptan	5.76	11.4	1.98	1.34	0.23
Diltiazem	3.93[a]	2.48	0.63	1.57	0.40
Disulfiram	1.05	1.13	1.08	1.00[c]	0.95
Eplerenone	0.96	1.48	1.54	2.03	2.02
Erythromycin	4.12	9.64	2.34	6.13	1.49
Imatinib	2.92	7.51	2.57	2.30	0.79
Midostaurin	1.00	1.28	1.28	1.11	1.11
Nelfinavir	4.29	19.2	4.48	1.24	0.32
Nelfinavir[b]	1.83	7.48	4.09	1.09	0.62
Nitrendipine	0.93	1.00	1.08	1.00[c]	1.08
Panobinostat	1.04	1.07	1.03	1.02	0.98
Paroxetine	0.97	1.32	1.36	1.16	1.20
Propiverine	1.46	1.57	1.08	1.42	0.97
Propranolol	0.89	1.00	1.12	1.00[c]	1.12
Simvastatin	1.24	1.00	0.81	1.00[c]	0.81
Tabimorelin	1.93	5.48	2.84	2.13	1.10
Tadalafil	0.90	3.30	3.67	2.83	3.14
Telaprevir	13.5	25.8	1.91	26.1	1.93
Telaprevir[b]	4.92	9.95	2.02	10.1	2.05
Terfenadine	1.19	1.10	0.92	1.00	0.84
Verapamil	2.92	6.09	2.09	8.71	2.99

[a]average AUCR weighted by number of subjects per study
[b]clinical IV midazolam studies
[c]predicted AUCR=1 since compound is not a TDI in hepatocytes
[d]predicted AUCR is reported as geometric mean

Supplemental Table 38. Observed and Predicted Inhibitor C_{max} and AUC Using Simcyp

Drug Name	Observed		Predicted[a]		Predicted/Observed		C_{max} and AUC Reference
	C_{max} (ng/mL)	AUC (ng·hr/mL)	C_{max} (ng/mL)	AUC (ng·hr/mL)	C_{max}	AUC	
Azithromycin	540	5800	4656	3947	0.86	0.68	(FDA, 2006)
Boceprevir	1723	5408	1981	5536	1.15	1.02	(FDA, 2011b)
Carfilzomib	5753	903	5055	602	0.88	0.67	(Wang et al., 2013)
Clarithromycin	2760	20215	2817	17165	1.02	0.85	(Chu et al., 1993)
Conivaptan	240	1176	242	1279	1.01	1.09	(FDA, 2005a)
Diltiazem	70.1	293	88.0	341	1.26	1.16	(Friedman et al., 2011)
Disulfiram	71.2	460	81.0	494	1.14	1.07	(McCance-Katz et al., 2014)
Eplerenone	2046	15786	2053	12070	1.00	0.76	(FDA, 2003)
Erythromycin	2530	6533	2137	8423	0.84	1.29	(Brannan et al., 1995)
Imatinib	2596	40100	2559	29863	0.99	0.74	(Peng et al., 2005)
Midostaurin	2326	9525	2205	15303	0.95	1.61	(Dutreix et al., 2013)
Nelfinavir	4000	26400	4269	27175	1.07	1.03	(FDA, 2005b)
Nitrendipine	8.00	31.8	7.20	43.0	0.90	1.35	(Soons et al., 1991)
Panobinostat	21.6	174	22.0	145	1.00	0.83	(Van Veggel et al., 2018)
Paroxetine	47.6	813	43.3	805	0.91	0.99	(Calvo et al., 2004)
Propiverine	65.4	692	61.0	510	0.93	0.74	(May et al., 2008)
Propranolol	39.4	130	39.8	144	1.01	1.11	(Dvornik et al., 1981)
Simvastatin	14.1	43.0	14.0	47.0	1.01	1.09	(Desager and Horsmans, 1996)
Tabimorelin	131	795	145	906	1.11	1.14	(Agerso et al., 2001)
Tadalafil	241	3695	235	4022	0.98	1.09	(Forgue et al., 2006)
Telaprevir	3510	22300	3655	23445	1.04	1.05	(FDA, 2011a)
Terfenadine	1.43	5.88	1.37	6.37	0.96	1.08	(Stern et al., 1998)
Verapamil	183	779	185	1047	1.01	1.34	(McTavish and Sorkin, 1989)

[a] C_{max} and AUC are reported as geometric mean

[b] time interval used to calculate average concentrations

C_{max}, maximum concentration; AUC, area under the curve

Supplemental References

ACD/pKa version 14, Advanced Chemistry Development, Inc., Toronto, On, Canada, www.acdlabs.com, 2021.

Adiwidjaja J, Boddy AV, and McLachlan AJ (2019) Implementation of a Physiologically Based Pharmacokinetic Modeling Approach to Guide Optimal Dosing Regimens for Imatinib and Potential Drug Interactions in Paediatrics. *Front Pharmacol* **10:**1672.

Agerso H, Ynddal L, Sogaard B, and Zdravkovic M (2001) Pharmacokinetic and pharmacodynamic modeling of NN703, a growth hormone secretagogue, after a single po dose to human volunteers. *J Clin Pharmacol* **41:**163-169.

BioByte cLogP, version 4.3, Biobyte Corp., Claremont, CA, USA, www.biobyte.com.

Brannan MD, Reidenberg P, Radwanski E, Shneyer L, Lin CC, Cayen MN, and Affrime MB (1995) Loratadine administered concomitantly with erythromycin: pharmacokinetic and electrocardiographic evaluations. *Clin Pharmacol Ther* **58:**269-278.

Burnier M, Fricker AF, Hayoz D, Nussberger J, and Brunner HR (1999) Pharmacokinetic and pharmacodynamic effects of YM087, a combined V1/V2 vasopressin receptor antagonist in normal subjects. *Eur J Clin Pharmacol* **55:**633-637.

Calvo G, García-Gea C, Luque A, Morte A, Dal-Ré R, and Barbanoj M (2004) Lack of Pharmacologic Interaction Between Paroxetine and Alprazolam at Steady State in Healthy Volunteers. *Journal of Clinical Psychopharmacology* **24:**268-276.

Chu S, Wilson DS, Deaton RL, Mackenthun AV, Eason CN, and Cavanaugh JH (1993) Single- and multiple-dose pharmacokinetics of clarithromycin, a new macrolide antimicrobial. *J Clin Pharmacol* **33:**719-726.

Desager JP and Horsmans Y (1996) Clinical pharmacokinetics of 3-hydroxy-3-methylglutaryl-coenzyme A reductase inhibitors. *Clin Pharmacokinet* **31:**348-371.

Dutreix C, Munarini F, Lorenzo S, Roesel J, and Wang Y (2013) Investigation into CYP3A4-mediated drug-drug interactions on midostaurin in healthy volunteers. *Cancer Chemother Pharmacol* **72:**1223-1234.

Dvornik D, Kraml M, Dubuc J, Patterson-Kreuscher S, Milosovich G, and Mullane JF (1981) Comparative bioavailability of propranolol: twice-daily versus four times-daily administration. *J Clin Pharmacol* **21:**472-476.

FDA (2003) Drug approval package: Inspra (Eplerenone). FDA application NDA 021437. FDA Silver Springs, MD.

FDA (2005a) Drug approval package: Vaprisol (conivaptan). FDA application NDA 021697. FDA Silver Springs, MD.

FDA (2005b) Drug approval package: Viracept (Nelfinavir mesylate). FDA application NDA021503. FDA Silver Springs, MD.

FDA (2006) Drug approval package: Azithromycin. FDA application ANDA065225. FDA Silver Springs, MD.

FDA (2011a) Drug approval package: Incivek (telaprevir). FDA application NDA 201917. FDA Silver Springs, MD.

FDA (2011b) Drug approval package: Victrelis (boceprevir). FDA application NDA 202258. FDA Silver Springs, MD.

Forgue ST, Patterson BE, Bedding AW, Payne CD, Phillips DL, Wrishko RE, and Mitchell MI (2006) Tadalafil pharmacokinetics in healthy subjects. *Br J Clin Pharmacol* **61:**280-288.

Friedman EJ, Fraser IP, Wang YH, Bergman AJ, Li CC, Larson PJ, Chodakewitz J, Wagner JA, and Stoch SA (2011) Effect of different durations and formulations of diltiazem on the single-dose pharmacokinetics of midazolam: how long do we go? *J Clin Pharmacol* **51:**1561-1570.

Holford N (2016) Absorption and Half-Life. *Transl Clin Pharmacol* **24:**157-160.

Johansson B (1990) Plasma protein binding of disulfiram and its metabolite diethylthiocarbamic acid methyl ester. *Journal of Pharmacy and Pharmacology* **42:**806-807.
Keefer CE, Kauffman GW, and Gupta RR (2013) Interpretable, probability-based confidence metric for continuous quantitative structure-activity relationship models. *J Chem Inf Model* **53:**368-383.
Kimoto E, Vourvahis M, Scialis RJ, Eng H, Rodrigues AD, and Varma MVS (2019) Mechanistic Evaluation of the Complex Drug-Drug Interactions of Maraviroc: Contribution of Cytochrome P450 3A, P-Glycoprotein and Organic Anion Transporting Polypeptide 1B1. *Drug Metab Dispos* **47:**493-503.
Kivisto KT, Lamberg TS, Kantola T, and Neuvonen PJ (1997) Plasma buspirone concentrations are greatly increased by erythromycin and itraconazole. *Clin Pharmacol Ther* **62:**348-354.
Kivisto KT, Lamberg TS, and Neuvonen PJ (1999) Interactions of buspirone with itraconazole and rifampicin: effects on the pharmacokinetics of the active 1-(2-pyrimidinyl)-piperazine metabolite of buspirone. *Pharmacol Toxicol* **84:**94-97.
Mahmood I and Sahajwalla C (1999) Clinical pharmacokinetics and pharmacodynamics of buspirone, an anxiolytic drug. *Clin Pharmacokinet* **36:**277-287.
May K, Giessmann T, Wegner D, Oertel R, Modess C, Oswald S, Braeter M, and Siegmund W (2008) Oral absorption of propiverine solution and of the immediate and extended release dosage forms: influence of regioselective intestinal elimination. *Eur J Clin Pharmacol* **64:**1085-1092.
McCance-Katz EF, Gruber VA, Beatty G, Lum P, Ma Q, DiFrancesco R, Hochreiter J, Wallace PK, Faiman MD, and Morse GD (2014) Interaction of disulfiram with antiretroviral medications: efavirenz increases while atazanavir decreases disulfiram effect on enzymes of alcohol metabolism. *Am J Addict* **23:**137-144.
McTavish D and Sorkin EM (1989) Verapamil. An updated review of its pharmacodynamic and pharmacokinetic properties, and therapeutic use in hypertension. *Drugs* **38:**19-76.
Obach RS, Walsky RL, Venkatakrishnan K, Gaman EA, Houston JB, and Tremaine LM (2006) The utility of in vitro cytochrome P450 inhibition data in the prediction of drug-drug interactions. *J Pharmacol Exp Ther* **316:**336-348.
Peng B, Lloyd P, and Schran H (2005) Clinical Pharmacokinetics of Imatinib. *Clinical Pharmacokinetics* **44:**879-894.
Simcyp Certera Simcyp Library Files. https://members.simcyp.com/account/libraryFiles).
Soons PA, Vogels BA, Roosemalen MC, Schoemaker HC, Uchida E, Edgar B, Lundahl J, Cohen AF, and Breimer DD (1991) Grapefruit juice and cimetidine inhibit stereoselective metabolism of nitrendipine in humans. *Clin Pharmacol Ther* **50:**394-403.
Stern RH, Smithers JA, and Olson SC (1998) Atorvastatin does not produce a clinically significant effect on the pharmacokinetics of terfenadine. *J Clin Pharmacol* **38:**753-757.
Stoschitzky K, Lindner W, Egginger G, Brunner F, Obermayer-Pietsch B, Passath A, and Klein W (1992) Racemic (R,S)-propranolol versus half-dosed optically pure (S)-propranolol in humans at steady state: Hemodynamic effects, plasma concentrations, and influence on thyroid hormone levels. *Clin Pharmacol Ther* **51:**445-453.
Van Veggel M, Westerman E, and Hamberg P (2018) Clinical Pharmacokinetics and Pharmacodynamics of Panobinostat. *Clin Pharmacokinet* **57:**21-29.
Wang Z, Yang J, Kirk C, Fang Y, Alsina M, Badros A, Papadopoulos K, Wong A, Woo T, Bomba D, Li J, and Infante JR (2013) Clinical pharmacokinetics, metabolism, and drug-drug interaction of carfilzomib. *Drug Metab Dispos* **41:**230-237.
Wisniowska B and Polak S (2016) Virtual Clinical Trial Toward Polytherapy Safety Assessment: Combination of Physiologically Based Pharmacokinetic/Pharmacodynamic-Based Modeling and Simulation Approach With Drug-Drug Interactions Involving Terfenadine as an Example. *J Pharm Sci* **105:**3415-3424.
Yadav J, Korzekwa K, and Nagar S (2018) Improved Predictions of Drug-Drug Interactions Mediated by Time-Dependent Inhibition of CYP3A. *Mol Pharm* **15:**1979-1995.